High Intensity Laser-Solid Interaction

Andrea Macchi

Istituto Nazionale per la Fisica della Materia (INFM)

Dipartimento di Fisica "Enrico Fermi", Università di Pisa

www.df.unipi.it/∼macchi

INFM

Department of Pure and Applied Physics,
Queen's University of Belfast, UK,
June 17th, 2004

UNIPI

Outlook

Outlook

- Overview of laser–solid interaction

Outlook

- Overview of laser–solid interaction
- Collisionless absorption mechanism

Outlook

- Overview of laser–solid interaction
- Collisionless absorption mechanism
  - Mode conversion:

Outlook

- Overview of laser–solid interaction
- Collisionless absorption mechanism
  - Mode conversion: resonance absorption, surface waves, . . .

Outlook

- Overview of laser–solid interaction
- Collisionless absorption mechanism
  - Mode conversion: resonance absorption, surface waves, . . .
  - Kinetic effects:

Outlook

- Overview of laser–solid interaction
- Collisionless absorption mechanism
  - Mode conversion: resonance absorption, surface waves, . . .
  - Kinetic effects: anomalous skin effect, vacuum heating, . . .

Outlook

- Overview of laser–solid interaction
- Collisionless absorption mechanism
  - Mode conversion: resonance absorption, surface waves, . . .
  - Kinetic effects: anomalous skin effect, vacuum heating, . . .
  - Some simulation results

Outlook

- Overview of laser–solid interaction
- Collisionless absorption mechanism
  - Mode conversion: resonance absorption, surface waves, . . .
  - Kinetic effects: anomalous skin effect, vacuum heating, . . .
  - Some simulation results
- "Fast" electrons and related instabilities

Outlook

- Overview of laser–solid interaction
- Collisionless absorption mechanism
  - Mode conversion: resonance absorption, surface waves, . . .
  - Kinetic effects: anomalous skin effect, vacuum heating, . . .
  - Some simulation results
- "Fast" electrons and related instabilities
- Laser–*nanosolid* (cluster) interaction

Interaction regime

Interaction regime

- Laser pulse: high intensity ($I_L \geq 10^{16}$ W/cm^2), short duration ($\tau_L \leq 1$ps)

Interaction regime

- Laser pulse: high intensity ($I_L \geq 10^{16}$ W/cm^2), short duration ($\tau_L \leq 1$ps)

- Plasma: overdense ($n_e \geq n_c \sim 10^{21}$ cm^{-3}), step boundary ($L = n_c/|\nabla n_e|_{@n_c} \ll \lambda_L$)

Interaction regime

- Laser pulse: high intensity ($I_L \geq 10^{16}$ W/cm^2), short duration ($\tau_L \leq 1$ps)

- Plasma: overdense ($n_e \geq n_c \sim 10^{21}$ cm^{-3}), step boundary ($L = n_c/|\nabla n_e|_{@n_c} \ll \lambda_L$)

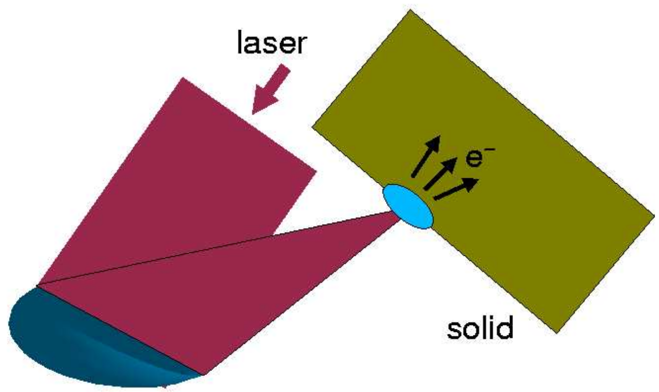

Interaction regime

- Laser pulse: high intensity ($I_L \geq 10^{16}$ W/cm^2), short duration ($\tau_L \leq 1$ps)

- Plasma: overdense ($n_e \geq n_c \sim 10^{21}$ cm^{-3}), step boundary ($L = n_c/|\nabla n_e|_{@n_c} \ll \lambda_L$)

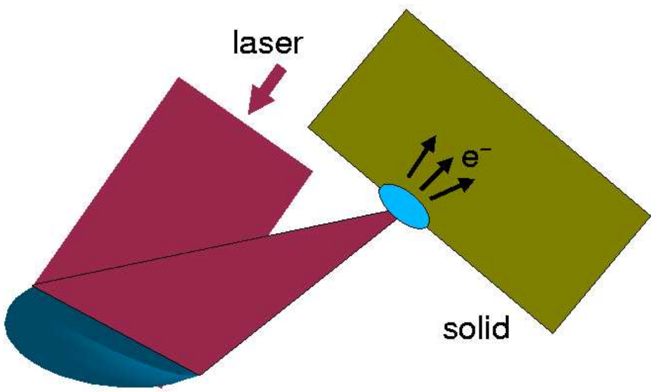

Laser–Solid Interaction is a route for laser energy conversion into thermal or suprathermal electrons and ions and into coherent and incoherent XUV radiation.

Interaction scenario

Interaction scenario

We may identify four stages of the interaction:

Interaction scenario

We may identify four stages of the interaction:

1. plasma production from fast ionization

Interaction scenario

We may identify four stages of the interaction:

1. plasma production from fast ionization

2. collisional absorption and plasma heating

Interaction scenario

We may identify four stages of the interaction:

1. plasma production from fast ionization

2. collisional absorption and plasma heating

3. collisionless absorption of laser energy and electron acceleration

Interaction scenario

We may identify four stages of the interaction:

1. plasma production from fast ionization
2. collisional absorption and plasma heating
3. collisionless absorption of laser energy and electron acceleration
4. electron energy transport and conversion (radiation, ions, fields . . .)

Stage 1: ionization and plasma production

Stage 1: ionization and plasma production

Field ionization by the laser pulse is "instantaneous" (faster than an optical cycle) when the laser field exceeds the atomic field ("barrier suppression" ionization):

$$E_L > e/r_B^2 = 5.1\times10^9\,\mathrm{V\ cm}^{-1} \Rightarrow I_L > 3.5\times10^{16}\,\mathrm{W\ cm}^{-2}$$

Stage 1: ionization and plasma production

Field ionization by the laser pulse is "instantaneous" (faster than an optical cycle) when the laser field exceeds the atomic field ("barrier suppression" ionization):

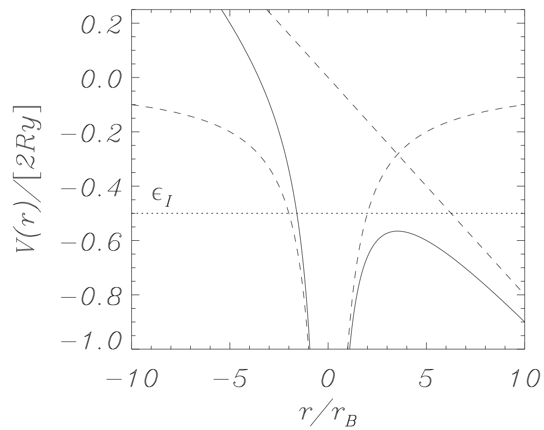

$$E_L > e/r_B^2 = 5.1\times10^9\ \text{V cm}^{-1} \Rightarrow I_L > 3.5\times10^{16}\ \text{W cm}^{-2}$$

Stage 1: ionization and plasma production

Field ionization by the laser pulse is "instantaneous" (faster than an optical cycle) when the laser field exceeds the atomic field ("barrier suppression" ionization):

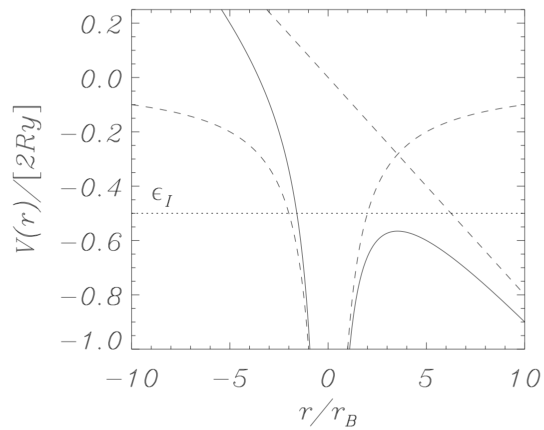

$$E_L > e/r_B^2 = 5.1\times10^9 \text{ V cm}^{-1} \Rightarrow I_L > 3.5\times10^{16} \text{ W cm}^{-2}$$

Oscillating free electrons contribute to collisional ionization (quiver energy $\mathcal{E}_{osc} \simeq 6$ keV at $I_L\lambda_L^2 = 3.5\times10^{16}$ W cm$^{-2}\mu$m^2).

The fields in the plasma

The fields in the plasma

Ionization of outer electrons is enough to make $\omega_p > \omega$ for any solid target.

The fields in the plasma

Ionization of outer electrons is enough to make $\omega_p > \omega$ for any solid target.The plasma dielectric function becomes negative:

$$\epsilon(\omega) = 1 - \frac{\omega_p^2}{\omega^2} = 1 - \frac{n_e}{n_c} < 0$$

As a first step, the fields in the plasma can be found from Fresnel formulas with refractive index n $= \sqrt{\epsilon(\omega)}$.

The fields in the plasma

Ionization of outer electrons is enough to make $\omega_p > \omega$ for any solid target.The plasma dielectric function becomes negative:

$$\epsilon(\omega) = 1 - \frac{\omega_p^2}{\omega^2} = 1 - \frac{n_e}{n_c} < 0$$

As a first step, the fields in the plasma can be found from Fresnel formulas with refractive index n $= \sqrt{\epsilon(\omega)}$.

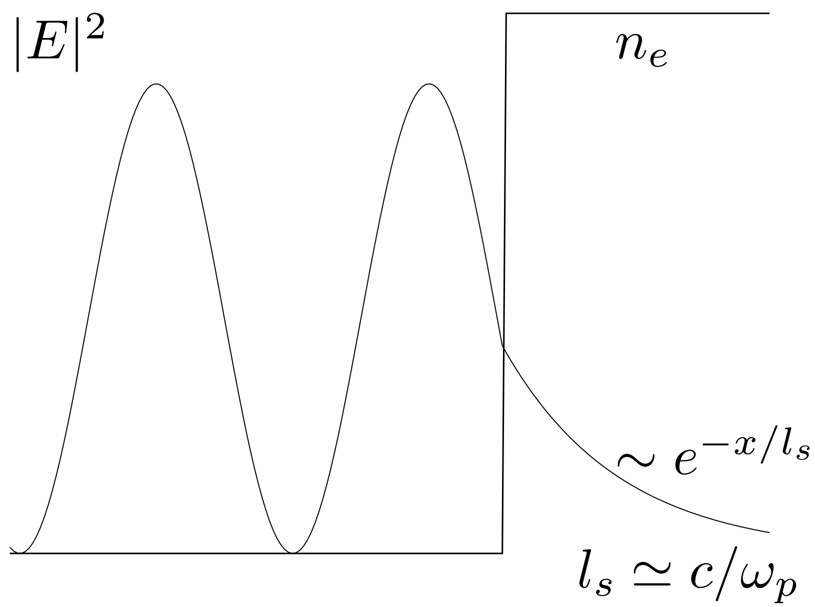

The forces on the plasma

The forces on the plasma

In addition to the electric force at frequency ω, the force at the plasma surface has a magnetic component at frequencies 0 and 2ω:

$$\mathbf{F} = -e(\underbrace{\mathbf{E}}_{\omega} + \underbrace{\mathbf{v} \times \mathbf{B}}_{0\omega+2\omega})$$

The forces on the plasma

In addition to the electric force at frequency ω, the force at the plasma surface has a magnetic component at frequencies 0 and 2ω:

$$\mathbf{F} = -e(\underbrace{\mathbf{E}}_{\omega} + \underbrace{\mathbf{v} \times \mathbf{B}}_{0\omega+2\omega})$$

The 0ω term corresponds to radiation pressure
[total pressure: $P = (1 + R)I/c$]

The forces on the plasma

In addition to the electric force at frequency ω, the force at the plasma surface has a magnetic component at frequencies 0 and 2ω:

$$\mathbf{F} = -e(\underbrace{\mathbf{E}}_{\omega} + \underbrace{\mathbf{v} \times \mathbf{B}}_{0\omega+2\omega})$$

The 0ω term corresponds to radiation pressure
[total pressure: $P = (1 + R)I/c$]

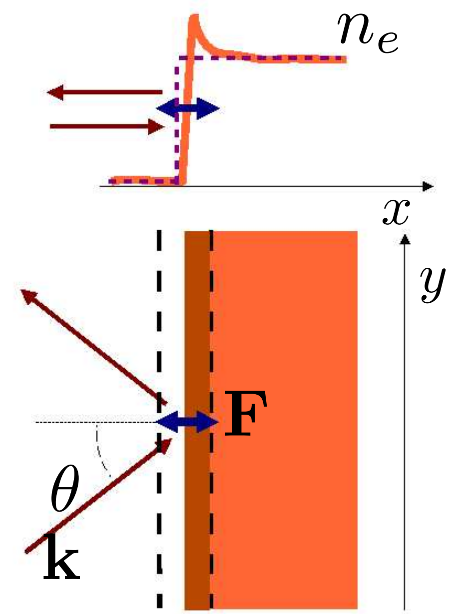

The forces on the plasma

In addition to the electric force at frequency ω, the force at the plasma surface has a magnetic component at frequencies 0 and 2ω:

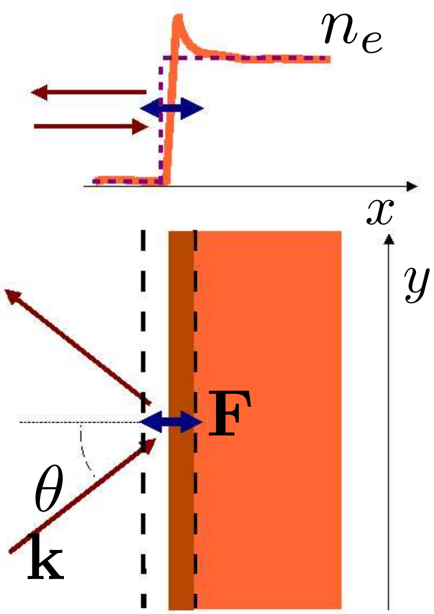

$$\mathbf{F} = -e(\underbrace{\mathbf{E}}_{\omega} + \underbrace{\mathbf{v} \times \mathbf{B}}_{0\omega+2\omega})$$

The 0ω term corresponds to radiation pressure [total pressure: $P = (1 + R)I/c$]

It turns out that the dynamics at the plasma surface is dominated by *the force component normal to the surface*. The latter strongly depends on polarization and incidence angle.

An useful trick: the boosted frame

An useful trick: the boosted frame

For planar geometry, the 2D problem of oblique incidence can be always reduced to a 1D problem of normal incidence by a Lorentz boost along the surface:

An useful trick: the boosted frame

For planar geometry, the 2D problem of oblique incidence can be always reduced to a 1D problem of normal incidence by a Lorentz boost along the surface:$\boldsymbol{\beta} = \beta\hat{\mathbf{y}}$, $\beta = \sin\theta$

An useful trick: the boosted frame

For planar geometry, the 2D problem of oblique incidence can be always reduced to a 1D problem of normal incidence by a Lorentz boost along the surface:$\boldsymbol{\beta} = \beta\hat{\mathbf{y}}$, $\beta = \sin\theta$[Bourdier, 1980].

$$k'_y = \gamma[k_y - (\omega/c)\beta] = \gamma(\omega/c)(\sin\theta - \sin\theta) = 0,$$

$$k'_x = k_x = k\cos\theta = k/\gamma\,, \qquad \omega' = \gamma(\omega - k_y\beta) = \omega/\gamma,$$

An useful trick: the boosted frame

For planar geometry, the 2D problem of oblique incidence can be always reduced to a 1D problem of normal incidence by a Lorentz boost along the surface:$\boldsymbol{\beta} = \beta\hat{\mathbf{y}}$, $\beta = \sin\theta$[Bourdier, 1980].

$$k'_y = \gamma[k_y - (\omega/c)\beta] = \gamma(\omega/c)(\sin\theta - \sin\theta) = 0,$$

$$k'_x = k_x = k\cos\theta = k/\gamma\,, \qquad \omega' = \gamma(\omega - k_y\beta) = \omega/\gamma,$$

$$E'_x = \gamma(E_x + \beta B_z) = \gamma E(\sin\theta - \sin\theta) = 0\,,\ E'_y = E_y\,,\ B'_z = B_z/\gamma.$$

An useful trick: the boosted frame

For planar geometry, the 2D problem of oblique incidence can be always reduced to a 1D problem of normal incidence by a Lorentz boost along the surface:$\boldsymbol{\beta} = \beta\hat{\mathbf{y}}$, $\beta = \sin\theta$[Bourdier, 1980].

$$k'_y = \gamma[k_y - (\omega/c)\beta] = \gamma(\omega/c)(\sin\theta - \sin\theta) = 0,$$

$$k'_x = k_x = k\cos\theta = k/\gamma\,, \qquad \omega' = \gamma(\omega - k_y\beta) = \omega/\gamma,$$

$$E'_x = \gamma(E_x + \beta B_z) = \gamma E(\sin\theta - \sin\theta) = 0\,,\ E'_y = E_y\,,\ B'_z = B_z/\gamma.$$

Transformation of the electric force component normal to the surface:

$$F_x = -eE_x \rightarrow F'_x = -e(\mathbf{v}' \times \mathbf{B}')_x \simeq -ec\beta B'_z$$

An useful trick: the boosted frame

For planar geometry, the 2D problem of oblique incidence can be always reduced to a 1D problem of normal incidence by a Lorentz boost along the surface:$\boldsymbol{\beta} = \beta\hat{\mathbf{y}}$, $\beta = \sin\theta$[Bourdier, 1980].

$$k'_y = \gamma[k_y - (\omega/c)\beta] = \gamma(\omega/c)(\sin\theta - \sin\theta) = 0,$$
$$k'_x = k_x = k\cos\theta = k/\gamma\,, \qquad \omega' = \gamma(\omega - k_y\beta) = \omega/\gamma,$$
$$E'_x = \gamma(E_x + \beta B_z) = \gamma E(\sin\theta - \sin\theta) = 0\,,\ E'_y = E_y\,,\ B'_z = B_z/\gamma.$$

Transformation of the electric force component normal to the surface:

$$F_x = -eE_x \rightarrow F'_x = -e(\mathbf{v}' \times \mathbf{B}')_x \simeq -ec\beta B'_z$$

This technique is very convenient for analytical and numerical modelling.

Stage 2: collisional absorption and thermalization

Stage 2: collisional absorption and thermalization

As soon as ionization produces free electrons the laser pulse energy is absorbed by electron–ion (e–I) collisions (inverse bremsstrahlung) and thermalizes by e–e collisions.

Stage 2: collisional absorption and thermalization

As soon as ionization produces free electrons the laser pulse energy is absorbed by electron–ion (e–I) collisions (inverse bremsstrahlung) and thermalizes by e–e collisions.

Rule of thumb to derive collision frequency ν_c:

$$\sigma_c \approx \pi b^2;$$

Stage 2: collisional absorption and thermalization

As soon as ionization produces free electrons the laser pulse energy is absorbed by electron–ion (e–I) collisions (inverse bremsstrahlung) and thermalizes by e–e collisions.

Rule of thumb to derive collision frequency ν_c:

$$\sigma_c \approx \pi b^2; \qquad Z_1 Z_2 e^2/b \approx mv^2;$$

Stage 2: collisional absorption and thermalization

As soon as ionization produces free electrons the laser pulse energy is absorbed by electron–ion (e–I) collisions (inverse bremsstrahlung) and thermalizes by e–e collisions.

Rule of thumb to derive collision frequency ν_c:

$$\sigma_c \approx \pi b^2; \qquad Z_1 Z_2 e^2/b \approx m v^2; \qquad \nu_c = n \sigma_c v_e \approx \frac{4\pi n Z_1^2 Z_2^2 e^4}{m^2 v^3}$$

Stage 2: collisional absorption and thermalization

As soon as ionization produces free electrons the laser pulse energy is absorbed by electron–ion (e–I) collisions (inverse bremsstrahlung) and thermalizes by e–e collisions.

Rule of thumb to derive collision frequency ν_c:

$$\sigma_c \approx \pi b^2; \qquad Z_1 Z_2 e^2/b \approx mv^2; \qquad \nu_c = n\sigma_c v_e \approx \frac{4\pi n Z_1^2 Z_2^2 e^4}{m^2 v^3}$$

e–e: $Z_{1,2} = -1$, $n = n_e$, $m = m_e/2$;

Stage 2: collisional absorption and thermalization

As soon as ionization produces free electrons the laser pulse energy is absorbed by electron–ion (e–I) collisions (inverse bremsstrahlung) and thermalizes by e–e collisions.

Rule of thumb to derive collision frequency ν_c:

$$\sigma_c \approx \pi b^2; \qquad Z_1 Z_2 e^2/b \approx m v^2; \qquad \nu_c = n \sigma_c v_e \approx \frac{4\pi n Z_1^2 Z_2^2 e^4}{m^2 v^3}$$

e–e: $Z_{1,2} = -1$, $n = n_e$, $m = m_e/2$; e–I: $Z_1 = Z$, $Z_2 = -1$, $n = n_i$, $m = m_e$

Stage 2: collisional absorption and thermalization

As soon as ionization produces free electrons the laser pulse energy is absorbed by electron–ion (e–I) collisions (inverse bremsstrahlung) and thermalizes by e–e collisions.

Rule of thumb to derive collision frequency ν_c:

$$\sigma_c \approx \pi b^2; \qquad Z_1 Z_2 e^2/b \approx m v^2; \qquad \nu_c = n \sigma_c v_e \approx \frac{4\pi n Z_1^2 Z_2^2 e^4}{m^2 v^3}$$

e–e: $Z_{1,2} = -1$, $n = n_e$, $m = m_e/2$; e–I: $Z_1 = Z$, $Z_2 = -1$, $n = n_i$, $m = m_e$
Exact result: multiply by $\sqrt{6}\ln(b_{max}/b_{min})$.

Stage 2: collisional absorption and thermalization

As soon as ionization produces free electrons the laser pulse energy is absorbed by electron–ion (e–I) collisions (inverse bremsstrahlung) and thermalizes by e–e collisions.

Rule of thumb to derive collision frequency ν_c:

$$\sigma_c \approx \pi b^2; \qquad Z_1 Z_2 e^2/b \approx m v^2; \qquad \nu_c = n \sigma_c v_e \approx \frac{4\pi n Z_1^2 Z_2^2 e^4}{m^2 v^3}$$

e–e: $Z_{1,2} = -1$, $n = n_e$, $m = m_e/2$; e–I: $Z_1 = Z$, $Z_2 = -1$, $n = n_i$, $m = m_e$
Exact result: multiply by $\sqrt{6}\ln(b_{max}/b_{min})$.

Effective dielectric function becomes (Drude's model)

$$\epsilon(\omega) = 1 - \frac{\omega_p^2}{\omega(\omega + i\nu_c)}$$

Inverse Bremsstrahlung

Inverse Bremsstrahlung

The rate of IB absorption ν_{IB} is estimated by equating the absorbed laser power density to the oscillation ("quiver") energy density absorbed via collisions:

Inverse Bremsstrahlung

The rate of IB absorption ν_{IB} is estimated by equating the absorbed laser power density to the oscillation ("quiver") energy density absorbed via collisions:

$$\nu_{IB}\epsilon(\omega)\frac{E_L^2}{4\pi} \doteq \nu_{eI}\frac{m_e}{2}n_e v_{osc}^2 = \nu_{eI} m_e n_e \left(\frac{eE_L}{m_e\omega}\right)^2$$

Inverse Bremsstrahlung

The rate of IB absorption ν_{IB} is estimated by equating the absorbed laser power density to the oscillation ("quiver") energy density absorbed via collisions:

$$\nu_{IB}\epsilon(\omega)\frac{E_L^2}{4\pi} \doteq \nu_{eI}\frac{m_e}{2}n_e v_{osc}^2 = \nu_{eI}m_e n_e\left(\frac{eE_L}{m_e\omega}\right)^2$$

$$\nu_{IB} \approx \nu_{eI}\frac{n_e}{n_c}\left(1-\frac{n_e}{n_c}\right)^{-1/2} \qquad\qquad (n_e/n_c = \omega_p^2/\omega^2)$$

Inverse Bremsstrahlung

The rate of IB absorption ν_{IB} is estimated by equating the absorbed laser power density to the oscillation ("quiver") energy density absorbed via collisions:

$$\nu_{IB}\epsilon(\omega)\frac{E_L^2}{4\pi} \doteq \nu_{eI}\frac{m_e}{2}n_e v_{osc}^2 = \nu_{eI}m_e n_e\left(\frac{eE_L}{m_e\omega}\right)^2$$

$$\nu_{IB} \approx \nu_{eI}\frac{n_e}{n_c}\left(1-\frac{n_e}{n_c}\right)^{-1/2} \qquad\qquad (n_e/n_c = \omega_p^2/\omega^2)$$

If the absorbed energy does not thermalizes quickly, the distribution function is depleted of slow electrons

Inverse Bremsstrahlung

The rate of IB absorption ν_{IB} is estimated by equating the absorbed laser power density to the oscillation ("quiver") energy density absorbed via collisions:

$$\nu_{IB}\epsilon(\omega)\frac{E_L^2}{4\pi} \doteq \nu_{eI}\frac{m_e}{2}n_e v_{osc}^2 = \nu_{eI}m_e n_e\left(\frac{eE_L}{m_e\omega}\right)^2$$

$$\nu_{IB} \approx \nu_{eI}\frac{n_e}{n_c}\left(1-\frac{n_e}{n_c}\right)^{-1/2} \qquad (n_e/n_c = \omega_p^2/\omega^2)$$

If the absorbed energy does not thermalizes quickly, the distribution function is depleted of slow electrons$\longrightarrow$ kinetic saturation of IB absorption

Inverse Bremsstrahlung

The rate of IB absorption ν_{IB} is estimated by equating the absorbed laser power density to the oscillation ("quiver") energy density absorbed via collisions:

$$\nu_{IB}\epsilon(\omega)\frac{E_L^2}{4\pi} \doteq \nu_{eI}\frac{m_e}{2}n_e v_{osc}^2 = \nu_{eI}m_e n_e\left(\frac{eE_L}{m_e\omega}\right)^2$$

$$\nu_{IB} \approx \nu_{eI}\frac{n_e}{n_c}\left(1-\frac{n_e}{n_c}\right)^{-1/2} \qquad (n_e/n_c = \omega_p^2/\omega^2)$$

If the absorbed energy does not thermalizes quickly, the distribution function is depleted of slow electrons$\longrightarrow$ kinetic saturation of IB absorption (Langdon effect, 1980).

Scaling laws for electron temperature

Scaling laws for electron temperature

Assuming isochoric heating, complete thermalization and diffusive transport, scaling laws for T_e and L_{th} (ablation depth) are found:

$$n_e \partial_t T_e = -\boldsymbol{\nabla} \cdot (\kappa \nabla T_e), \qquad \kappa = \frac{n_e T_e}{m_e \nu_{eI}}, \qquad \nu_{eI} = \frac{Z n_e e^4 \ln \Lambda}{m_e^{1/2} T_e^{3/2}}$$

Scaling laws for electron temperature

Assuming isochoric heating, complete thermalization and diffusive transport, scaling laws for T_e and L_{th} (ablation depth) are found:

$$n_e \partial_t T_e = -\boldsymbol{\nabla} \cdot (\kappa \nabla T_e), \qquad \kappa = \frac{n_e T_e}{m_e \nu_{eI}}, \quad \nu_{eI} = \frac{Z n_e e^4 \ln \Lambda}{m_e^{1/2} T_e^{3/2}}$$

$$\nabla \sim L_{th}^{-1}, \qquad \partial_t \sim t^{-1} \qquad ; I_{abs} t \approx n_e T_e L_{th} \text{ (energy balance)}$$

Scaling laws for electron temperature

Assuming isochoric heating, complete thermalization and diffusive transport, scaling laws for T_e and L_{th} (ablation depth) are found:

$$n_e \partial_t T_e = -\boldsymbol{\nabla} \cdot (\kappa \nabla T_e), \qquad \kappa = \frac{n_e T_e}{m_e \nu_{eI}}, \qquad \nu_{eI} = \frac{Z n_e e^4 \ln \Lambda}{m_e^{1/2} T_e^{3/2}}$$

$$\nabla \sim L_{th}^{-1}, \qquad \partial_t \sim t^{-1} \qquad ; I_{abs} t \approx n_e T_e L_{th} \text{ (energy balance)}$$

$$\begin{aligned} T_e &\approx C^{2/9} Z^{2/9} n_e^{-2/9} I_{abs}^{4/9} t^{2/9} = 1.5 Z^{2/9} n_{e,23}^{-2/9} I_{abs,16}^{4/9} t_{10}^{2/9} \text{ keV}, \\ L_{th} &\approx C^{-2/9} Z^{-2/9} n_e^{-7/9} I_{abs}^{5/9} t^{7/9} = 4 \times 10^{-2} Z^{-2/9} n_{e,23}^{-7/9} I_{abs,16}^{5/9} t_{10}^{7/9} \ \mu\text{m}. \end{aligned}$$

$(C = [m_e^{1/2} e^4 \ln \Lambda])$.

Scaling laws for electron temperature

Assuming isochoric heating, complete thermalization and diffusive transport, scaling laws for T_e and L_{th} (ablation depth) are found:

$$n_e \partial_t T_e = -\boldsymbol{\nabla} \cdot (\kappa \nabla T_e), \qquad \kappa = \frac{n_e T_e}{m_e \nu_{eI}}, \qquad \nu_{eI} = \frac{Z n_e e^4 \ln \Lambda}{m_e^{1/2} T_e^{3/2}}$$

$$\nabla \sim L_{th}^{-1}, \qquad \partial_t \sim t^{-1} \qquad ; I_{abs} t \approx n_e T_e L_{th} \text{ (energy balance)}$$

$$\begin{aligned} T_e &\approx C^{2/9} Z^{2/9} n_e^{-2/9} I_{abs}^{4/9} t^{2/9} = 1.5 Z^{2/9} n_{e,23}^{-2/9} I_{abs,16}^{4/9} t_{10}^{2/9} \text{ keV}, \\ L_{th} &\approx C^{-2/9} Z^{-2/9} n_e^{-7/9} I_{abs}^{5/9} t^{7/9} = 4 \times 10^{-2} Z^{-2/9} n_{e,23}^{-7/9} I_{abs,16}^{5/9} t_{10}^{7/9} \ \mu\text{m}. \end{aligned}$$

$(C = [m_e^{1/2} e^4 \ln \Lambda])$.

Stage 3: collisionless absorption

Stage 3: collisionless absorption

The collision frequency and the IB rate drop with increasing T_e and/or laser intensity I_L (runaway effect):

Stage 3: collisionless absorption

The collision frequency and the IB rate drop with increasing T_e and/or laser intensity I_L (runaway effect):

$$\nu_{eI} \sim v_e^{-3} \quad ; \quad v_e \approx \mathsf{max}(v_{th}, v_{osc}) \quad ; \quad v_{th} \sim T_e^{1/2} \quad ; \quad v_{osc} \sim (I_L \lambda_L^2)^{1/2}$$

Stage 3: collisionless absorption

The collision frequency and the IB rate drop with increasing T_e and/or laser intensity I_L (runaway effect):

$$\nu_{eI} \sim v_e^{-3} \quad ; \quad v_e \approx \mathsf{max}(v_{th}, v_{osc}) \quad ; \quad v_{th} \sim T_e^{1/2} \quad ; \quad v_{osc} \sim (I_L \lambda_L^2)^{1/2}$$

$\Rightarrow$ at high irradiances absorption is dominated by collisionless processes.

Stage 3: collisionless absorption

The collision frequency and the IB rate drop with increasing T_e and/or laser intensity I_L (runaway effect):

$$\nu_{eI} \sim v_e^{-3} \quad ; \quad v_e \approx \max(v_{th}, v_{osc}) \quad ; \quad v_{th} \sim T_e^{1/2} \quad ; \quad v_{osc} \sim (I_L \lambda_L^2)^{1/2}$$

$\Rightarrow$ at high irradiances absorption is dominated by collisionless processes.

Weak absorption dependence on target material
[Price et al, PRL **75**, 252 (1995)].

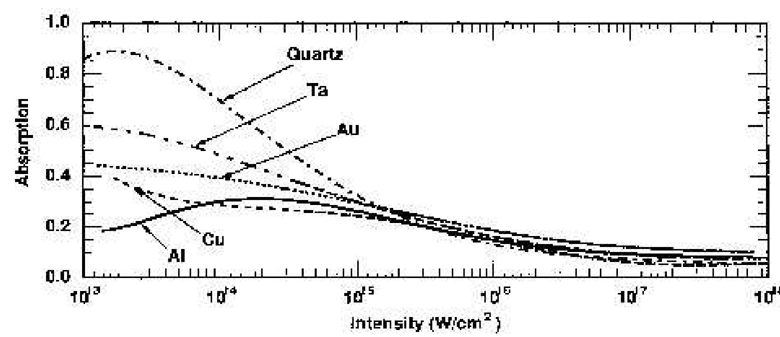

FIG. 1. Absorption fraction vs peak laser intensity for aluminum, copper, gold, tantalum, and quartz targets. In Figs. 1, 3, 4, and 5 laser intensity is the temporal and spatial peak value of the laser intensity.

Where does absorption come from?

Where does absorption come from?

Poynting's theorem $\Rightarrow$ the net energy absorption per unit volume and per cycle is given by $\langle \mathbf{J} \cdot \mathbf{E} \rangle$

Where does absorption come from?

Poynting's theorem $\Rightarrow$ the net energy absorption per unit volume and per cycle is given by $\langle \mathbf{J} \cdot \mathbf{E} \rangle \Rightarrow$ the phase shift between $\mathbf{J}$ and $\mathbf{E}$ must be $\neq \pi/2$.

Where does absorption come from?

Poynting's theorem $\Rightarrow$ the net energy absorption per unit volume and per cycle is given by $\langle \mathbf{J} \cdot \mathbf{E} \rangle \Rightarrow$ the phase shift between $\mathbf{J}$ and $\mathbf{E}$ must be $\neq \pi/2$.

For an ideal, "fluid" plasma $\mathbf{J} = i\omega_p^2/\omega \mathbf{E} \Rightarrow \langle \mathbf{J} \cdot \mathbf{E} \rangle = 0$.

In the absence of collisions, absorption can be due only to:

Where does absorption come from?

Poynting's theorem $\Rightarrow$ the net energy absorption per unit volume and per cycle is given by $\langle \mathbf{J} \cdot \mathbf{E} \rangle \Rightarrow$ the phase shift between $\mathbf{J}$ and $\mathbf{E}$ must be $\neq \pi/2$.

For an ideal, "fluid" plasma $\mathbf{J} = i\omega_p^2/\omega \mathbf{E} \Rightarrow \langle \mathbf{J} \cdot \mathbf{E} \rangle = 0$.

In the absence of collisions, absorption can be due only to:

- mode conversion (i.e. linear or nonlinear excitation of waves)

Where does absorption come from?

Poynting's theorem $\Rightarrow$ the net energy absorption per unit volume and per cycle is given by $\langle \mathbf{J} \cdot \mathbf{E} \rangle \Rightarrow$ the phase shift between $\mathbf{J}$ and $\mathbf{E}$ must be $\neq \pi/2$.

For an ideal, "fluid" plasma $\mathbf{J} = i\omega_p^2/\omega \mathbf{E} \Rightarrow \langle \mathbf{J} \cdot \mathbf{E} \rangle = 0$.

In the absence of collisions, absorption can be due only to:

- mode conversion (i.e. linear or nonlinear excitation of waves)

- kinetic effects (the distribution function is modified leading to a different phase between $\mathbf{J}$ and $\mathbf{E}$.

Some general relations

Some general relations

Poynting's theorem in 1D yields (neglecting field generation)

$$\partial_x S + J_x E_x + J_y E_y = 0$$

Some general relations

Poynting's theorem in 1D yields (neglecting field generation)

$$\partial_x S + J_x E_x + J_y E_y = 0$$

From $4\pi J_x + \partial_t E_x = 0$ one obtains $J_x E_x = -\partial_t E_x^2/8\pi$.

Some general relations

Poynting's theorem in 1D yields (neglecting field generation)

$$\partial_x S + J_x E_x + J_y E_y = 0$$

From $4\pi J_x + \partial_t E_x = 0$ one obtains $J_x E_x = -\partial_t E_x^2 / 8\pi$.

For periodic, steady–state fields $\langle J_x E_x \rangle = 0$.

Some general relations

Poynting's theorem in 1D yields (neglecting field generation)

$$\partial_x S + J_x E_x + J_y E_y = 0$$

From $4\pi J_x + \partial_t E_x = 0$ one obtains $J_x E_x = -\partial_t E_x^2/8\pi$.

For periodic, steady–state fields $\langle J_x E_x \rangle = 0$.

All steady–state absorption in 1D comes from $\langle J_y E_y \rangle$.

Some general relations

Poynting's theorem in 1D yields (neglecting field generation)

$$\partial_x S + J_x E_x + J_y E_y = 0$$

From $4\pi J_x + \partial_t E_x = 0$ one obtains $J_x E_x = -\partial_t E_x^2/8\pi$.

For periodic, steady–state fields $\langle J_x E_x \rangle = 0$.

All steady–state absorption in 1D comes from $\langle J_y E_y \rangle$.

This constraint may be however violated: non–steady state effects, aperiodic motion, 2D effects,. . .

What is the absorption mechanism?

What is the absorption mechanism?

The solution of the Vlasov-Maxwell system should in principle contain all effects leading to absorption.

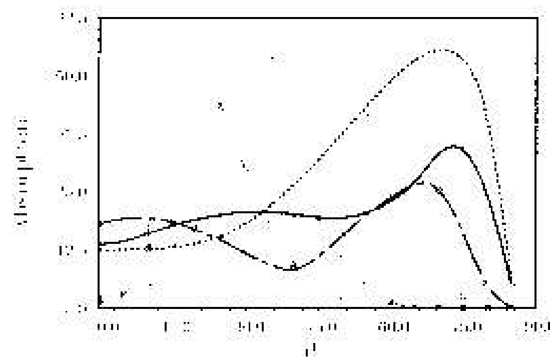

Fig. 6. Absorption versus angle of incidence. The parameters common to the bold curves are T_e = 10 keV, n/n_c = 25; the other parameters for theses curves are $I\lambda^2 = 10^{15}$ W cm^{-2} μm^2, L/λ = 0.023 (solid); $I\lambda^2 = 10^{18}$ W cm^{-2} μm^2, L/λ = 0.046 (chained dashed); $I\lambda^2 = 10^{[illegible]}$ W cm^{-2} μm^2, L/λ = 0.023 (dashed). The parameters common to the rest of the lines are T_e = 10 keV, n/n_e = 2; the remaining parameters are $I\lambda^2 = 10^{18}$ W cm^{-2} μm^2, L/λ = 0.15 (solid); $I\lambda^2 = 10^{16}$ W cm^{-2} μm^2, L/λ = 0.15 (chained-dashed); $I\lambda^2 = 10^{15}$ W cm^{-2} μm^2, L/λ = 1.25 (dashed).

What is the absorption mechanism?

The solution of the Vlasov-Maxwell system should in principle contain all effects leading to absorption.

Vlasov simulations (1D)

[Ruhl & Mulser, Phys. Lett. A **205** (1995) 388].

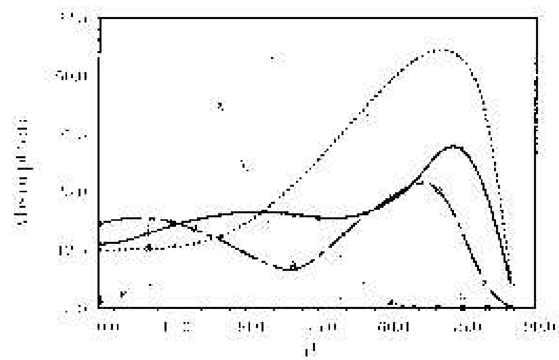

Fig. 6. Absorption versus angle of incidence. The parameters common to the bold curves are $T_e = 10$ keV, $n/n_c = 25$; the other parameters for these curves are $I\lambda^2 = 10^{19}$ W cm^{-2} μm^2, $L/\lambda = 0.023$ (solid); $I\lambda^2 = 10^{18}$ W cm^{-2} μm^2, $L/\lambda = 0.046$ (chained dashed); $I\lambda^2 = 10^{17}$ W cm^{-2} μm^2, $L/\lambda = 0.023$ (dashed). The parameters common to the rest of the lines are $T_e = 10$ keV, $n/n_c = 2$; the remaining parameters are $I\lambda^2 = 10^{18}$ W cm^{-2} μm^2, $L/\lambda = 0.15$ (solid); $I\lambda^2 = 10^{16}$ W cm^{-2} μm^2, $L/\lambda = 0.15$ (chained-dashed); $I\lambda^2 = 10^{16}$ W cm^{-2} μm^2, $L/\lambda = 1.25$ (dashed).

What is the absorption mechanism?

The solution of the Vlasov-Maxwell system should in principle contain all effects leading to absorption.

Vlasov simulations (1D)

[Ruhl & Mulser, Phys. Lett. A **205** (1995) 388].

Absorption scaling with laser and target parameters (e.g. I_L, n_e, $L = n_e/|\boldsymbol{\nabla} n_e|$, incidence angle θ, . . .) is complex due to the overlap and competition of several processes,

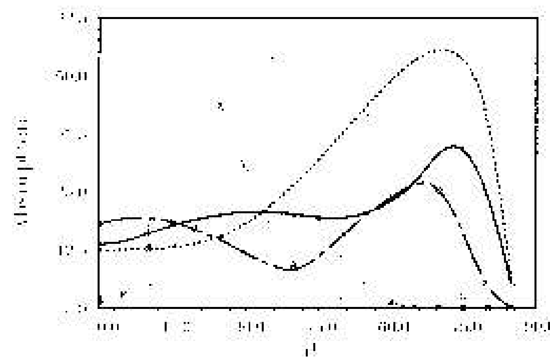

Fig. 6. Absorption versus angle of incidence. The parameters common to the bold curves are T_e = 10 keV, n/n_c = 25; the other parameters for theses curves are $I\lambda^2 = 10^{15}$ W cm^{-2} μm^2, L/λ = 0.023 (solid); $I\lambda^2 = 10^{18}$ W cm^{-2} μm^2, L/λ = 0.046 (chained dashed); $I\lambda^2 = 10^{17}$ W cm^{-2} μm^2, L/λ = 0.023 (dashed). The parameters common to the rest of the lines are T_e = 10 keV, n/n_c = 2; the remaining parameters are $I\lambda^2 = 10^{18}$ W cm^{-2} μm^2, L/λ = 0.15 (solid); $I\lambda^2 = 10^{16}$ W cm^{-2} μm^2, L/λ = 0.15 (chained-dashed); $I\lambda^2 = 10^{16}$ W cm^{-2} μm^2, L/λ = 1.25 (dashed).

What is the absorption mechanism?

The solution of the Vlasov-Maxwell system should in principle contain all effects leading to absorption.

Vlasov simulations (1D)

[Ruhl & Mulser, Phys. Lett. A **205** (1995) 388].

Absorption scaling with laser and target parameters (e.g. I_L, n_e, $L = n_e/|\nabla n_e|$, incidence angle θ, . . .) is complex due to the overlap and competition of several processes,e.g.:

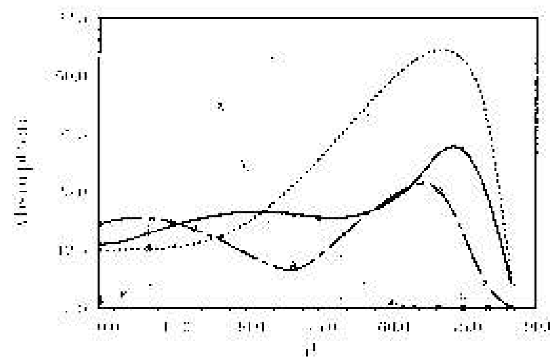

Fig. 6. Absorption versus angle of incidence. The parameters common to the bold curves are T_e = 10 keV, n/n_c = 25; the other parameters for these curves are $I\lambda^2 = 10^{15}$ W cm^{-2} μm^2, $L/\lambda = 0.023$ (solid); $I\lambda^2 = 10^{18}$ W cm^{-2} μm^2, $L/\lambda = 0.046$ (chained dashed); $I\lambda^2 = 10^{17}$ W cm^{-2} μm^2, $L/\lambda = 0.023$ (dashed). The parameters common to the rest of the lines are T_e = 10 keV, n/n_c = 2; the remaining parameters are $I\lambda^2 = 10^{18}$ W cm^{-2} μm^2, $L/\lambda = 0.15$ (solid); $I\lambda^2 = 10^{16}$ W cm^{-2} μm^2, $L/\lambda = 0.15$ (chained-dashed); $I\lambda^2 = 10^{16}$ W cm^{-2} μm^2, $L/\lambda = 1.25$ (dashed).

- resonance absorption

What is the absorption mechanism?

The solution of the Vlasov-Maxwell system should in principle contain all effects leading to absorption.

Vlasov simulations (1D)

[Ruhl & Mulser, Phys. Lett. A **205** (1995) 388].

Absorption scaling with laser and target parameters (e.g. I_L, n_e, $L = n_e/|\boldsymbol{\nabla} n_e|$, incidence angle θ, . . .) is complex due to the overlap and competition of several processes,e.g.:

- resonance absorption
- anomalous skin effect

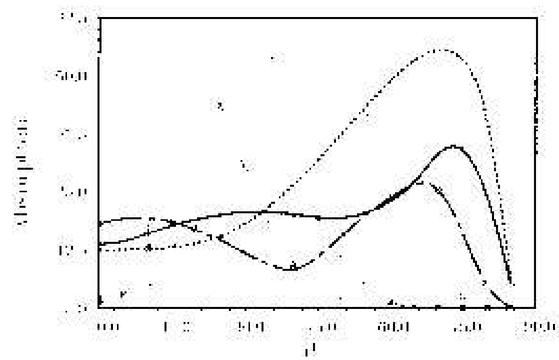

Fig. 6. Absorption versus angle of incidence. The parameters common to the bold curves are T_e = 10 keV, n/n_c = 25; the other parameters for theses curves are $I\lambda^2 = 10^{18}$ W cm^{-2} μm^2, L/λ = 0.023 (solid); $I\lambda^2 = 10^{18}$ W cm^{-2} μm^2, L/λ = 0.046 (chained dashed); $I\lambda^2 = 10^{17}$ W cm^{-2} μm^2, L/λ = 0.023 (dashed). The parameters common to the rest of the lines are T_e = 10 keV, n/n_c = 2; the remaining parameters are $I\lambda^2 = 10^{18}$ W cm^{-2} μm^2, L/λ = 0.15 (solid); $I\lambda^2 = 10^{16}$ W cm^{-2} μm^2, L/λ = 0.15 (chained-dashed); $I\lambda^2 = 10^{15}$ W cm^{-2} μm^2, L/λ = 1.25 (dashed).

What is the absorption mechanism?

The solution of the Vlasov-Maxwell system should in principle contain all effects leading to absorption.

Vlasov simulations (1D)

[Ruhl & Mulser, Phys. Lett. A **205** (1995) 388].

Absorption scaling with laser and target parameters (e.g. I_L, n_e, $L = n_e/|\boldsymbol{\nabla} n_e|$, incidence angle θ, . . .) is complex due to the overlap and competition of several processes,e.g.:

- resonance absorption
- anomalous skin effect
- vacuum heating

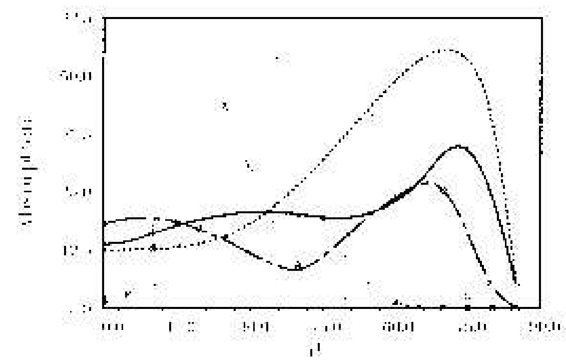

Fig. 6. Absorption versus angle of incidence. The parameters common to the bold curves are T_e = 10 keV, n/n_c = 25; the other parameters for theses curves are $I\lambda^2 = 10^{18}$ W cm^{-2} μm^2, L/λ = 0.023 (solid); $I\lambda^2 = 10^{18}$ W cm^{-2} μm^2, L/λ = 0.046 (chained dashed); $I\lambda^2 = 10^{17}$ W cm^{-2} μm^2, L/λ = 0.023 (dashed). The parameters common to the rest of the lines are T_e = 10 keV, n/n_c = 2; the remaining parameters are $I\lambda^2 = 10^{18}$ W cm^{-2} μm^2, L/λ = 0.15 (solid); $I\lambda^2 = 10^{16}$ W cm^{-2} μm^2, L/λ = 0.15 (chained-dashed); $I\lambda^2 = 10^{15}$ W cm^{-2} μm^2, L/λ = 1.25 (dashed).

What is the absorption mechanism?

The solution of the Vlasov-Maxwell system should in principle contain all effects leading to absorption.

Vlasov simulations (1D)

[Ruhl & Mulser, Phys. Lett. A **205** (1995) 388].

Absorption scaling with laser and target parameters (e.g. I_L, n_e, $L = n_e/|\boldsymbol{\nabla} n_e|$, incidence angle θ, . . .) is complex due to the overlap and competition of several processes,e.g.:

- resonance absorption
- anomalous skin effect
- vacuum heating . . . *and more*. . .

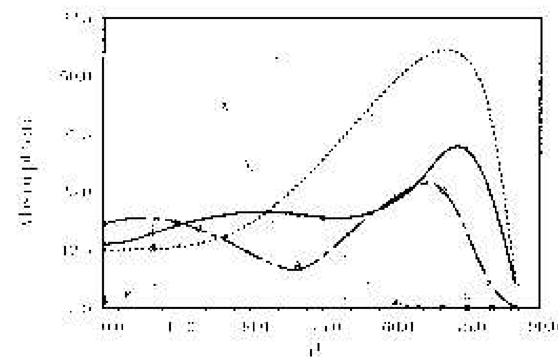

Fig. 6. Absorption versus angle of incidence. The parameters common to the bold curves are T_e = 10 keV, n/n_c = 25; the other parameters for theses curves are $I\lambda^2 = 10^{18}$ W cm^{-2} μm^2, $L/\lambda = 0.023$ (solid); $I\lambda^2 = 10^{18}$ W cm^{-2} μm^2, $L/\lambda = 0.046$ (chained dashed); $I\lambda^2 = 10^{[illegible]}$ W cm^{-2} μm^2, $L/\lambda = 0.023$ (dashed). The parameters common to the rest of the lines are T_e = 10 keV, n/n_c = 2; the remaining parameters are $I\lambda^2 = 10^{18}$ W cm^{-2} μm^2, $L/\lambda = 0.15$ (solid); $I\lambda^2 = 10^{16}$ W cm^{-2} μm^2, $L/\lambda = 0.15$ (chained-dashed); $I\lambda^2 = 10^{[illegible]}$ W cm^{-2} μm^2, $L/\lambda = 1.25$ (dashed).

Schematic of 1D mechanisms

Schematic of 1D mechanisms

Resonance absorption: collective plasma oscillation excited where $\omega = \omega_p$

Schematic of 1D mechanisms

Resonance absorption: collective plasma oscillation excited where $\omega = \omega_p$

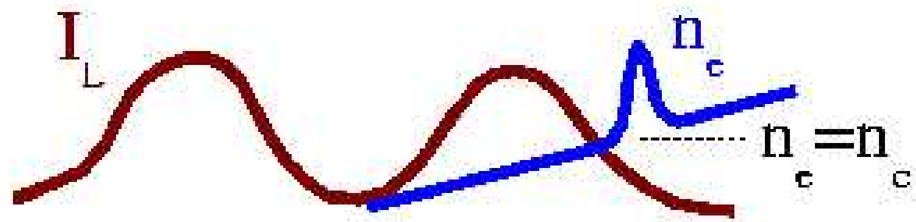

Schematic of 1D mechanisms

Resonance absorption: collective plasma oscillation excited where $\omega = \omega_p$

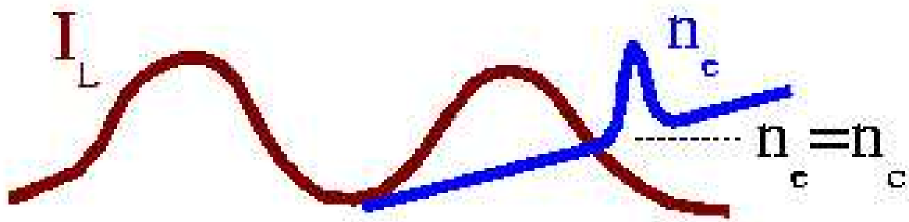

Anomalous skin effect: electrons "collide" with the plasma boundary and move non–adiabatically into the evanescent field

Schematic of 1D mechanisms

Resonance absorption: collective plasma oscillation excited where $\omega = \omega_p$

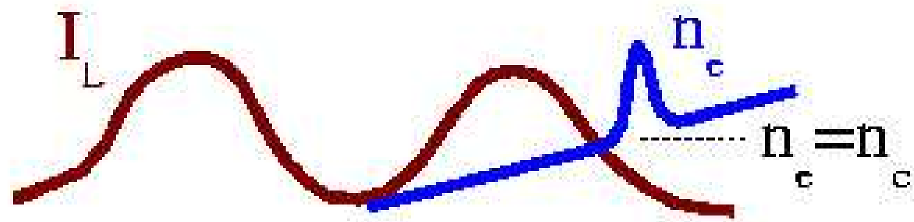

Anomalous skin effect: electrons "collide" with the plasma boundary and move non–adiabatically into the evanescent field

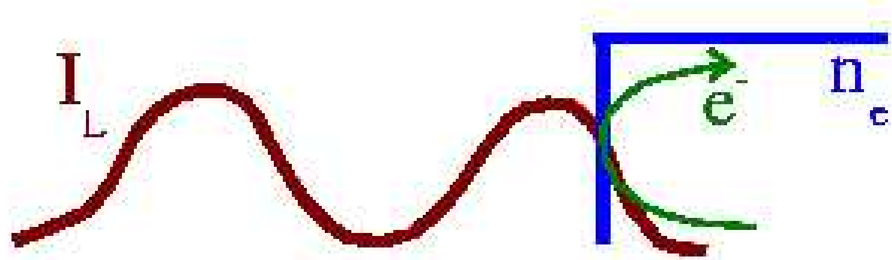

Schematic of 1D mechanisms

Resonance absorption: collective plasma oscillation excited where $\omega = \omega_p$

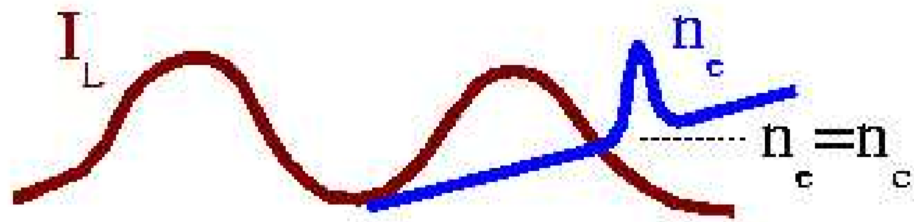

Anomalous skin effect: electrons “collide” with the plasma boundary and move non–adiabatically into the evanescent field

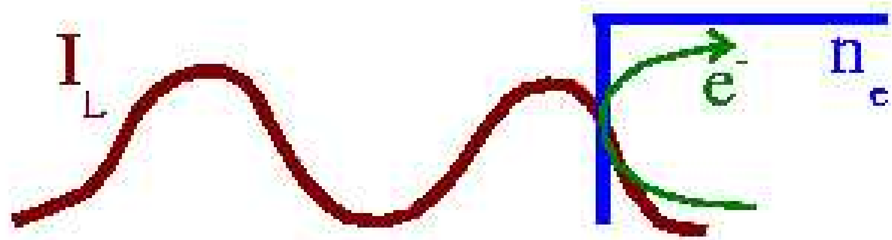

Vacuum heating: electrons cross the plasma boundary and return with high velocity

Schematic of 1D mechanisms

Resonance absorption: collective plasma oscillation excited where $\omega = \omega_p$

Anomalous skin effect: electrons “collide” with the plasma boundary and move non–adiabatically into the evanescent field

Vacuum heating: electrons cross the plasma boundary and return with high velocity

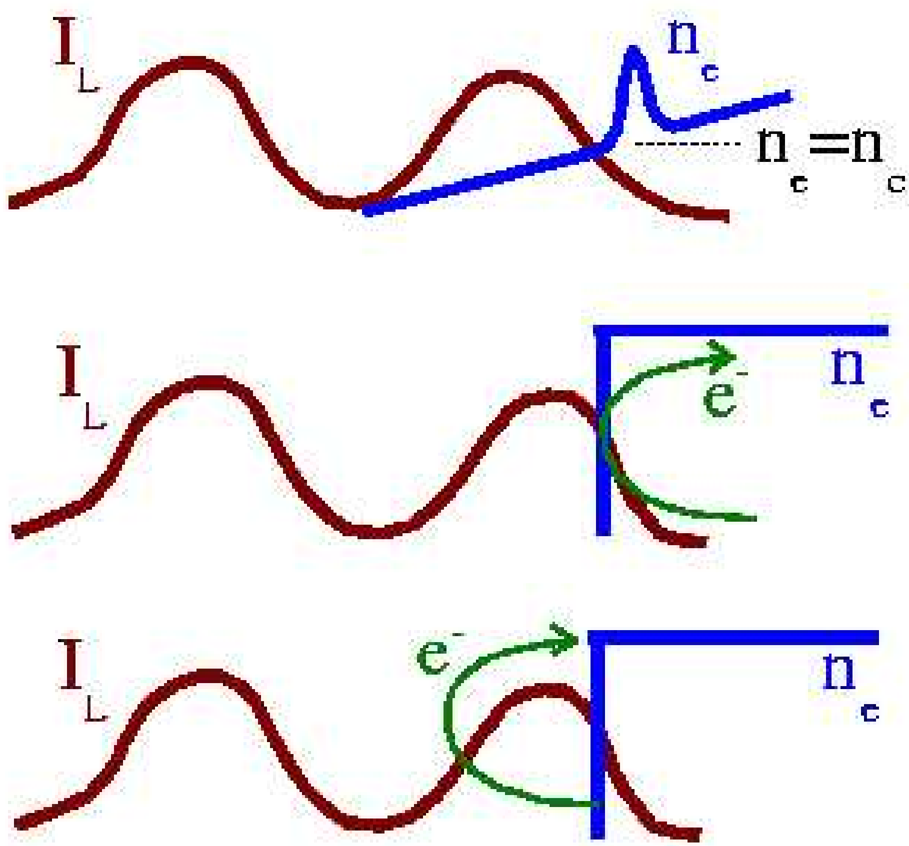

Schematic of 1D mechanisms

Resonance absorption: collective plasma oscillation excited where $\omega = \omega_p$

Anomalous skin effect: electrons "collide" with the plasma boundary and move non–adiabatically into the evanescent field

Vacuum heating: electrons cross the plasma boundary and return with high velocity

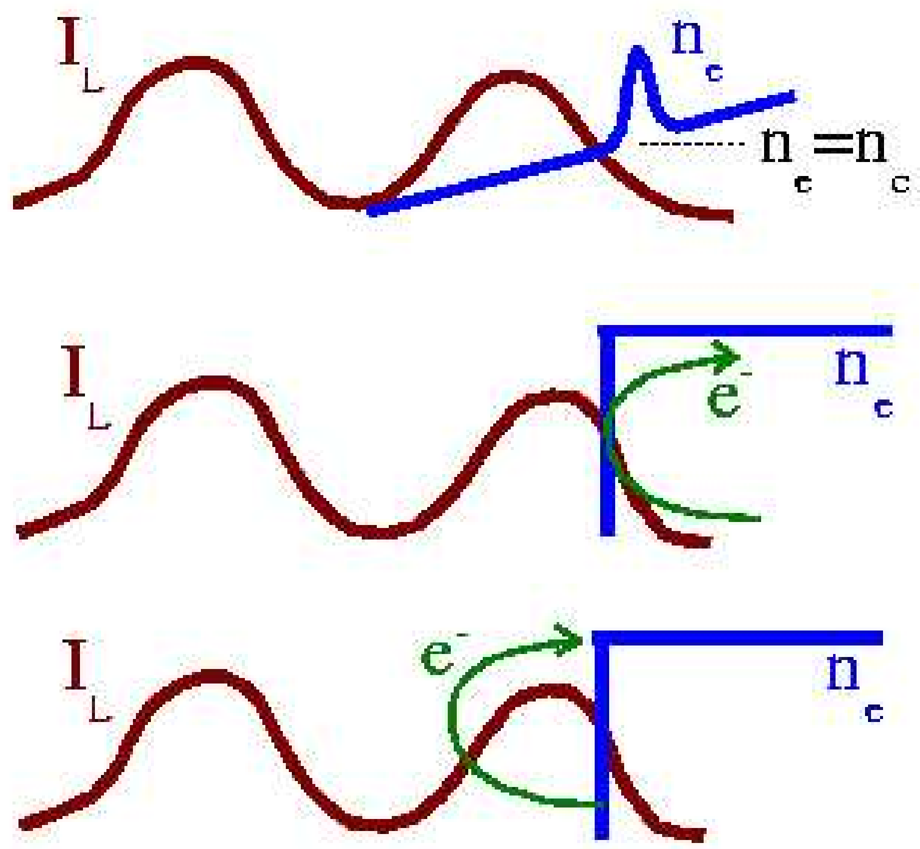

Resonance absorption

Resonance absorption

It is the mode conversion of the incident EM wave (the laser pulse) into a plasma wave of the same frequency ($\omega_p = \omega_L$).

Resonance absorption

It is the mode conversion of the incident EM wave (the laser pulse) into a plasma wave of the same frequency ($\omega_p = \omega_L$).

Linearized 1D Poisson–Euler system with external field $\mathbf{E}_d$ ("capacitor" model):

$$\begin{aligned}
\nabla \cdot \mathbf{E} &= -4\pi e(n_e - n_0) \equiv -4\pi e \delta n_e, \\
\partial_t \delta n_e &= -\nabla \cdot (n_e \mathbf{v}) \simeq -n_0 \nabla \cdot \mathbf{v} - \mathbf{v} \cdot \nabla n_0, \\
m_e(\partial_t - \mathbf{v} \cdot \nabla)\mathbf{v} &\simeq m_e \partial_t \mathbf{v} = -e(\mathbf{E} + \mathbf{E}_d).
\end{aligned}$$

Resonance absorption

It is the mode conversion of the incident EM wave (the laser pulse) into a plasma wave of the same frequency ($\omega_p = \omega_L$).

Linearized 1D Poisson–Euler system with external field $\mathbf{E}_d$ ("capacitor" model):

$$\begin{aligned}
\nabla \cdot \mathbf{E} &= -4\pi e(n_e - n_0) \equiv -4\pi e \delta n_e, \\
\partial_t \delta n_e &= -\nabla \cdot (n_e \mathbf{v}) \simeq -n_0 \nabla \cdot \mathbf{v} - \mathbf{v} \cdot \nabla n_0, \\
m_e(\partial_t - \mathbf{v} \cdot \nabla)\mathbf{v} &\simeq m_e \partial_t \mathbf{v} = -e(\mathbf{E} + \mathbf{E}_d). \\
\delta n_e &= \frac{1}{4\pi e} \frac{\boldsymbol{\nabla} n_0 \cdot (\mathbf{E} + \mathbf{E}_d)}{n_0 - n_c} \qquad (n_c = \omega^2/4\pi e^2).
\end{aligned}$$

Resonance at $n_e = n_c$ (requires: $\boldsymbol{\nabla} n_0 \cdot \mathbf{E}_d \neq 0$).

Resonance absorption

It is the mode conversion of the incident EM wave (the laser pulse) into a plasma wave of the same frequency ($\omega_p = \omega_L$).

Linearized 1D Poisson–Euler system with external field $\mathbf{E}_d$ ("capacitor" model):

$$\begin{aligned}
\nabla \cdot \mathbf{E} &= -4\pi e(n_e - n_0) \equiv -4\pi e \delta n_e, \\
\partial_t \delta n_e &= -\nabla \cdot (n_e \mathbf{v}) \simeq -n_0 \nabla \cdot \mathbf{v} - \mathbf{v} \cdot \nabla n_0, \\
m_e(\partial_t - \mathbf{v} \cdot \nabla)\mathbf{v} &\simeq m_e \partial_t \mathbf{v} = -e(\mathbf{E} + \mathbf{E}_d). \\
\delta n_e &= \frac{1}{4\pi e} \frac{\boldsymbol{\nabla} n_0 \cdot (\mathbf{E} + \mathbf{E}_d)}{n_0 - n_c} \qquad (n_c = \omega^2 / 4\pi e^2).
\end{aligned}$$

Resonance at $n_e = n_c$ (requires: $\boldsymbol{\nabla} n_0 \cdot \mathbf{E}_d \neq 0$).

Schematic of resonance absorption

Schematic of resonance absorption

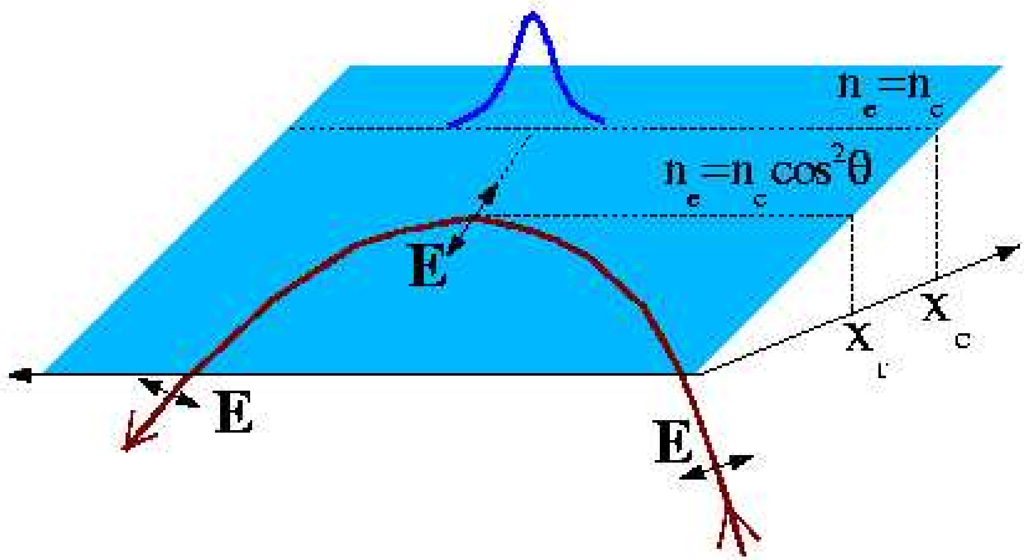

Schematic of resonance absorption

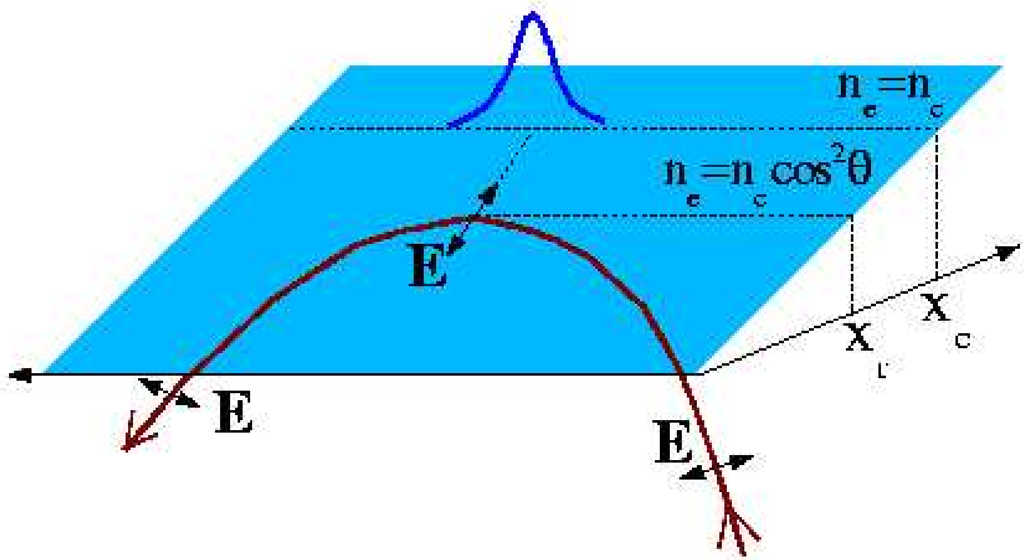

Adapted from C. E. Max (Les Houches lectures, 1980)

Schematic of resonance absorption

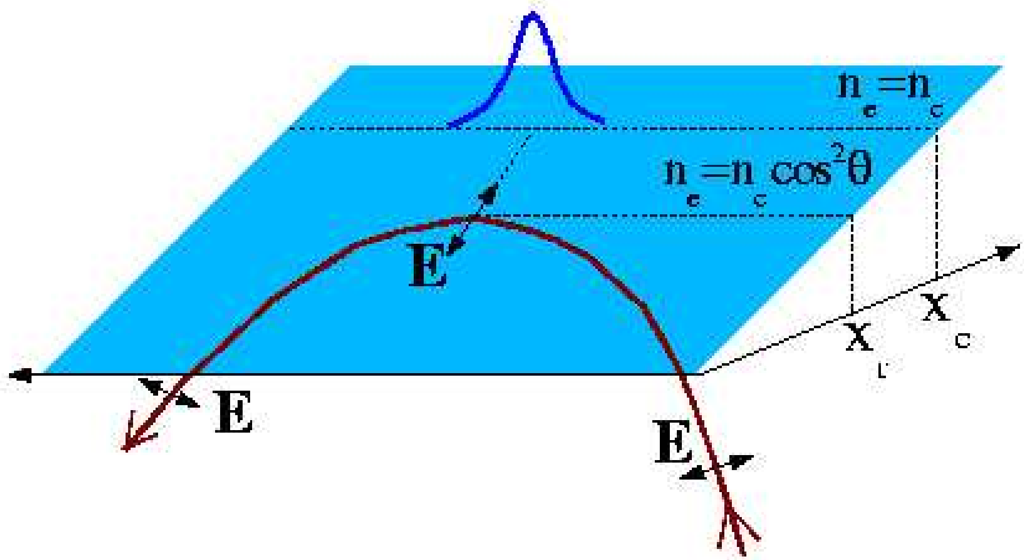

Adapted from C. E. Max (Les Houches lectures, 1980)

Oblique incidence, p–polarization, and "gentle" gradients, i.e. $L \gg (\lambda\, ,\, v_{osc})$, are required.

Schematic of resonance absorption

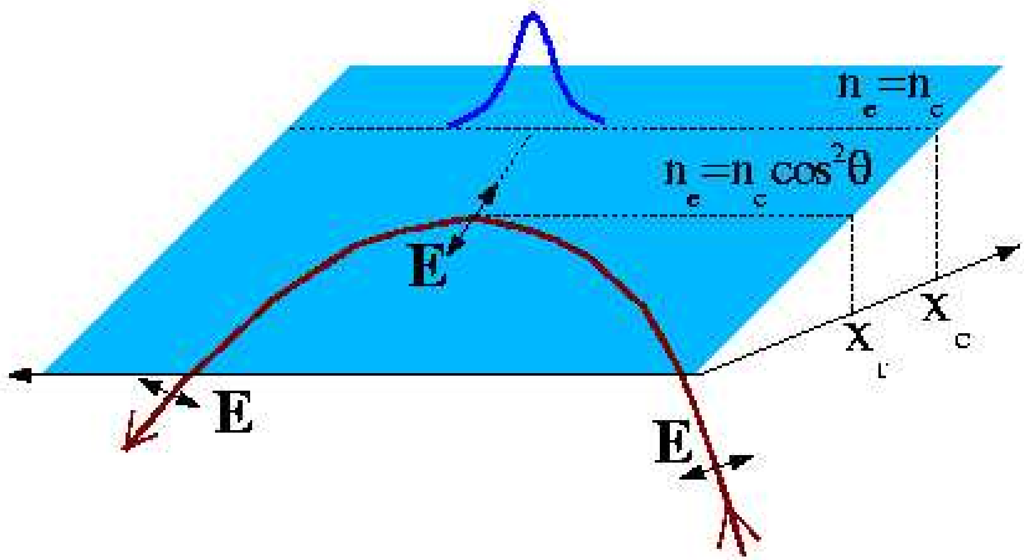

Adapted from C. E. Max (Les Houches lectures, 1980)

Oblique incidence, p–polarization, and "gentle" gradients, i.e. $L \gg (\lambda\,,\,v_{osc})$, are required.
The laser field is evanescent at $x = x_c$

Schematic of resonance absorption

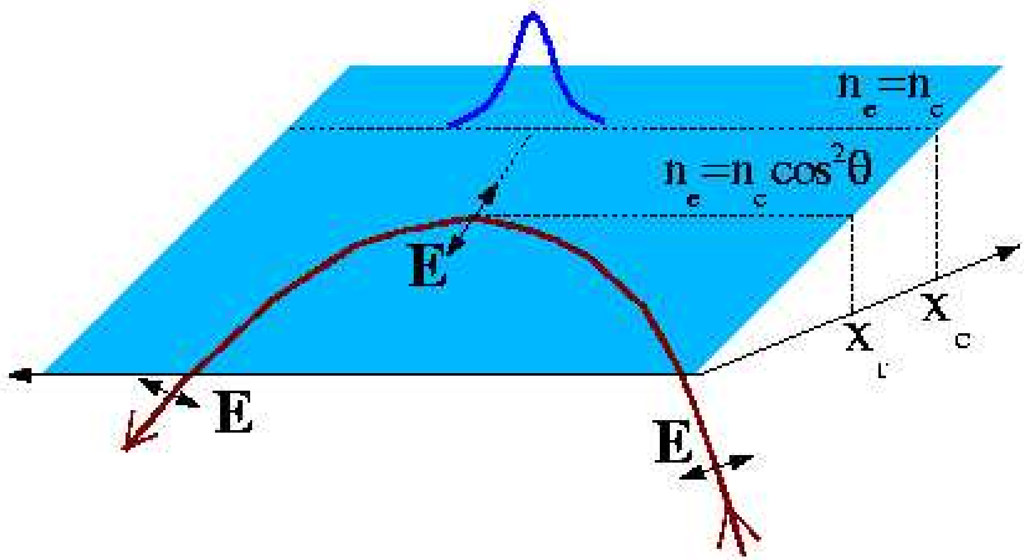

Adapted from C. E. Max (Les Houches lectures, 1980)

Oblique incidence, p–polarization, and "gentle" gradients, i.e. $L \gg (\lambda\,,\,v_{osc})$, are required.
The laser field is evanescent at $x = x_c \Rightarrow$ optimal absorption angle depends on density gradient L:

Schematic of resonance absorption

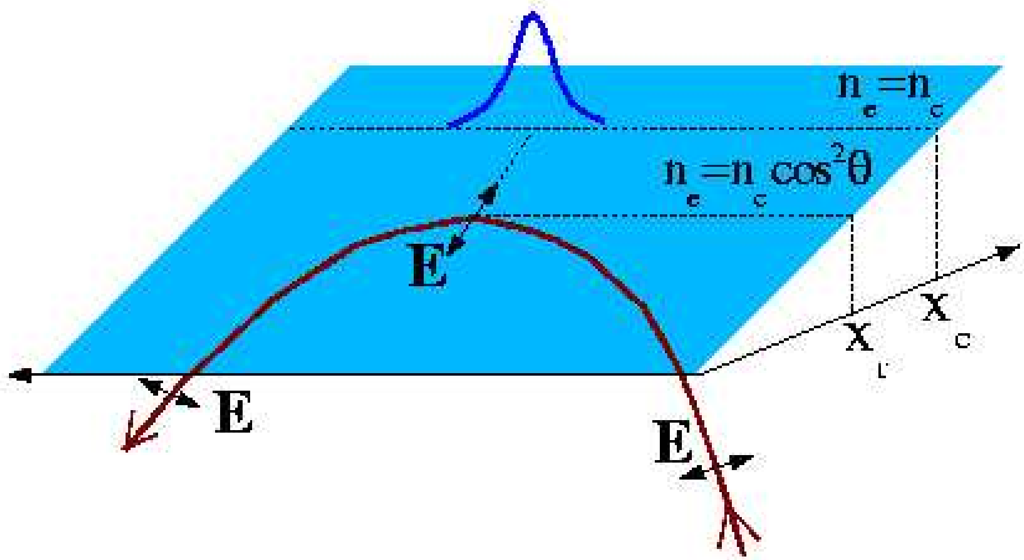

Adapted from C. E. Max (Les Houches lectures, 1980)

Oblique incidence, p–polarization, and "gentle" gradients, i.e. $L \gg (\lambda\,,\, v_{osc})$, are required.
The laser field is evanescent at $x = x_c \Rightarrow$ optimal absorption angle depends on density gradient L: $\sin\theta_o \simeq 0.8(c/\omega L)^{1/3}$.

Schematic of resonance absorption

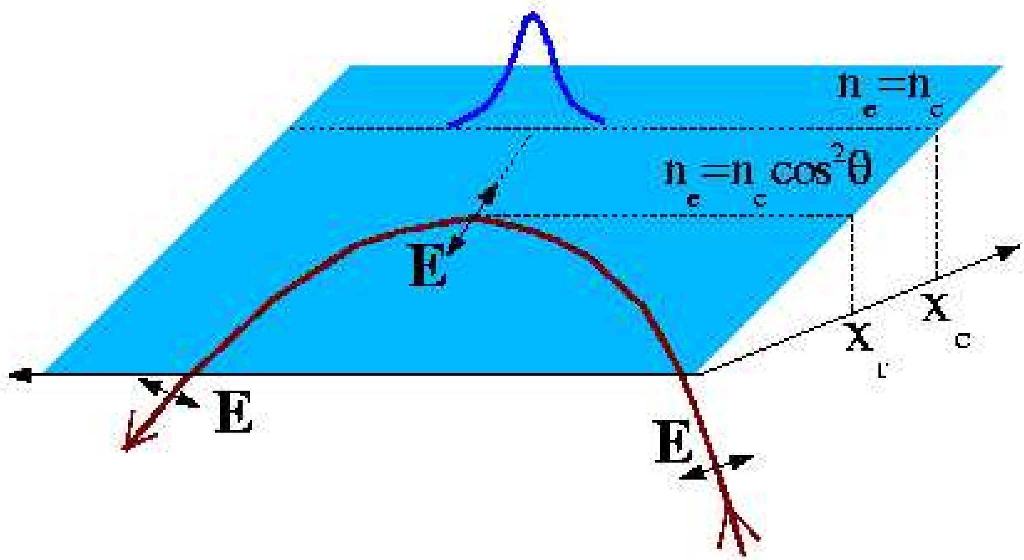

Adapted from C. E. Max (Les Houches lectures, 1980)

Oblique incidence, p–polarization, and "gentle" gradients, i.e. $L \gg (\lambda\,,\, v_{osc})$, are required.
The laser field is evanescent at $x = x_c \Rightarrow$ optimal absorption angle depends on density gradient L: $\sin\theta_o \simeq 0.8(c/\omega L)^{1/3}$.
In a warm plasma, the plasma oscillation propagates in the $n_e < n_c$ region and can accelerate electrons.

Vlasov simulation of resonance absorption

Vlasov simulation of resonance absorption

Numerical solution of the Vlasov-Poisson system within the capacitor approximation (uniform $\mathbf{E}_d$)

Vlasov simulation of resonance absorption

Numerical solution of the Vlasov-Poisson system within the capacitor approximation (uniform $\mathbf{E}_d$)

n_e, E_x

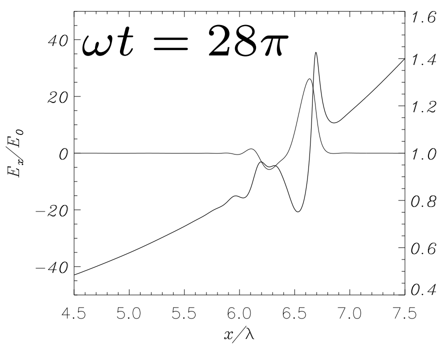

$f_e(x, p_x)$

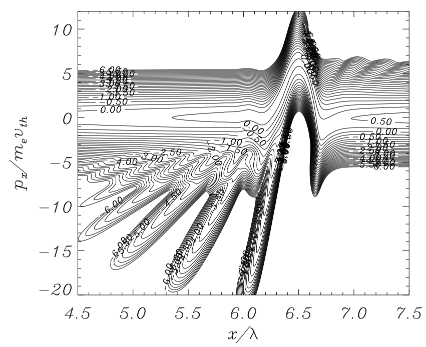

"Linear" stage: a resonantly excited plasma wave propagates towards the low density or "underdense" region ($\omega_p < \omega$) region. Electrons are accelerated by the wave field.

Vlasov simulation of resonance absorption

Numerical solution of the Vlasov-Poisson system within the capacitor approximation (uniform $\mathbf{E}_d$)

n_e, E_x $\qquad\qquad$ $f_e(x, p_x)$

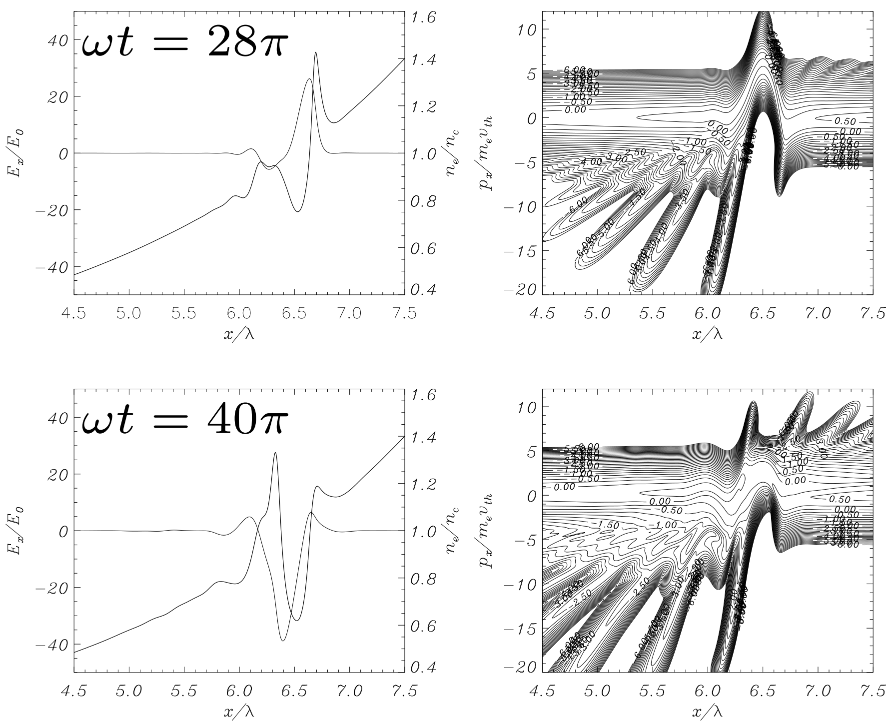

"Linear" stage: a resonantly excited plasma wave propagates towards the low density or "underdense" region ($\omega_p < \omega$) region. Electrons are accelerated by the wave field.

"Nonlinear" stage: the plasma density profile is strongly modified. Additional fast electrons bunches are generated at resonance and propagate into the *over-dense* plasma ($\omega_p > \omega$).

Vlasov simulation of resonance absorption

Numerical solution of the Vlasov-Poisson system within the capacitor approximation (uniform $\mathbf{E}_d$)

$n_e,\ E_x$ $\qquad\qquad$ $f_e(x, p_x)$

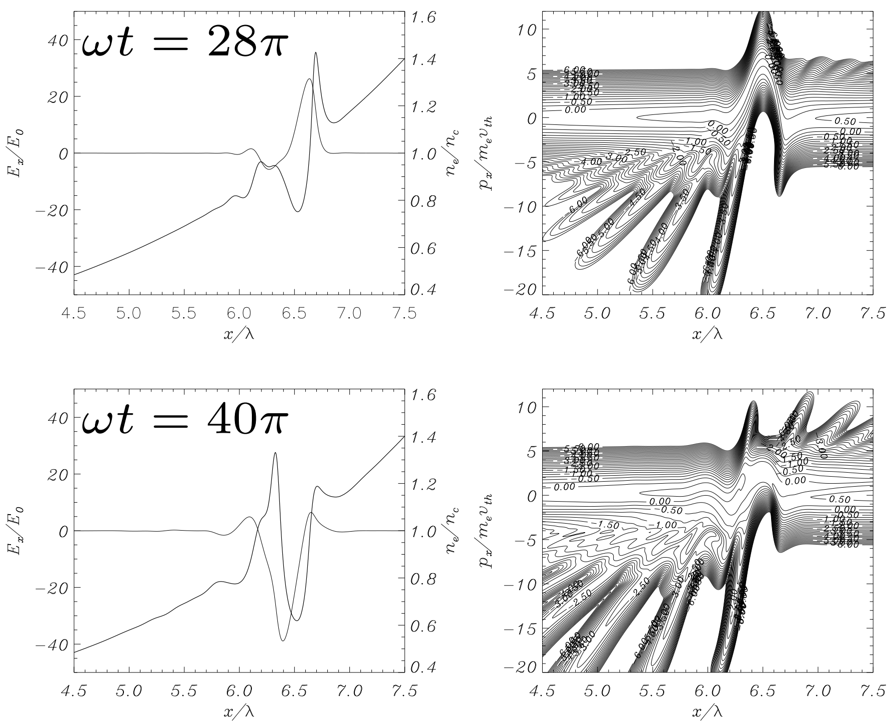

"Linear" stage: a resonantly excited plasma wave propagates towards the low density or "underdense" region ($\omega_p < \omega$) region. Electrons are accelerated by the wave field.

"Nonlinear" stage: the plasma density profile is strongly modified. Additional fast electrons bunches are generated at resonance and propagate into the *overdense* plasma ($\omega_p > \omega$).

A. Macchi and H. Ruhl, GSI Report, Darmstadt, 2000

“2ω” resonance absorption

"2ω" resonance absorption

At normal incidence ($\theta = 0$), a longitudinal, electrostatic oscillation can be driven by $\mathbf{v} \times \mathbf{B}$ force at 2ω along $\hat{\mathbf{x}}$ even for step–like density gradients ($L = 0$).

"2ω" resonance absorption

At normal incidence ($\theta = 0$), a longitudinal, electrostatic oscillation can be driven by $\mathbf{v} \times \mathbf{B}$ force at 2ω along $\hat{\mathbf{x}}$ even for step–like density gradients ($L = 0$).

$$(\mathbf{v} \times \mathbf{B})_x = \frac{e^2 E_L^2(0)}{2 m_e c^2 l_s} e^{-2x/l_s - 2i\omega t}$$

“2ω” resonance absorption

At normal incidence ($\theta = 0$), a longitudinal, electrostatic oscillation can be driven by $\mathbf{v} \times \mathbf{B}$ force at 2ω along $\hat{\mathbf{x}}$ even for step–like density gradients ($L = 0$).

$$(\mathbf{v} \times \mathbf{B})_x = \frac{e^2 E_L^2(0)}{2 m_e c^2 l_s} e^{-2x/l_s - 2i\omega t}$$

(perturbative)

For $n_e < 4n_c$, the oscillation propagates as a plasma wave with maximum amplitude when $2\omega = \sqrt{\omega_p^2 + 4v_{th}^2/l_s^2} \simeq \omega_p$.

"2ω" resonance absorption

At normal incidence ($\theta = 0$), a longitudinal, electrostatic oscillation can be driven by $\mathbf{v} \times \mathbf{B}$ force at 2ω along $\hat{\mathbf{x}}$ even for step–like density gradients ($L = 0$).

$$(\mathbf{v} \times \mathbf{B})_x = \frac{e^2 E_L^2(0)}{2 m_e c^2 l_s} e^{-2x/l_s - 2i\omega t}$$

(perturbative)

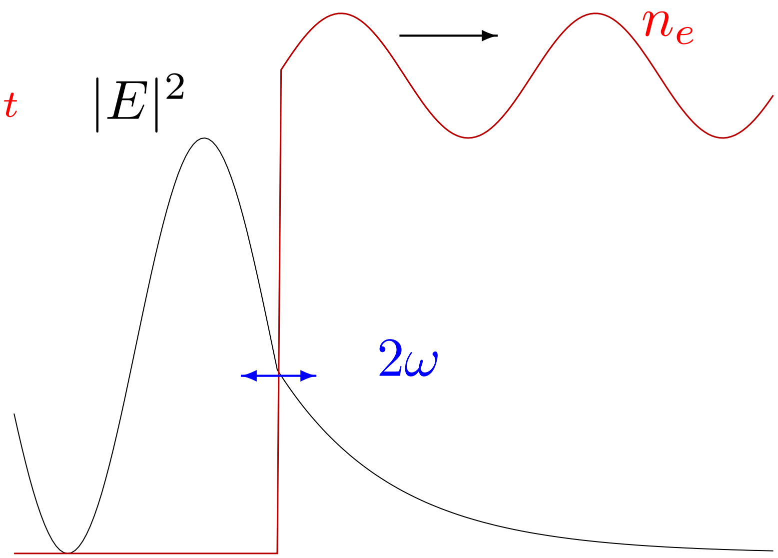

For $n_e < 4n_c$, the oscillation propagates as a plasma wave with maximum amplitude when $2\omega = \sqrt{\omega_p^2 + 4v_{th}^2/l_s^2} \simeq \omega_p$.

The anomalous skin effect

The anomalous skin effect

In a plasma in thermal equilibrium when $v_{th}/\omega > c/\omega_p$,
(being $v_{th} = \sqrt{T_e/m_e}$)
the conductivity becomes non–local.

The anomalous skin effect

In a plasma in thermal equilibrium when $v_{th}/\omega > c/\omega_p$,
(being $v_{th} = \sqrt{T_e/m_e}$)
the conductivity becomes non–local.

In such conditions the local phase between $\mathbf{J}$ and $\mathbf{E}$ may be different from $\pi/2 \rightarrow \langle \mathbf{J} \cdot \mathbf{E} \rangle \neq 0$.

The anomalous skin effect

In a plasma in thermal equilibrium when $v_{th}/\omega > c/\omega_p$,
(being $v_{th} = \sqrt{T_e/m_e}$)
the conductivity becomes non–local.

In such conditions the local phase between $\mathbf{J}$ and $\mathbf{E}$ may be different from $\pi/2 \rightarrow \langle \mathbf{J} \cdot \mathbf{E} \rangle \neq 0$.

The above condition also states that electrons cross the skin layer in a time shorter than the field period $T = 2\pi/\omega$: their motion is thus non–adiabatic.

The anomalous skin effect

In a plasma in thermal equilibrium when $v_{th}/\omega > c/\omega_p$,
(being $v_{th} = \sqrt{T_e/m_e}$)
the conductivity becomes non–local.

In such conditions the local phase between $\mathbf{J}$ and $\mathbf{E}$ may be different from $\pi/2 \rightarrow \langle \mathbf{J} \cdot \mathbf{E} \rangle \neq 0$.

The above condition also states that electrons cross the skin layer in a time shorter than the field period $T = 2\pi/\omega$: their motion is thus non–adiabatic.

[E. S. Weibel, Phys. Fluids **10**, 741 (1967)].

Theory of the anomalous skin effect

Theory of the anomalous skin effect

Boltzmann–Vlasov and Maxwell's equations are solved in 1D

Theory of the anomalous skin effect

Boltzmann–Vlasov and Maxwell's equations are solved in 1D (normal incidence assumed for simplicity):

Theory of the anomalous skin effect

Boltzmann–Vlasov and Maxwell's equations are solved in 1D (normal incidence assumed for simplicity):

$$\partial_t f + v_x \partial_x f - \frac{e}{m_e}\left(\mathbf{E} + \frac{\mathbf{v}}{c} \times \mathbf{B}\right) \cdot \partial_{\mathbf{v}} f = -\nu (f - F_M),$$

$$\partial_x E_y = i\frac{\omega}{c} B_z\,, \qquad \partial_x B_z = -\frac{4\pi}{c} j_y\,.$$

(F_M: Maxwell distribution)

Theory of the anomalous skin effect

Boltzmann–Vlasov and Maxwell's equations are solved in 1D (normal incidence assumed for simplicity):

$$\partial_t f + v_x \partial_x f - \frac{e}{m_e}\left(\mathbf{E} + \frac{\mathbf{v}}{c} \times \mathbf{B}\right) \cdot \partial_{\mathbf{v}} f = -\nu(f - F_M),$$

$$\partial_x E_y = i\frac{\omega}{c} B_z \,, \qquad \partial_x B_z = -\frac{4\pi}{c} j_y \,.$$

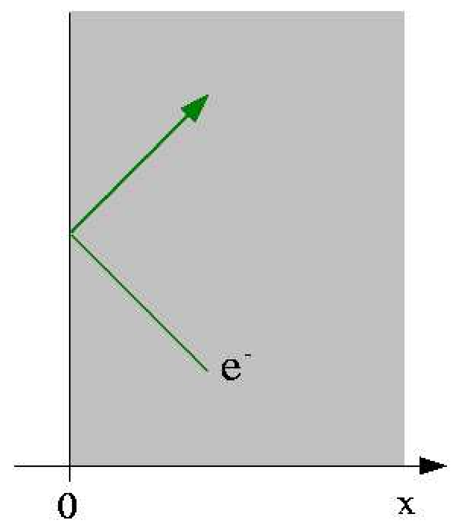

(F_M: Maxwell distribution)

Specular reflection at $x = 0$ is assumed:
$f(x = 0, v_x, v_y) = f(x = 0, -v_x, v_y)$

Anomalous skin effect absorption

Anomalous skin effect absorption

Absorption degree A_{abs} and extinction length l_s in the limit $l_s \ll v_{th}/\omega$:

$$P_{abs} = \int_{-\infty}^{+\infty} dx \langle J_y E_y \rangle \equiv A_{abs}(c|E_L|^2/4\pi)$$

$$A_{abs} = \frac{8}{3\sqrt{3}} \left(\frac{v_{th}}{c} \frac{\omega_L^2}{\omega_p^2} \right)^{1/3} , \qquad l_s = \left(\frac{c^2 v_{th}}{\omega_p^2 \omega_L} \right)^{1/3} .$$

Anomalous skin effect absorption

Absorption degree A_{abs} and extinction length l_s in the limit $l_s \ll v_{th}/\omega$:

$$P_{abs} = \int_{-\infty}^{+\infty} dx \langle J_y E_y \rangle \equiv A_{abs}(c|E_L|^2/4\pi)$$

$$A_{abs} = \frac{8}{3\sqrt{3}} \left(\frac{v_{th}}{c} \frac{\omega_L^2}{\omega_p^2} \right)^{1/3} , \qquad l_s = \left(\frac{c^2 v_{th}}{\omega_p^2 \omega_L} \right)^{1/3} .$$

ASE $+$ simple diffusion model for heat losses [i.e. $T_e = T_e(t)$] explains well absorption data by Price et al. in solid target at $I \leq 10^{18}$ W cm^{-2}.
[Rozmus et al, Phys. Plasmas **3**, 360 (1996)]

On the boundary conditions

On the boundary conditions

When is it correct to assume electron reflection at the plasma surface?

On the boundary conditions

When is it correct to assume electron reflection at the plasma surface?

For a step–density, warm plasma in equilibrium, the Debye sheath field E_s confines electrons:

$$\begin{cases} -en_eE_s - \boldsymbol{\nabla} n_eT_e = 0 \\ \partial_x E_s = 4\pi e(n_i - n_e) \end{cases}$$

On the boundary conditions

When is it correct to assume electron reflection at the plasma surface?

For a step–density, warm plasma in equilibrium, the Debye sheath field E_s confines electrons:

$$\left\{ \begin{array}{l} -en_e E_s - \boldsymbol{\nabla} n_e T_e = 0 \\ \partial_x E_s = 4\pi e(n_i - n_e) \end{array} \right. \quad \rightarrow E_s \approx \frac{T_e}{e\lambda_D}$$

On the boundary conditions

When is it correct to assume electron reflection at the plasma surface?

For a step–density, warm plasma in equilibrium, the Debye sheath field E_s confines electrons:

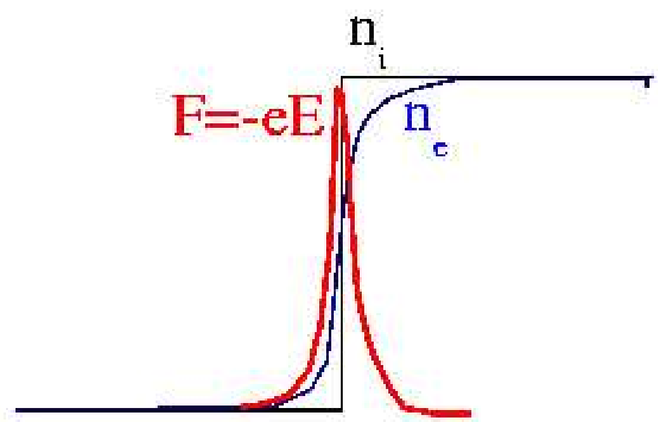

$$\left\{ \begin{array}{l} -en_eE_s - \nabla n_eT_e = 0 \\ \partial_x E_s = 4\pi e(n_i - n_e) \end{array} \right. \quad \rightarrow E_s \approx \frac{T_e}{e\lambda_D}$$

In an external field E_d, electrons are reflected from the sheath if $v_{osc} = eE_d/m_e\omega < v_{th}$.
Since the sheath is very thin ($\approx \lambda_D$) , $E_s \sim \delta(x)$ may be assumed (reflecting boundary).

From skin effect to “vacuum heating” absorption

From skin effect to "vacuum heating" absorption

The regime $v_{osc} < v_{th}$ corresponds to skin absorption.

From skin effect to “vacuum heating” absorption

The regime $v_{osc} < v_{th}$ corresponds to skin absorption.

When $v_{osc} > v_{th}$, electrons are dragged into vacuum
$\longrightarrow$ vacuum heating absorption [Brunel 1987].

For a p–polarized laser pulse at oblique incidence

$$E_d \sim (\omega/\omega_p)E_L \longrightarrow I/c > n_e T_e$$

for VH absorption.

From skin effect to “vacuum heating” absorption

The regime $v_{osc} < v_{th}$ corresponds to skin absorption.

When $v_{osc} > v_{th}$, electrons are dragged into vacuum
$\longrightarrow$ vacuum heating absorption [Brunel 1987].

For a p–polarized laser pulse at oblique incidence

$$E_d \sim (\omega/\omega_p)E_L \longrightarrow I/c > n_e T_e$$

for VH absorption. (Radiation pressure exceeds plasma pressure).

At normal incidence, the $\mathbf{v} \times \mathbf{B}$ force may drive VH.

Simple electrostatic model of “Vacuum heating”

Simple electrostatic model of "Vacuum heating"

When $v_{osc} = eE_d/m_e\omega > v_{th}$, cold fluid equations may be used for modelling of the plasma in a strong external field $E_d = E_{d0}\cos\omega t$.

Simple electrostatic model of "Vacuum heating"

When $v_{osc} = eE_d/m_e\omega > v_{th}$, cold fluid equations may be used for modelling of the plasma in a strong external field $E_d = E_{d0}\cos\omega t$.

Euler–Poisson 1D system ("capacitor" model):

$$\left\{ \begin{array}{rcl} 4\pi j_x & = & \partial_t E_e \,, \\ \partial_x E_x & = & 4\pi e(n_0 - n_e)\,, \\ \frac{dv_x}{dt} & = & -\frac{e}{m_e}(E_e + E_d). \end{array} \right.$$

Simple electrostatic model of "Vacuum heating"

When $v_{osc} = eE_d/m_e\omega > v_{th}$, cold fluid equations may be used for modelling of the plasma in a strong external field $E_d = E_{d0}\cos\omega t$.

Euler–Poisson 1D system ("capacitor" model):

$$\left\{\begin{array}{rcl} 4\pi j_x &=& \partial_t E_e\,, \\ \partial_x E_x &=& 4\pi e(n_0 - n_e)\,, \\ \frac{dv_x}{dt} &=& -\frac{e}{m_e}(E_e + E_d). \end{array}\right.$$

+ Lagrangian coordinates:
$x = x_0 + \xi(x_0, t)\,,\;\; \partial_t\xi = v_x$

$$\Rightarrow\;\; \frac{d^2\xi}{dt^2} = \left\{\begin{array}{ll} -\omega_p^2\xi - eE_d/m_e & (x_0 + \xi > 0) \\ +\omega_p^2 x_0 - eE_d/m_e & (x_0 + \xi < 0) \end{array}\right.$$

Simple electrostatic model of "Vacuum heating"

When $v_{osc} = eE_d/m_e\omega > v_{th}$, cold fluid equations may be used for modelling of the plasma in a strong external field $E_d = E_{d0}\cos\omega t$.

Euler–Poisson 1D system ("capacitor" model):

$$\left\{ \begin{array}{rcl} 4\pi j_x & = & \partial_t E_e \,, \\ \partial_x E_x & = & 4\pi e(n_0 - n_e)\,, \\ \frac{dv_x}{dt} & = & -\frac{e}{m_e}(E_e + E_d). \end{array} \right.$$

+ Lagrangian coordinates:
$x = x_0 + \xi(x_0, t)\,,\;\; \partial_t \xi = v_x$

$$\Rightarrow \;\; \frac{d^2\xi}{dt^2} = \left\{ \begin{array}{ll} -\omega_p^2\xi - eE_d/m_e & (x_0 + \xi > 0) \\ +\omega_p^2 x_0 - eE_d/m_e & (x_0 + \xi < 0) \end{array} \right.$$

Electrons crossing the surface towards vacuum $(x_0 + \xi < 0)$ feel a discontinous force with an effective secular acceleration $\omega_p^2 x_0$.

“Vacuum heating” or interface phase mixing

“Vacuum heating” or interface phase mixing

Numerical solution of the equation of motion in Lagrangian coordinates:

$$\frac{d^2\xi}{dt^2} = \begin{cases} -\omega_p^2\xi - eE_d/m_e & (x_0 + \xi > 0) \\ \omega_p^2 x_0 - eE_d/m_e & (x_0 + \xi < 0) \end{cases}$$

“Vacuum heating” or interface phase mixing

Numerical solution of the equation of motion in Lagrangian coordinates:

$$\frac{d^2\xi}{dt^2} = \begin{cases} -\omega_p^2\xi - eE_d/m_e & (x_0+\xi>0) \\ \omega_p^2 x_0 - eE_d/m_e & (x_0+\xi<0) \end{cases}$$

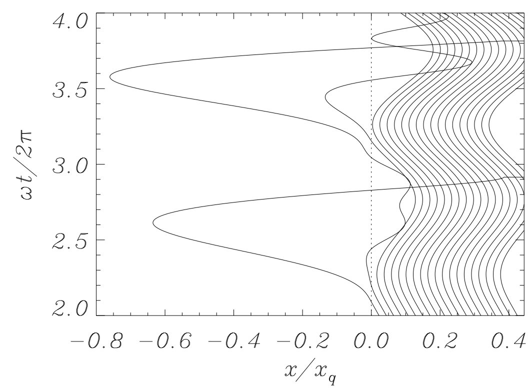

An irregular aperiodic motion is observed with electrons re–entering the plasma with energy ≈ the oscillation energy in vacuum.

“Vacuum heating” or interface phase mixing

Numerical solution of the equation of motion in Lagrangian coordinates:

$$\frac{d^2\xi}{dt^2} = \begin{cases} -\omega_p^2\xi - eE_d/m_e & (x_0+\xi>0) \\ \omega_p^2 x_0 - eE_d/m_e & (x_0+\xi<0) \end{cases}$$

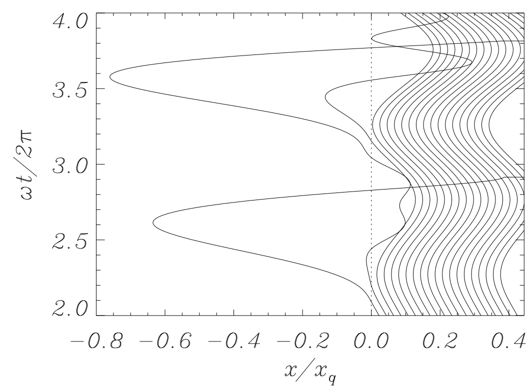

An irregular aperiodic motion is observed with electrons re–entering the plasma with energy ≈ the oscillation energy in vacuum. Electron pulses (“jets”) are produced with the frequency of E_d:

“Vacuum heating” or interface phase mixing

Numerical solution of the equation of motion in Lagrangian coordinates:

$$\frac{d^2\xi}{dt^2} = \begin{cases} -\omega_p^2\xi - eE_d/m_e & (x_0+\xi>0) \\ \omega_p^2 x_0 - eE_d/m_e & (x_0+\xi<0) \end{cases}$$

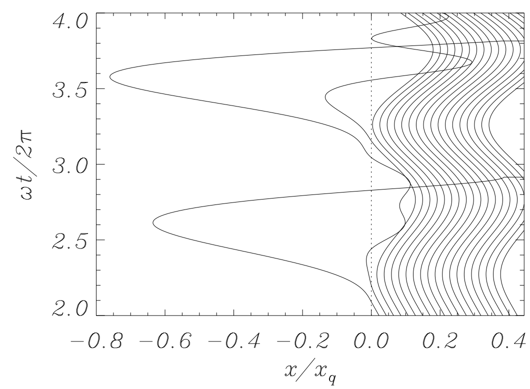

An irregular aperiodic motion is observed with electrons re–entering the plasma with energy $\approx$ the oscillation energy in vacuum.
Electron pulses (“jets”) are produced with the frequency of E_d:
– $\omega = \omega_L$ for oblique incidence, p–polarization ($E_d \sim E_L \sin\theta$),

“Vacuum heating” or interface phase mixing

Numerical solution of the equation of motion in Lagrangian coordinates:

$$\frac{d^2\xi}{dt^2} = \begin{cases} -\omega_p^2\xi - eE_d/m_e & (x_0+\xi>0) \\ \omega_p^2 x_0 - eE_d/m_e & (x_0+\xi<0) \end{cases}$$

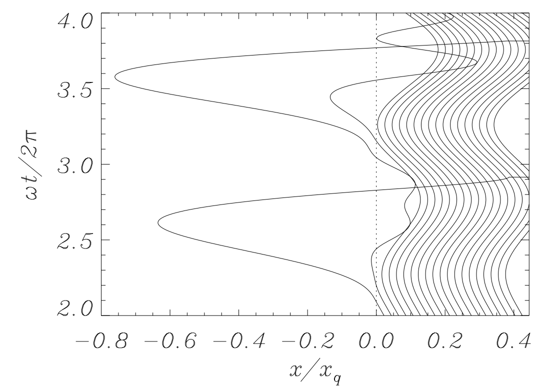

An irregular aperiodic motion is observed with electrons re–entering the plasma with energy ≈ the oscillation energy in vacuum.
Electron pulses (“jets”) are produced with the frequency of E_d:
– $\omega = \omega_L$ for oblique incidence, p–polarization ($E_d \sim E_L \sin\theta$),
– $\omega = 2\omega_L$ otherwise ($E_d \sim (\mathbf{v}\times\mathbf{B})_x$).

“Vacuum heating” or interface phase mixing

Numerical solution of the equation of motion in Lagrangian coordinates:

$$\frac{d^2\xi}{dt^2} = \begin{cases} -\omega_p^2\xi - eE_d/m_e & (x_0+\xi>0) \\ \omega_p^2 x_0 - eE_d/m_e & (x_0+\xi<0) \end{cases}$$

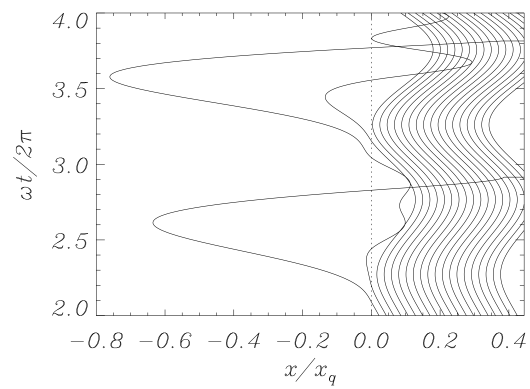

An irregular aperiodic motion is observed with electrons re–entering the plasma with energy $\approx$ the oscillation energy in vacuum.
Electron pulses (“jets”) are produced with the frequency of E_d:
– $\omega = \omega_L$ for oblique incidence, p–polarization ($E_d \sim E_L \sin\theta$),
– $\omega = 2\omega_L$ otherwise ($E_d \sim (\mathbf{v}\times\mathbf{B})_x$).
Similar behavior is observed in fully self–consistent PIC simulations.

“Vacuum heating” or interface phase mixing

Numerical solution of the equation of motion in Lagrangian coordinates:

$$\frac{d^2\xi}{dt^2} = \begin{cases} -\omega_p^2\xi - eE_d/m_e & (x_0+\xi>0) \\ \omega_p^2 x_0 - eE_d/m_e & (x_0+\xi<0) \end{cases}$$

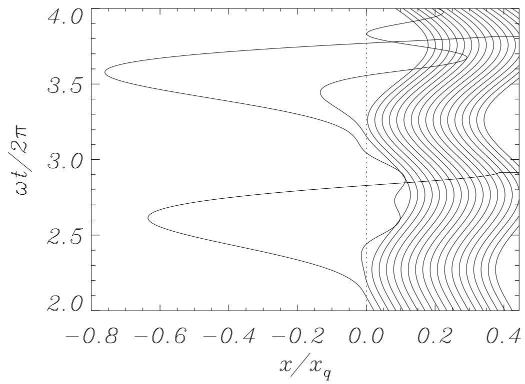

An irregular aperiodic motion is observed with electrons re–entering the plasma with energy $\approx$ the oscillation energy in vacuum.
Electron pulses (“jets”) are produced with the frequency of E_d:
– $\omega = \omega_L$ for oblique incidence, p–polarization ($E_d \sim E_L \sin\theta$),
– $\omega = 2\omega_L$ otherwise ($E_d \sim (\mathbf{v}\times\mathbf{B})_x$).
Similar behavior is observed in fully self–consistent PIC simulations.

The “moving mirror”

The "moving mirror"

In the regime $I/c > n_e T_e$, the whole density profile is modified by the laser force:

The "moving mirror"

In the regime $I/c > n_e T_e$, the whole density profile is modified by the laser force:the critical surface oscillates at ω or 2ω (depending on angle and polarization)

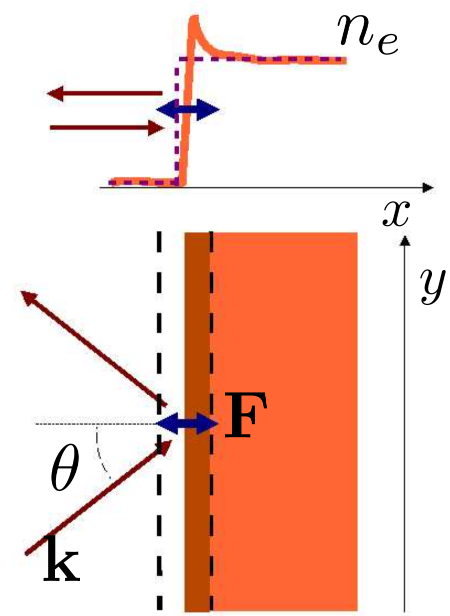

The "moving mirror"

In the regime $I/c > n_e T_e$, the whole density profile is modified by the laser force:the critical surface oscillates at ω or 2ω (depending on angle and polarization)

$\longrightarrow$ "moving mirror" effect: generation of high harmonics 3ω, 4ω, $\ldots$, $n\omega$ $\ldots$

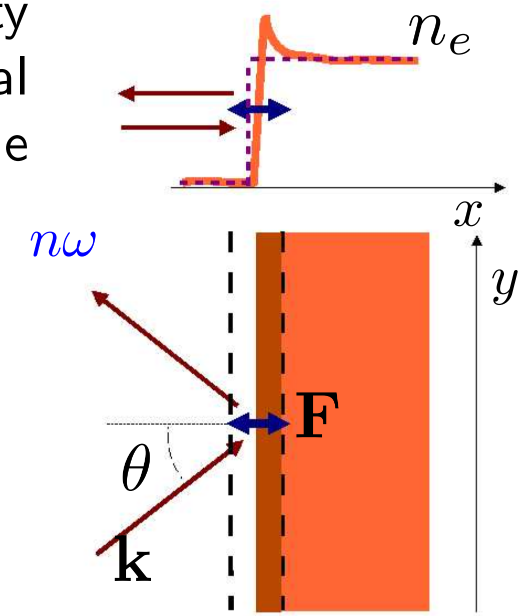

Ion acceleration

Ion acceleration

The secular ponderomotive force (radiation pressure) acts on electron and creates a charge separation layer with a *back–holding field* that then accelerates ions.

Ion acceleration

The secular ponderomotive force (radiation pressure) acts on electron and creates a charge separation layer with a *back–holding field* that then accelerates ions.

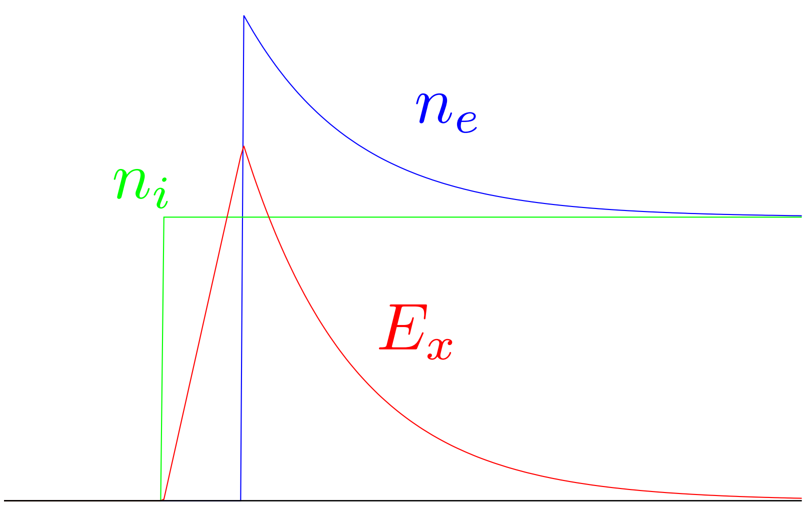

Ion acceleration

The secular ponderomotive force (radiation pressure) acts on electron and creates a charge separation layer with a *back–holding field* that then accelerates ions.

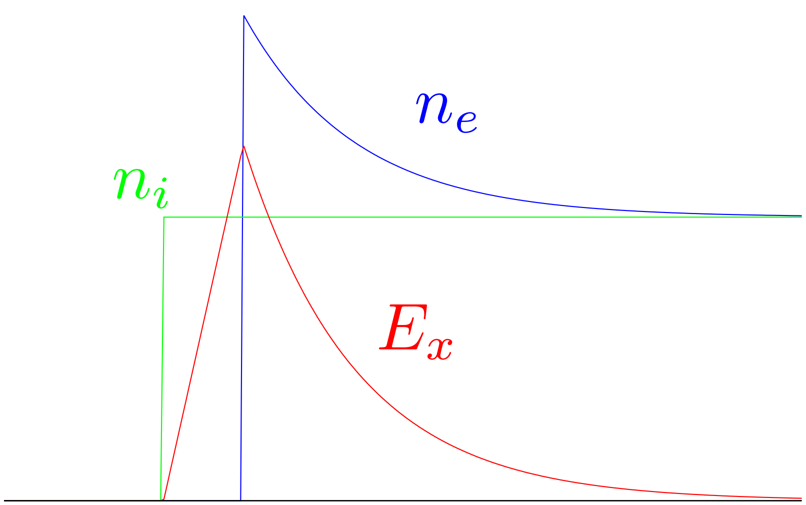

Ions will pile up forming a so–called "shock" front.

Ion acceleration

The secular ponderomotive force (radiation pressure) acts on electron and creates a charge separation layer with a *back–holding field* that then accelerates ions.

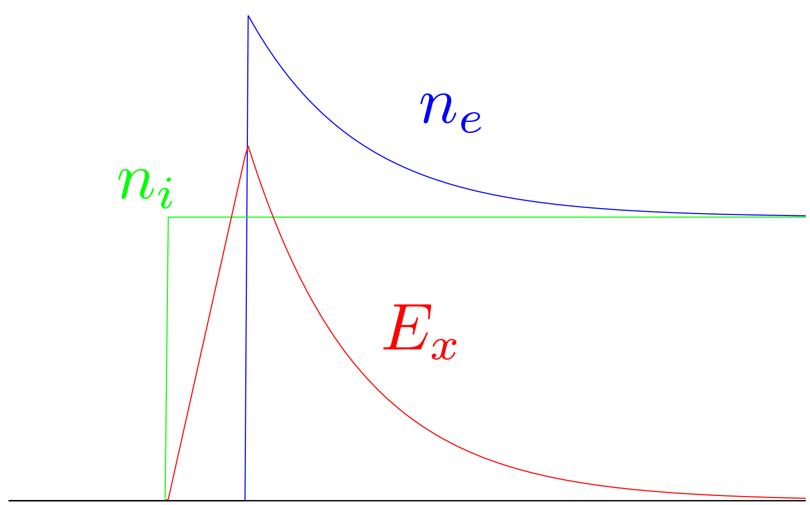

Ions will pile up forming a so–called "shock" front.

But the process is *not* stationary: ions will go across the electron front leading to "breaking" of the shock front.

A simple (heuristic) model

A simple (heuristic) model

Use a simple "step" profile as in figure.

A simple (heuristic) model

Use a simple "step" profile as in figure.
Assume the PM force "follows" electrons and that the "screening length" l_s is nearly constant during compression.

A simple (heuristic) model

Use a simple "step" profile as in figure.
Assume the PM force "follows" electrons and that the "screening length" l_s is nearly constant during compression.
Assume electrons "bound" to ions in region B.

A simple (heuristic) model

Use a simple "step" profile as in figure.
Assume the PM force "follows" electrons and that the "screening length" l_s is nearly constant during compression.
Assume electrons "bound" to ions in region B.

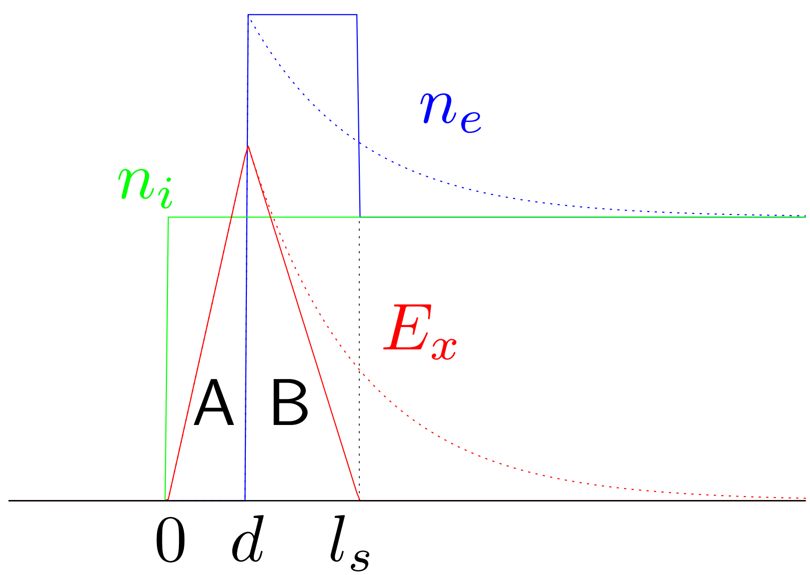

A simple (heuristic) model

Use a simple "step" profile as in figure.
Assume the PM force "follows" electrons and that the "screening length" l_s is nearly constant during compression.
Assume electrons "bound" to ions in region B.

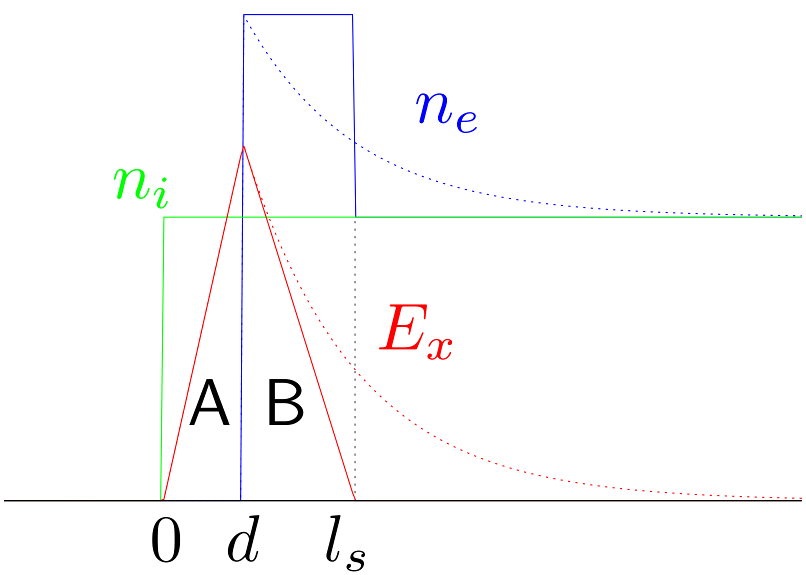

Ions in region A never reach electrons again and form a shelf.

A simple (heuristic) model

Use a simple "step" profile as in figure.
Assume the PM force "follows" electrons and that the "screening length" l_s is nearly constant during compression.
Assume electrons "bound" to ions in region B.

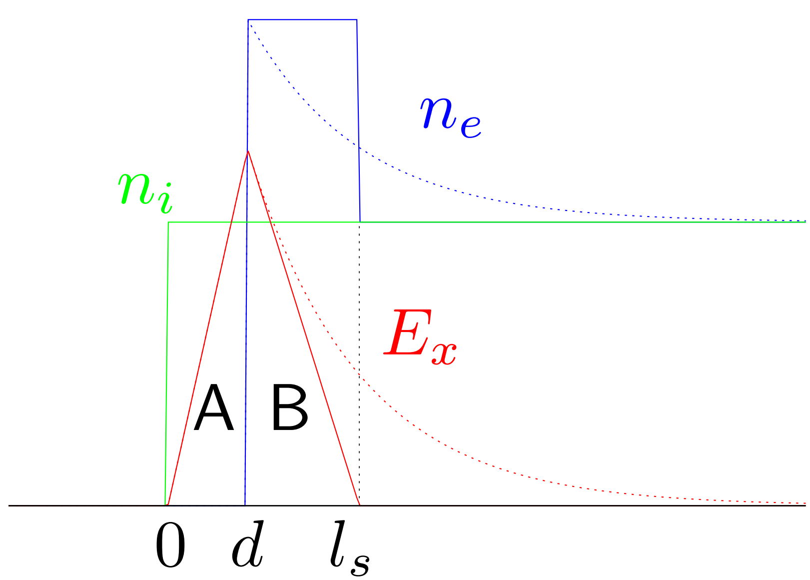

Ions in region A never reach electrons again and form a shelf.
Ions in region B pile up forming the "shock" front.

A simple (heuristic) model

Use a simple "step" profile as in figure.
Assume the PM force "follows" electrons and that the "screening length" l_s is nearly constant during compression.
Assume electrons "bound" to ions in region B.

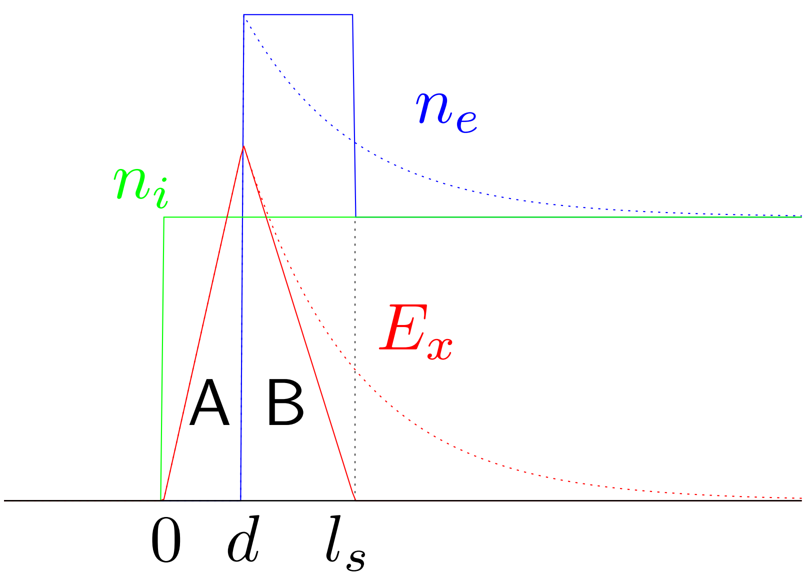

Ions in region A never reach electrons again and form a shelf.
Ions in region B pile up forming the "shock" front.
If E_x is linear, all ions reach the $x = l_s$ position at the same time: *breaking* of the shock.

Model predictions

Model predictions

- Electric field in region B: $E(x_0) = E_0\,(1 - x_0/l_s)$

  with $eE_0 n_e l_s/2 \simeq 2I/c$

Model predictions

- Electric field in region B: $E(x_0) = E_0\,(1 - x_0/l_s)$

  with $eE_0 n_e l_s/2 \simeq 2I/c$

- Ion displacement: $\xi(x_0, t) = (q_i E_0/2m_i)\,(1 - x_0/l_s)\,t^2$

Model predictions

- Electric field in region B: $E(x_0) = E_0\,(1 - x_0/l_s)$

  with $eE_0 n_e l_s/2 \simeq 2I/c$

- Ion displacement: $\xi(x_0, t) = (q_i E_0/2m_i)\,(1 - x_0/l_s)\,t^2$

- Time to reach electrons: $\tau_i = \sqrt{2 l_s m_i / q_i E_0}$

Model predictions

- Electric field in region B: $E(x_0) = E_0\,(1 - x_0/l_s)$

  with $eE_0 n_e l_s/2 \simeq 2I/c$

- Ion displacement: $\xi(x_0, t) = (q_i E_0/2m_i)\,(1 - x_0/l_s)\,t^2$

- Time to reach electrons: $\tau_i = \sqrt{2 l_s m_i / q_i E_0}$

- Maximum ion velocity $v_{max} = \sqrt{2 l_s q_i E_0/m_i} \simeq \sqrt{I/m_i n_i c}$

  with $v_{max} = 2 v_s$ (average shock speed)

Model predictions

- Electric field in region B: $E(x_0) = E_0\,(1 - x_0/l_s)$

  with $eE_0 n_e l_s/2 \simeq 2I/c$

- Ion displacement: $\xi(x_0, t) = (q_i E_0/2m_i)\,(1 - x_0/l_s)\,t^2$

- Time to reach electrons: $\tau_i = \sqrt{2l_s m_i/q_i E_0}$

- Maximum ion velocity $v_{max} = \sqrt{2l_s q_i E_0/m_i} \simeq \sqrt{I/m_i n_i c}$

  with $v_{max} = 2v_s$ (average shock speed)

Numerical results

Numerical results

Ion density profile at different times from PIC simulation:

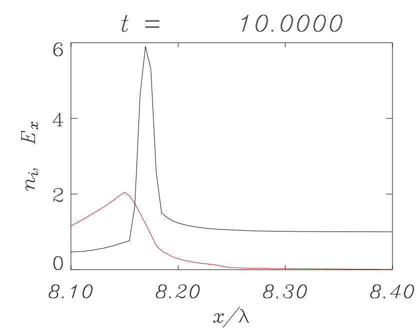

– The shock front forms

Numerical results

Ion density profile at different times from PIC simulation:

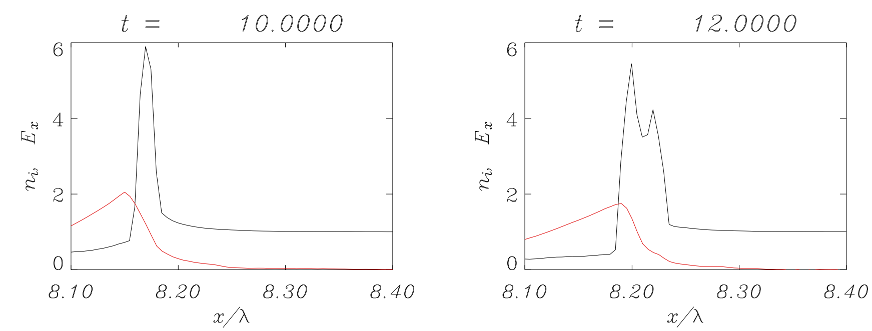

– The shock front forms

– Shock breaks

Numerical results

Ion density profile at different times from PIC simulation:

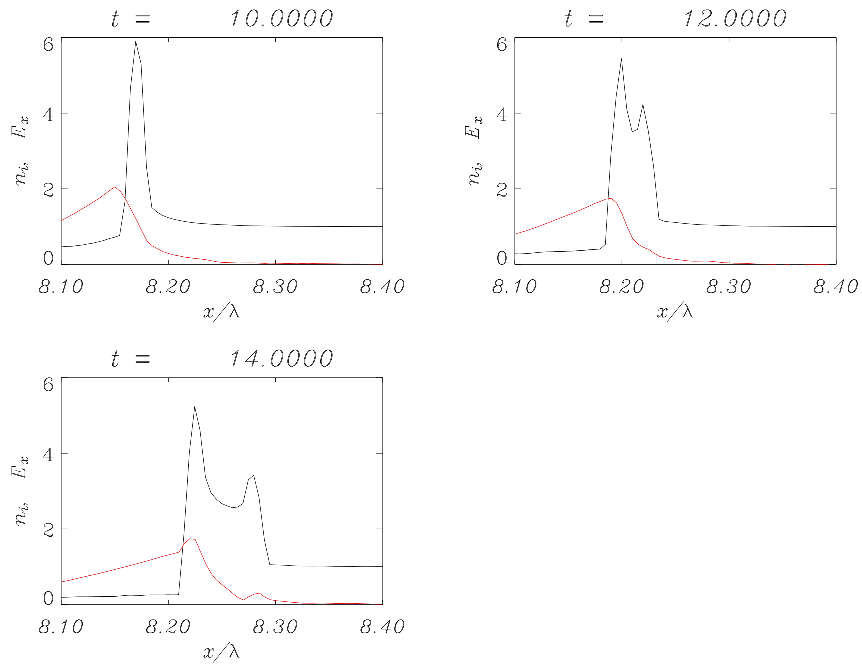

– The shock front forms

– Shock breaks

– Secondary shock forms

Numerical results

Ion density profile at different times from PIC simulation:

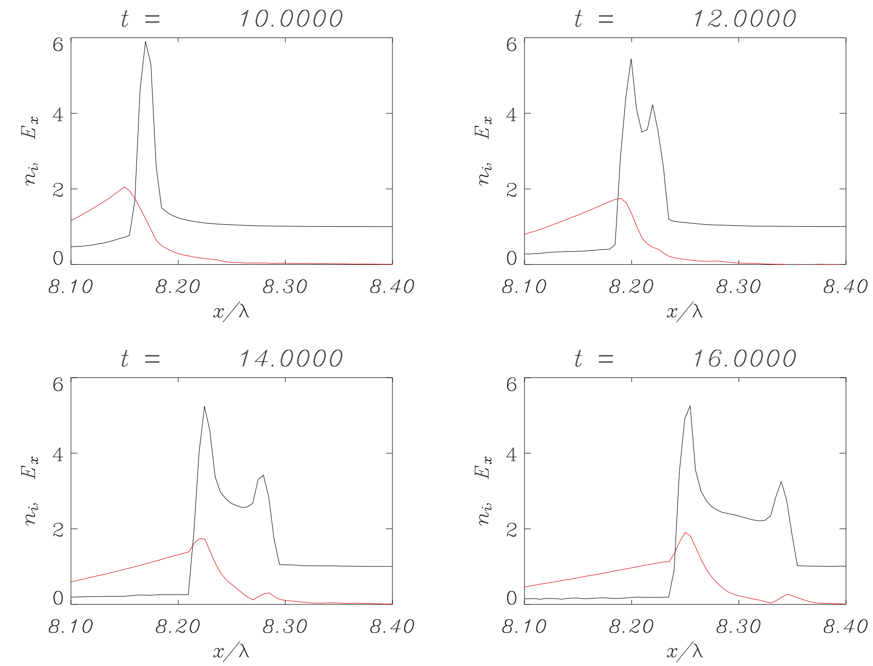

– The shock front forms

– Shock breaks

– Secondary shock forms

– 2nd shock speed $v_2 \simeq 2v_s$

Numerical results

Ion density profile at different times from PIC simulation:

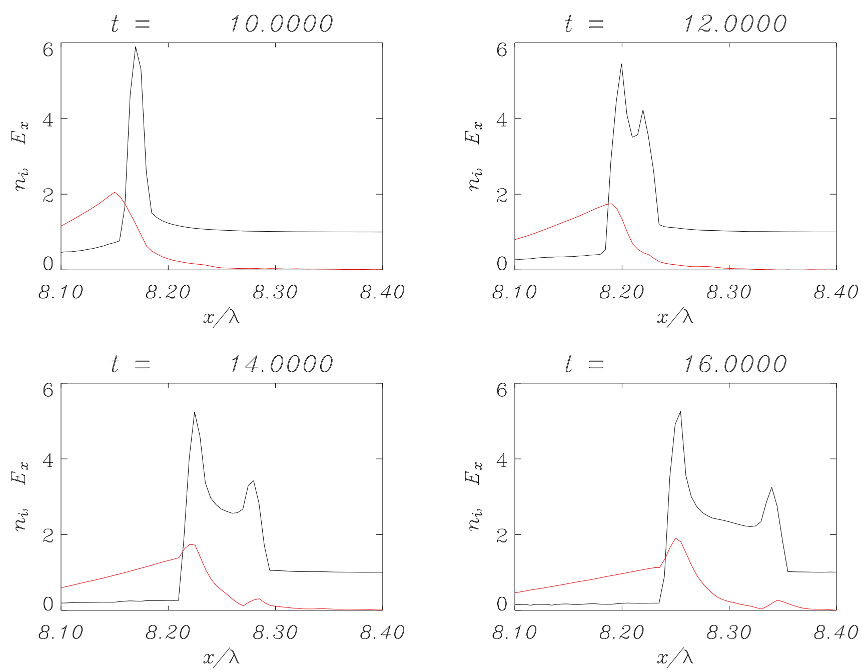

– The shock front forms

– Shock breaks

– Secondary shock forms

– 2nd shock speed $v_2 \simeq 2v_s$

Good agreement with simple model

Beyond 1D effects

Beyond 1D effects

What happens in 2D (or 3D)?

Beyond 1D effects

What happens in 2D (or 3D)?

- 2D mode conversion: surface waves

Beyond 1D effects

What happens in 2D (or 3D)?

- 2D mode conversion: surface waves
- Profile modification by ponderomotive hole boring

Beyond 1D effects

What happens in 2D (or 3D)?

- 2D mode conversion: surface waves
- Profile modification by ponderomotive hole boring
- Surface instabilities and corrugations

Beyond 1D effects

What happens in 2D (or 3D)?

- 2D mode conversion: surface waves
- Profile modification by ponderomotive hole boring
- Surface instabilities and corrugations
- Magnetic collimation of “fast” electrons
- . . .

Surface waves

Surface waves

A step–boundary, overdense plasma supports *surface waves*:

Surface waves

A step–boundary, overdense plasma supports *surface waves*:

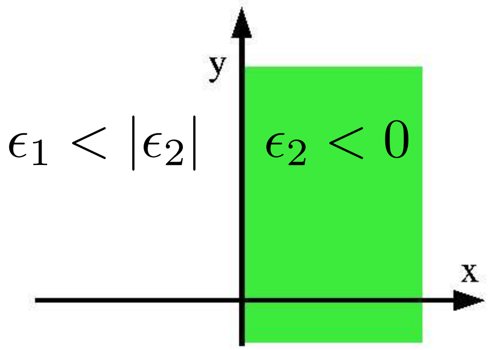

Surface waves

A step–boundary, overdense plasma supports *surface waves*:

$$E_y = E_0 \left[\theta(-x)e^{q_- x} + \theta(x)e^{-q_+ x}\right] e^{iky-i\omega t}$$

$$B_z = \frac{i\omega}{q\_c} E_0 \left[\theta(-x)e^{q_- x} + \theta(x)e^{-q_+ x}\right] e^{iky-i\omega t}$$

$$E_x = ikE_0 \left[\theta(-x)\frac{e^{q_- x}}{q_-} - \theta(x)\frac{e^{-q_+ x}}{q_+}\right] e^{iky-i\omega t}$$

$$\delta n_e = \eta_e \delta(x) e^{iky-i\omega t}$$

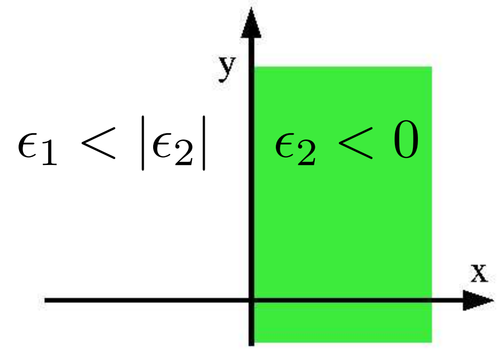

$\epsilon_2 = 1 - \frac{\omega_p^2}{\omega^2} = 1 - \frac{n_e}{n_c}$
< -1 if $n_0 > 2n_c$

Surface waves

A step–boundary, overdense plasma supports *surface waves*:

$$E_y = E_0 \left[\theta(-x)e^{q_- x} + \theta(x)e^{-q_+ x}\right] e^{iky-i\omega t}$$

$$B_z = \frac{i\omega}{q\_c}E_0 \left[\theta(-x)e^{q_- x} + \theta(x)e^{-q_+ x}\right] e^{iky-i\omega t}$$

$$E_x = ikE_0 \left[\theta(-x)\frac{e^{q_- x}}{q_-} - \theta(x)\frac{e^{-q_+ x}}{q_+}\right] e^{iky-i\omega t}$$

$$\delta n_e = \eta_e \delta(x) e^{iky-i\omega t}$$

$$k^2 = \frac{\omega^2}{c^2}\frac{\epsilon_1|\epsilon_2|}{|\epsilon_2| - \epsilon_1} = \frac{\omega^2}{c^2}\frac{\omega_p^2 - \omega^2}{\omega_p^2 - 2\omega^2}$$

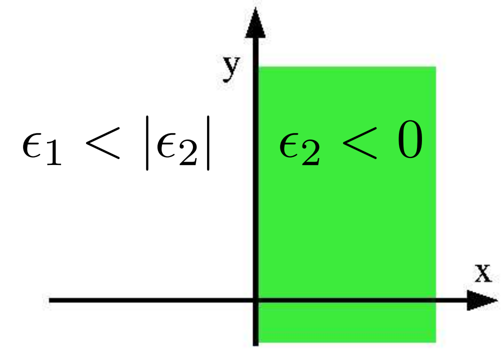

$\epsilon_2 = 1 - \frac{\omega_p^2}{\omega^2} = 1 - \frac{n_e}{n_c}$
< -1 if $n_0 > 2n_c$

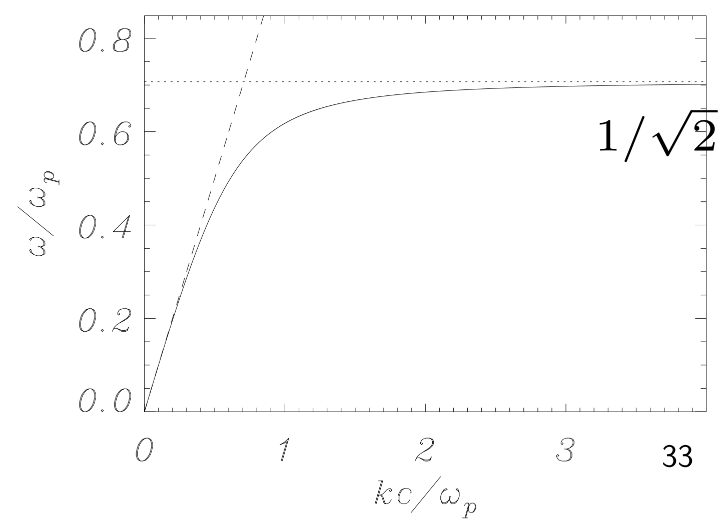

Surface wave absorption II

Surface wave absorption II

Linear mode conversion of the laser pulse into a SW at a plane vacuum–plasma interface requires $\omega_L = \omega_s$, $k_L \sin\theta = k_s$ where $k_L = \omega_L/c$
($L \rightarrow$laser, $s \rightarrow$SW).

Surface wave absorption II

Linear mode conversion of the laser pulse into a SW at a plane vacuum–plasma interface requires $\omega_L = \omega_s$, $k_L \sin\theta = k_s$ where $k_L = \omega_L/c$ ($L \rightarrow$laser, $s \rightarrow$SW).

For SWs $\omega_s < k_s c$

Surface wave absorption II

Linear mode conversion of the laser pulse into a SW at a plane vacuum–plasma interface requires $\omega_L = \omega_s$, $k_L \sin\theta = k_s$ where $k_L = \omega_L/c$ ($L \rightarrow$laser, $s \rightarrow$SW).

For SWs $\omega_s < k_s c \longrightarrow$ phase matching is *not* possible!

Surface wave absorption II

Linear mode conversion of the laser pulse into a SW at a plane vacuum–plasma interface requires $\omega_L = \omega_s$, $k_L \sin\theta = k_s$ where $k_L = \omega_L / c$ ($L \rightarrow$laser, $s \rightarrow$SW).

For SWs $\omega_s < k_s c \longrightarrow$ phase matching is *not* possible!

Structured targets are required, e.g. *grating* targets:

$$k_L \sin\theta = k_s + k_g \qquad (k_g\text{: grating wavevector})$$

Surface wave absorption II

Linear mode conversion of the laser pulse into a SW at a plane vacuum–plasma interface requires $\omega_L = \omega_s$, $k_L \sin\theta = k_s$ where $k_L = \omega_L/c$ ($L \to$laser, $s \to$SW).

For SWs $\omega_s < k_s c \longrightarrow$ phase matching is *not* possible!

Structured targets are required, e.g. *grating* targets:

$$k_L \sin\theta = k_s + k_g \qquad (k_g\text{: grating wavevector})$$

Peak absorption occurs at optimal incidence angle $\sin\theta = \frac{k_s(\omega_L)+k_g}{\omega_L/c}$

Two–surface wave decay

Two–surface wave decay

In *nonlinear* mode conversion, e.g. a **three-wave process**, phase matching at a planar surface is possible

Two–surface wave decay

In *nonlinear* mode conversion, e.g. a **three-wave process**, phase matching at a planar surface is possible

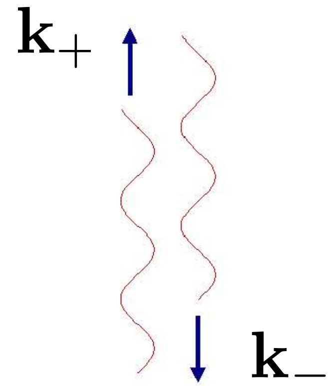

Two–surface wave decay

In *nonlinear* mode conversion, e.g. a **three-wave process**, phase matching at a planar surface is possible

$$\omega_0 = \omega_+ + \omega_-$$
$$k_0 = k_+ + k_-$$

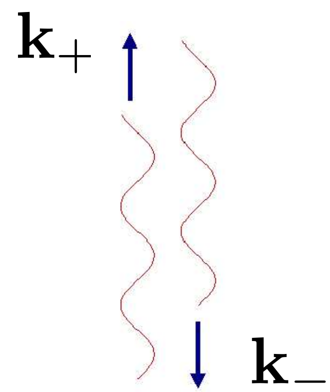

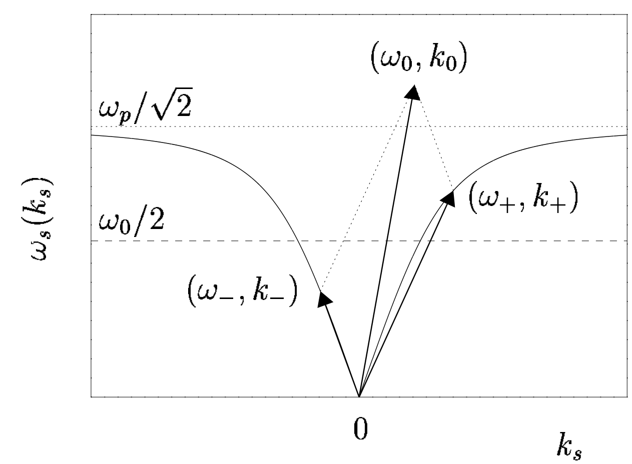

Two–surface wave decay

In *nonlinear* mode conversion, e.g. a **three-wave process**, phase matching at a planar surface is possible

$$\omega_0 = \omega_+ + \omega_-$$
$$k_0 = k_+ + k_-$$

One expects $\omega_0 = \omega_L$,
$k_0 = k_L \sin\theta \rightarrow \omega_\pm = \omega_L/2 \pm \delta\omega$

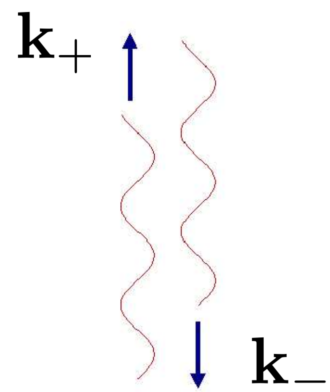

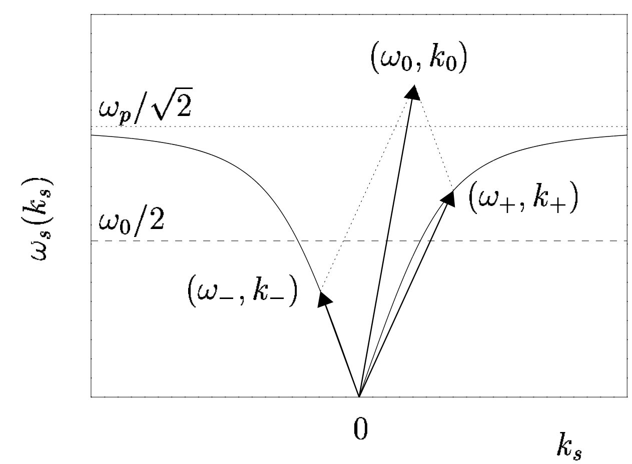

Two–surface wave decay

In *nonlinear* mode conversion, e.g. a **three-wave process**, phase matching at a planar surface is possible

$$\omega_0 = \omega_+ + \omega_-$$
$$k_0 = k_+ + k_-$$

One expects $\omega_0 = \omega_L$,
$k_0 = k_L \sin\theta \rightarrow \omega_\pm = \omega_L/2 \pm \delta\omega$

However, also the $\mathbf{v}\times\mathbf{B}$ force at $2\omega_L$ may drive TSWD at normal incidence: $k_+ = -k_-$, $\omega_\pm = \omega_L$.
[Macchi et al, PRL **87**, 205004 (2001); Phys. Plasmas **9**, 1704 (2002).]

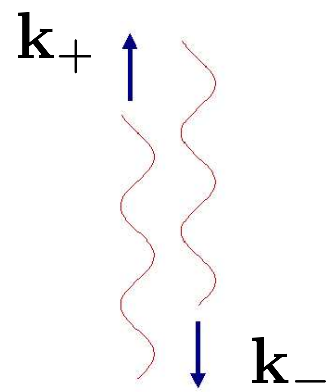

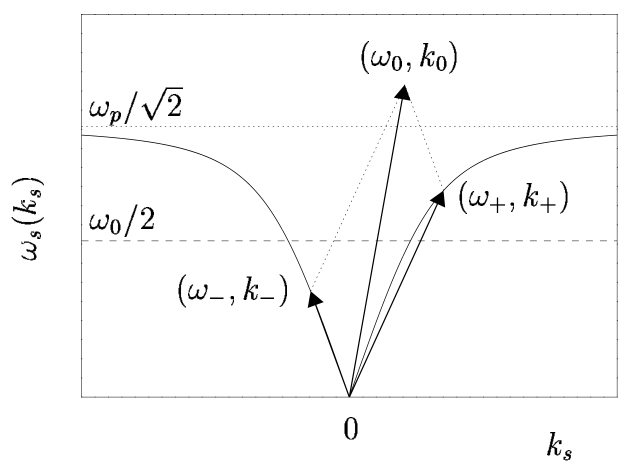

Numerical observations: "$\mathrm{v} \times \mathrm{B}$"–driven TSWD

Numerical observations: "$\mathbf{v} \times \mathbf{B}$"–driven TSWD

2D Simulations for s-polarization and normal laser incidence show the generation of a standing surface wave:

Numerical observations: "$\mathbf{v} \times \mathbf{B}$"–driven TSWD

2D Simulations for s-polarization and normal laser incidence show the generation of a standing surface wave:evidence of a "$2\omega \longrightarrow \omega + \omega$" TSWD pumped by the $\mathbf{v} \times \mathbf{B}$ force at 2ω.

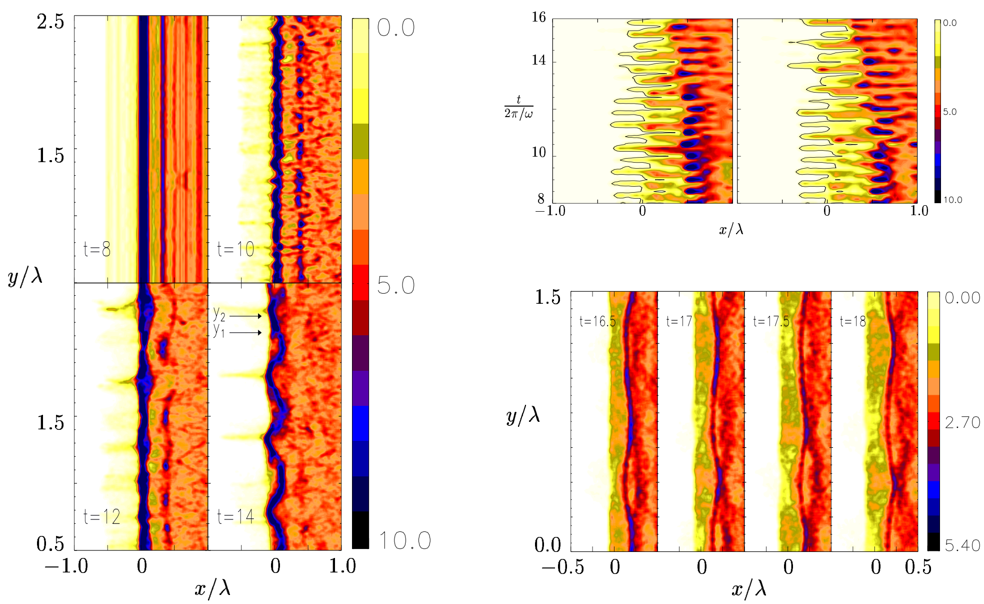

“Funneling” and focusing of fast electrons

“Funneling” and focusing of fast electrons

2D Vlasov simulations [Ruhl, Macchi et al, PRL **82**, 2095 (1999)]

“Funneling” and focusing of fast electrons

2D Vlasov simulations [Ruhl, Macchi et al, PRL **82**, 2095 (1999)]

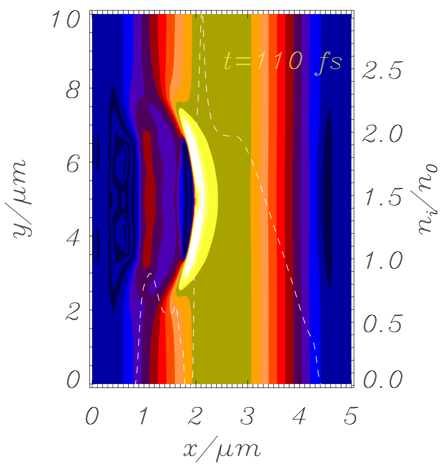

The radiation pressure modifies the plasma profile (hole boring).

“Funneling” and focusing of fast electrons

2D Vlasov simulations [Ruhl, Macchi et al, PRL **82**, 2095 (1999)]

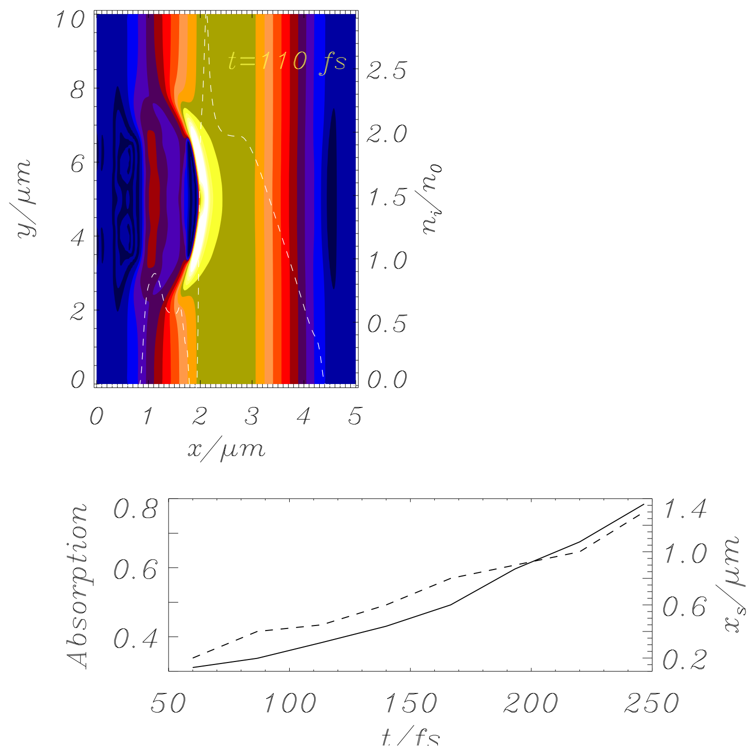

The radiation pressure modifies the plasma profile (hole boring).

A time–dependent, increasing absorption is found.

“Funneling” and focusing of fast electrons

2D Vlasov simulations [Ruhl, Macchi et al, PRL **82**, 2095 (1999)]

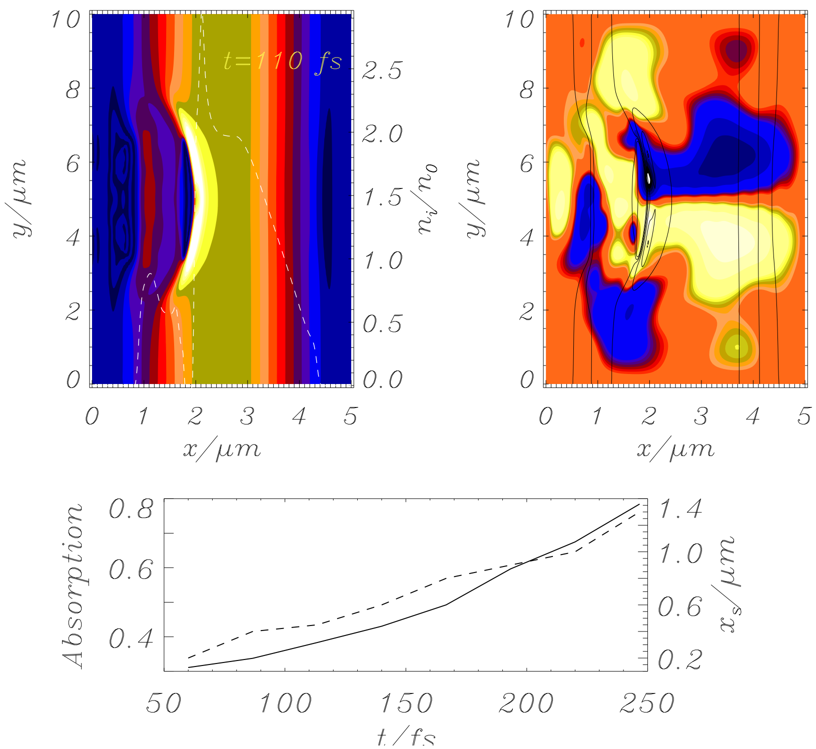

The radiation pressure modifies the plasma profile (hole boring).

A time–dependent, increasing absorption is found.

“Funneling” and focusing of fast electrons

2D Vlasov simulations [Ruhl, Macchi et al, PRL **82**, 2095 (1999)]

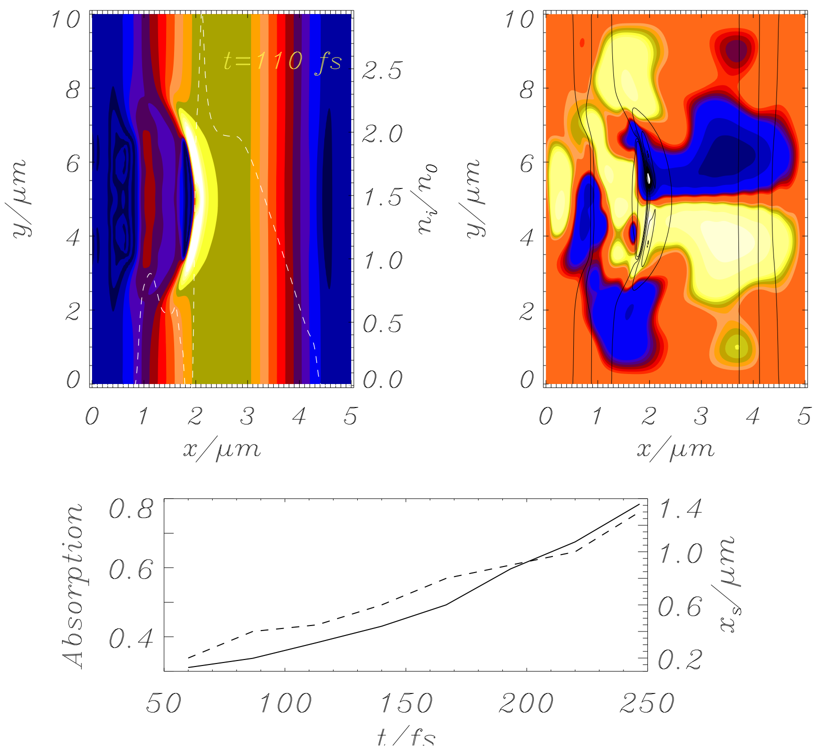

The radiation pressure modifies the plasma profile (hole boring).

A time–dependent, increasing absorption is found.

The fast electrons are focused by the deformed surface (“funnel effect”) and collimated by self–generated magnetic fields.

Pioneering numerical work: Wilks et al, PRL 1992.

"Funneling" and focusing of fast electrons

2D Vlasov simulations [Ruhl, Macchi et al, PRL **82**, 2095 (1999)]

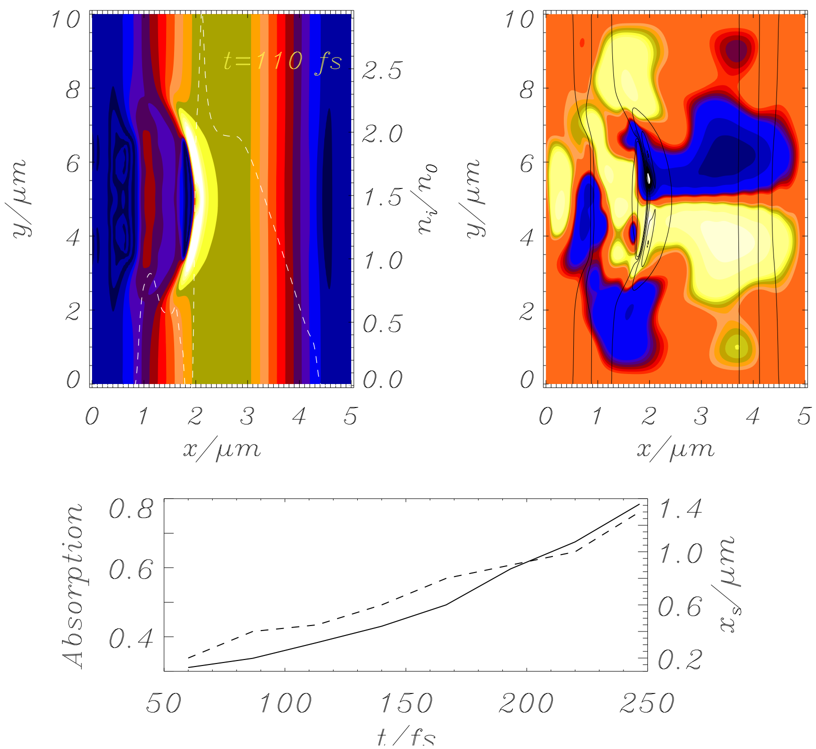

The radiation pressure modifies the plasma profile (hole boring).

A time–dependent, increasing absorption is found.

The fast electrons are focused by the deformed surface ("funnel effect") and collimated by self–generated magnetic fields.

Pioneering numerical work: Wilks et al, PRL 1992.

Filaments and corrugations

Filaments and corrugations

n_i

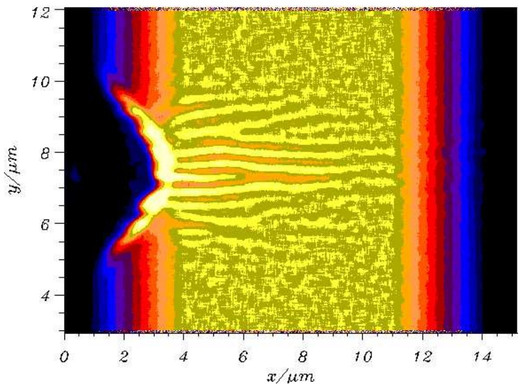

Filaments and corrugations

n_i

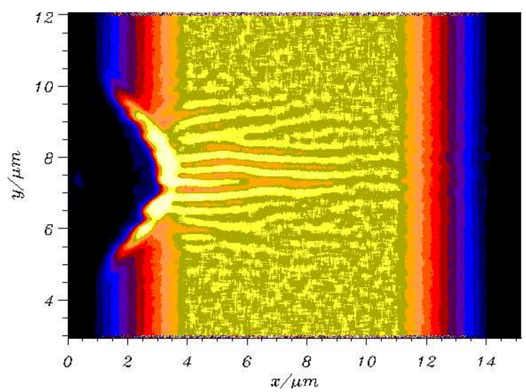

B_z

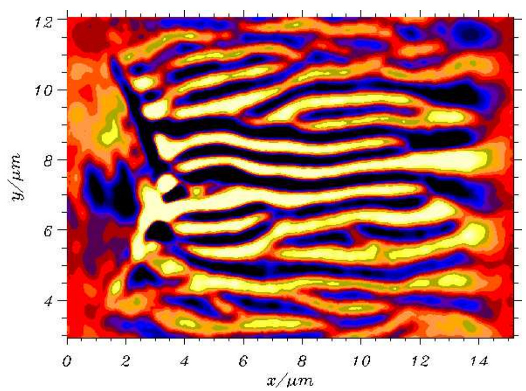

Filaments and corrugations

n_i

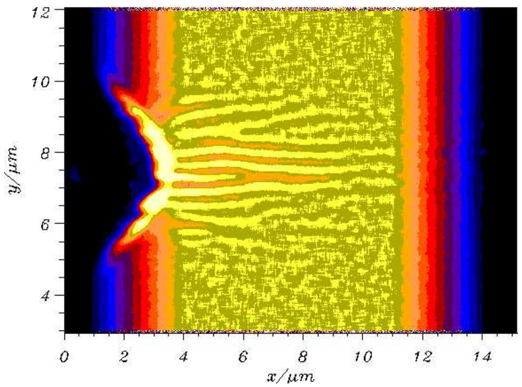

B_z

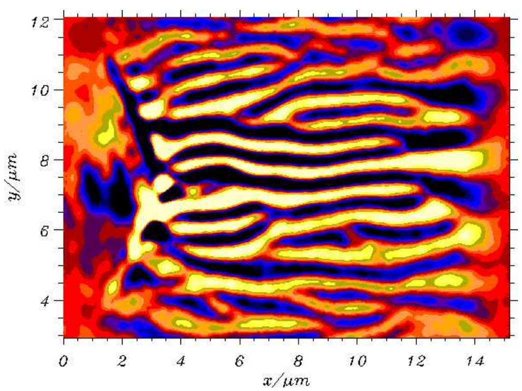

PIC simulations by H. Ruhl,
in Mulser et al., Las. Phys (1999).

Filaments and corrugations

n_i

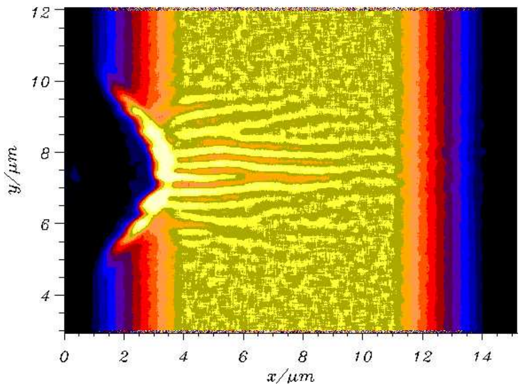

B_z

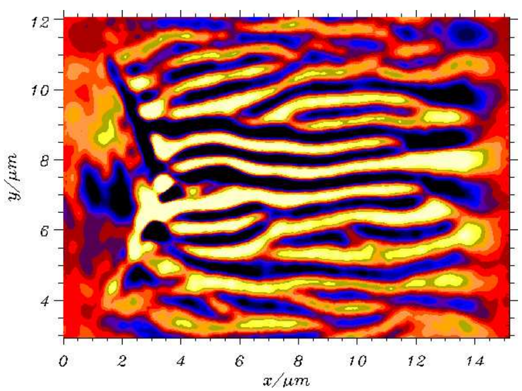

PIC simulations by H. Ruhl,
in Mulser et al., Las. Phys (1999).

- breakup of electron current into many filaments

Filaments and corrugations

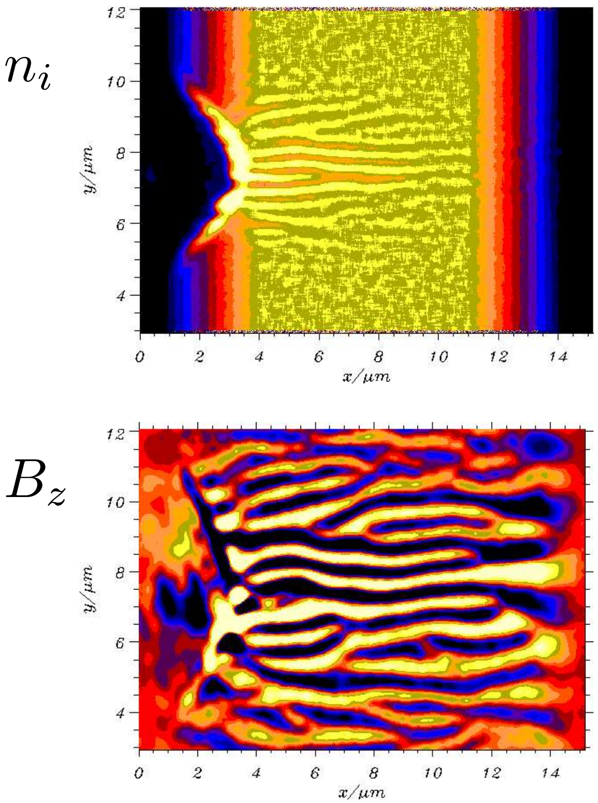

PIC simulations by H. Ruhl,
in Mulser et al., Las. Phys (1999).

- breakup of electron current into many filaments

- filament size scales with laser wavelength

Filaments and corrugations

n_i

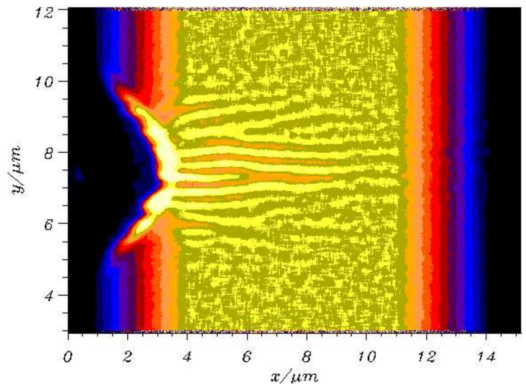

B_z

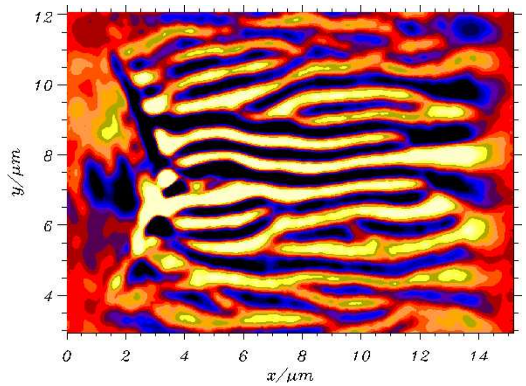

PIC simulations by H. Ruhl,
in Mulser et al., Las. Phys (1999).

- breakup of electron current into many filaments

- filament size scales with laser wavelength

- spatial correlation with surface corrugations

Where do corrugations come from?

Where do corrugations come from?

Experiments at high intensity show the onset of surface corrugations in a very short time (≤ 30 fs).

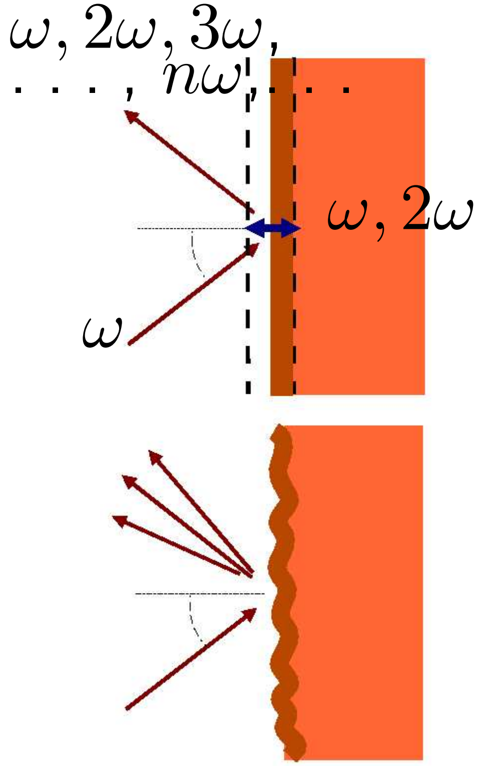

Where do corrugations come from?

Experiments at high intensity show the onset of surface corrugations in a very short time (≤ 30 fs).
This is too fast for Rayleigh–Taylor–like instabilities with
$\Gamma_{RT} \simeq \sqrt{k_{RT} g} \simeq (400 \text{ fs})^{-1}$
for $2\pi/k_{RT} \simeq \lambda_L = 1\ \mu$m

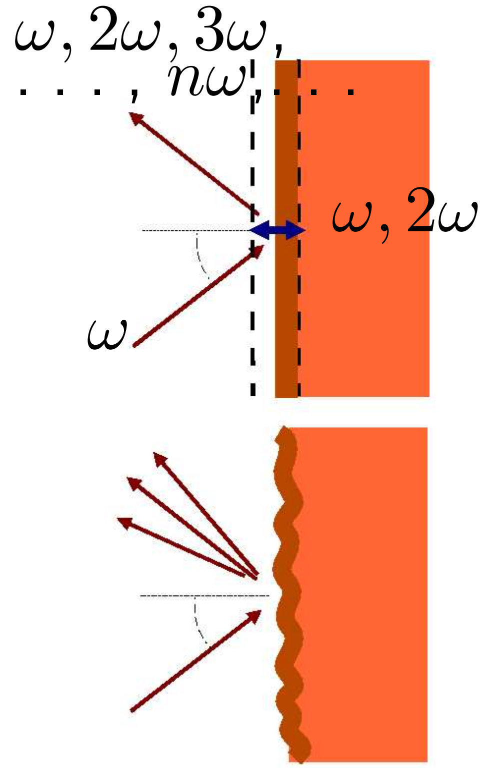

Where do corrugations come from?

Experiments at high intensity show the onset of surface corrugations in a very short time (≤ 30 fs).
This is too fast for Rayleigh–Taylor–like instabilities with
$\Gamma_{RT} \simeq \sqrt{k_{RT} g} \simeq (400 \text{ fs})^{-1}$
for $2\pi/k_{RT} \simeq \lambda_L = 1$ μm
(even if $g \simeq 10^{20}$ cm/s^2 !)

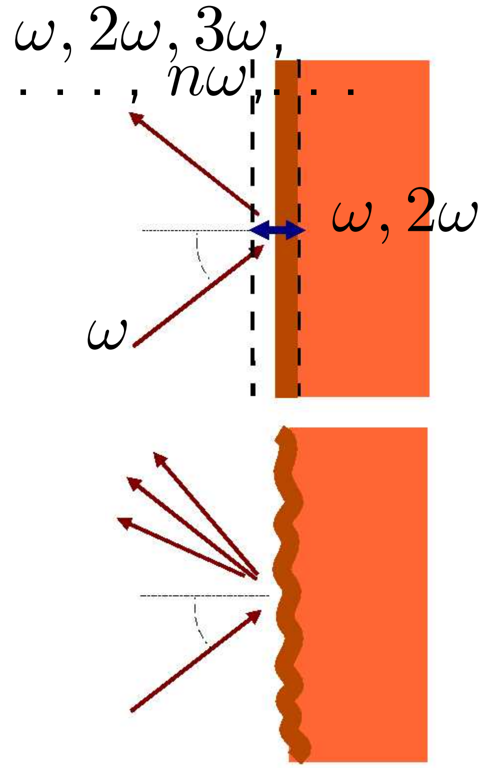

Where do corrugations come from?

Experiments at high intensity show the onset of surface corrugations in a very short time (≤ 30 fs).
This is too fast for Rayleigh–Taylor–like instabilities with
$\Gamma_{RT} \simeq \sqrt{k_{RT}g} \simeq (400\ \text{fs})^{-1}$
for $2\pi/k_{RT} \simeq \lambda_L = 1\ \mu$m
(even if $g \simeq 10^{20}$ cm/s^2 !)
$\Rightarrow$ the mechanism must be of electronic nature.

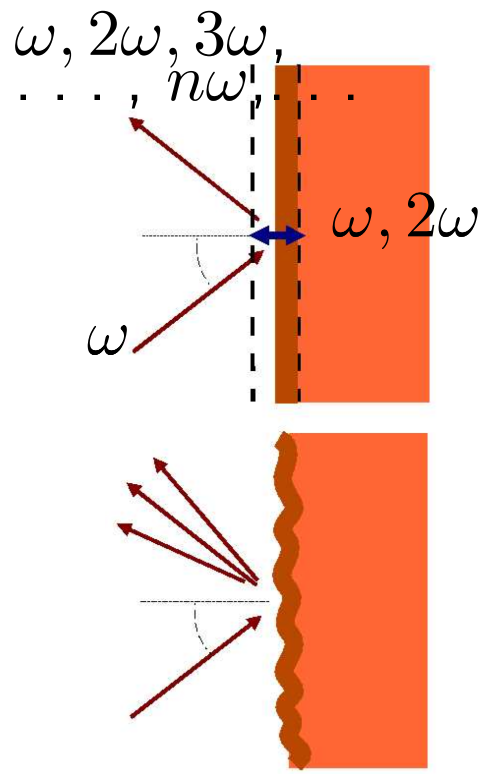

Where do corrugations come from?

Experiments at high intensity show the onset of surface corrugations in a very short time (≤ 30 fs).
This is too fast for Rayleigh–Taylor–like instabilities with
$\Gamma_{RT} \simeq \sqrt{k_{RT} g} \simeq (400 \text{ fs})^{-1}$
for $2\pi/k_{RT} \simeq \lambda_L = 1\ \mu$m
(even if $g \simeq 10^{20}$ cm/s^2 !)
$\Rightarrow$ the mechanism must be of electronic nature.
The effect is detrimental to high harmonic generation from "moving mirrors".

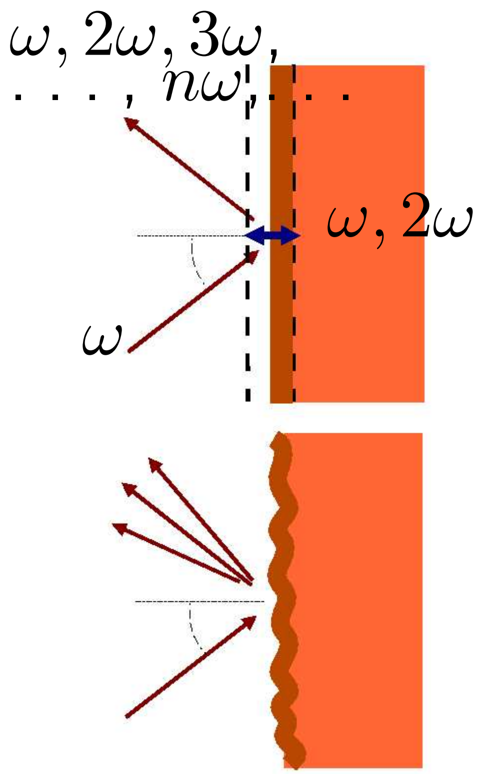

Fast electron transport

Fast electron transport

The current j_f of "fast" electrons entering the target is huge:

Fast electron transport

The current j_f of "fast" electrons entering the target is huge:

Laser irradiance $I\lambda^2 = 10^{18} - 10^{20}$ W cm$^{-2}\mu$m^2 i.e. $a_0 = 0.85 - -8.5$

Fast electron transport

The current j_f of "fast" electrons entering the target is huge:

Laser irradiance $I\lambda^2 = 10^{18} - 10^{20}$ W cm$^{-2}\mu$m^2 i.e. $a_0 = 0.85 - -8.5$

Energy per electron $\mathcal{E}_f \approx (\sqrt{1 + a_0^2} - 1)m_e c^2 \simeq 150$ keV $- -3.8$ MeV

Fast electron transport

The current j_f of "fast" electrons entering the target is huge:

Laser irradiance $I\lambda^2 = 10^{18} - 10^{20}$ W cm$^{-2}\mu$m^2 i.e. $a_0 = 0.85 - -8.5$

Energy per electron $\mathcal{E}_f \approx (\sqrt{1 + a_0^2} - 1)m_e c^2 \simeq 150$ keV $- -3.8$ MeV

Flux energy balance: $A_f I_L = n_f \mathcal{E}_f v_f$

Fast electron transport

The current j_f of "fast" electrons entering the target is huge:

Laser irradiance $I\lambda^2 = 10^{18} - 10^{20}$ W cm$^{-2}\mu$m^2 i.e. $a_0 = 0.85 - -8.5$

Energy per electron $\mathcal{E}_f \approx (\sqrt{1+a_0^2} - 1)m_e c^2 \simeq 150$ keV $- -3.8$ MeV

Flux energy balance: $A_f I_L = n_f \mathcal{E}_f v_f$with absorption $A_f \approx 10\%$ yields

$n_f \approx 1.8 \times 10^{20} - 5 \times 10^{20}$ cm^{-3}, $j_f \approx 3.7 \times 10^{11} - 2.4 \times 10^{12}$ A cm^{-2}

Fast electron transport

The current j_f of "fast" electrons entering the target is huge:

Laser irradiance $I\lambda^2 = 10^{18} - 10^{20}$ W cm$^{-2}\mu$m^2 i.e. $a_0 = 0.85 - -8.5$

Energy per electron $\mathcal{E}_f \approx (\sqrt{1+a_0^2} - 1)m_e c^2 \simeq 150$ keV $- -3.8$ MeV

Flux energy balance: $A_f I_L = n_f \mathcal{E}_f v_f$with absorption $A_f \approx 10\%$ yields

$n_f \approx 1.8 \times 10^{20} - 5 \times 10^{20}$ cm^{-3}, $j_f \approx 3.7 \times 10^{11} - 2.4 \times 10^{12}$ A cm^{-2}

Over a focal spot with radius $r_s \simeq 5\mu$m, $I_f \approx 2.9 \times 10^5 - -1.8 \times 10^6$ A

Fast electron transport

The current j_f of "fast" electrons entering the target is huge:

Laser irradiance $I\lambda^2 = 10^{18} - 10^{20}$ W cm$^{-2}\mu$m^2 i.e. $a_0 = 0.85 - -8.5$

Energy per electron $\mathcal{E}_f \approx (\sqrt{1+a_0^2} - 1)m_e c^2 \simeq 150$ keV $- -3.8$ MeV

Flux energy balance: $A_f I_L = n_f \mathcal{E}_f v_f$with absorption $A_f \approx 10\%$ yields

$n_f \approx 1.8 \times 10^{20} - 5 \times 10^{20}$ cm^{-3}, $j_f \approx 3.7 \times 10^{11} - 2.4 \times 10^{12}$ A cm^{-2}

Over a focal spot with radius $r_s \simeq 5\mu$m, $I_f \approx 2.9 \times 10^5 - -1.8 \times 10^6$ A

$\Rightarrow$ *current neutralization* by "background" electrons is needed to avoid "self-stopping" by associated *electric* and *magnetic* fields.

Current neutralization

Current neutralization

Neutralization of the "fast" electron current $\mathbf{j}_f$ by a current $\mathbf{j}_s$ of "slow" background electrons within a time:

$$\tau_c \approx \begin{cases} \nu_{eI}/\omega_p^2 & \text{(collisional plasma)}, \\ 1/\omega_p & \text{(collisionless plasma)} \end{cases}$$

Current neutralization

Neutralization of the "fast" electron current $\mathbf{j}_f$ by a current $\mathbf{j}_s$ of "slow" background electrons within a time:

$$\tau_c \approx \begin{cases} \nu_{eI}/\omega_p^2 & \text{(collisional plasma),} \\ 1/\omega_p & \text{(collisionless plasma)} \end{cases}$$

Typically $\tau_c < 1$ fs when $n_s \geq 10^{22}$ cm$^{-3} \gg n_f$.

Current neutralization

Neutralization of the "fast" electron current $\mathbf{j}_f$ by a current $\mathbf{j}_s$ of "slow" background electrons within a time:

$$\tau_c \approx \begin{cases} \nu_{eI}/\omega_p^2 & \text{(collisional plasma),} \\ 1/\omega_p & \text{(collisionless plasma)} \end{cases}$$

Typically $\tau_c < 1$ fs when $n_s \geq 10^{22}$ cm$^{-3} \gg n_f$.

The equilibrium condition of opposite, neutralizing currents $\mathbf{j}_f = -\mathbf{j}_s$ is however affected by instabilities and additional effects.

Where do filaments come from?

Where do filaments come from?

In a collisions–dominated plasma current filamentation may be due to the electrothermal instability [Haines, PRL **47**, 917 (1981).]

Where do filaments come from?

In a collisions–dominated plasma current filamentation may be due to the electrothermal instability [Haines, PRL **47**, 917 (1981).]

In the regime of relativistic fast electrons, the "Weibel", collisionless filamentation instability is often invoked.

Where do filaments come from?

In a collisions–dominated plasma current filamentation may be due to the electrothermal instability [Haines, PRL **47**, 917 (1981).]

In the regime of relativistic fast electrons, the "Weibel", collisionless filamentation instability is often invoked.

Another possibility is that the filamentary structure already arises during the acceleration stage due to surface instabilities [Macchi et. al].

Where do filaments come from?

In a collisions–dominated plasma current filamentation may be due to the electrothermal instability [Haines, PRL **47**, 917 (1981).]

In the regime of relativistic fast electrons, the "Weibel", collisionless filamentation instability is often invoked.

Another possibility is that the filamentary structure already arises during the acceleration stage due to surface instabilities [Macchi et. al].

So far, experimental indications are not exhaustive

Where do filaments come from?

In a collisions–dominated plasma current filamentation may be due to the electrothermal instability [Haines, PRL **47**, 917 (1981).]

In the regime of relativistic fast electrons, the "Weibel", collisionless filamentation instability is often invoked.

Another possibility is that the filamentary structure already arises during the acceleration stage due to surface instabilities [Macchi et. al].

So far, experimental indications are not exhaustive(Do filaments actually occur? What is their scale? What is the driving mechanism? . . .)

On the “Weibel” current filamentation (CF) instability

On the “Weibel” current filamentation (CF) instability

An equilibrium configuration with two electron populations carrying opposite and neutralizing currents $(n_1 v_1 = -n_2 v_2)$ is unstable due to electromagnetic, transverse perturbations (Weibel transverse instability)

On the "Weibel" current filamentation (CF) instability

An equilibrium configuration with two electron populations carrying opposite and neutralizing currents $(n_1 v_1 = -n_2 v_2)$ is unstable due to electromagnetic, transverse perturbations (Weibel transverse instability)and for electrostatic, longitudinal perturbations (*two–stream* instability).

On the "Weibel" current filamentation (CF) instability

An equilibrium configuration with two electron populations carrying opposite and neutralizing currents $(n_1 v_1 = -n_2 v_2)$ is unstable due to electromagnetic, transverse perturbations (Weibel transverse instability)and for electrostatic, longitudinal perturbations (*two–stream* instability).

In the relativistic regime $(v_1 \rightarrow c)$ the longitudinal modes are coupled to the transverse ones for asymmetrical initial equilibria $(v_1 \neq v_2)$ [Califano et al. PRE 1998].

On the "Weibel" current filamentation (CF) instability

An equilibrium configuration with two electron populations carrying opposite and neutralizing currents ($n_1 v_1 = -n_2 v_2$) is unstable due to electromagnetic, transverse perturbations (Weibel transverse instability)and for electrostatic, longitudinal perturbations (*two–stream* instability).

In the relativistic regime ($v_1 \rightarrow c$) the longitudinal modes are coupled to the transverse ones for asymmetrical initial equilibria ($v_1 \neq v_2$) [Califano et al. PRE 1998].
The most unstable wavevector $\mathbf{k} = (k_{\|}, \mathbf{k}_{\perp})$ has $k_{\perp} \neq 0$
$\rightarrow$ fields structures have finite length along the beams direction.

On the “Weibel” current filamentation (CF) instability

An equilibrium configuration with two electron populations carrying opposite and neutralizing currents $(n_1 v_1 = -n_2 v_2)$ is unstable due to electromagnetic, transverse perturbations (Weibel transverse instability)and for electrostatic, longitudinal perturbations (*two–stream* instability).

In the relativistic regime $(v_1 \rightarrow c)$ the longitudinal modes are coupled to the transverse ones for asymmetrical initial equilibria $(v_1 \neq v_2)$ [Califano et al. PRE 1998].
The most unstable wavevector $\mathbf{k} = (k_{\|}, \mathbf{k}_{\perp})$ has $k_{\perp} \neq 0$
$\rightarrow$ fields structures have finite length along the beams direction.

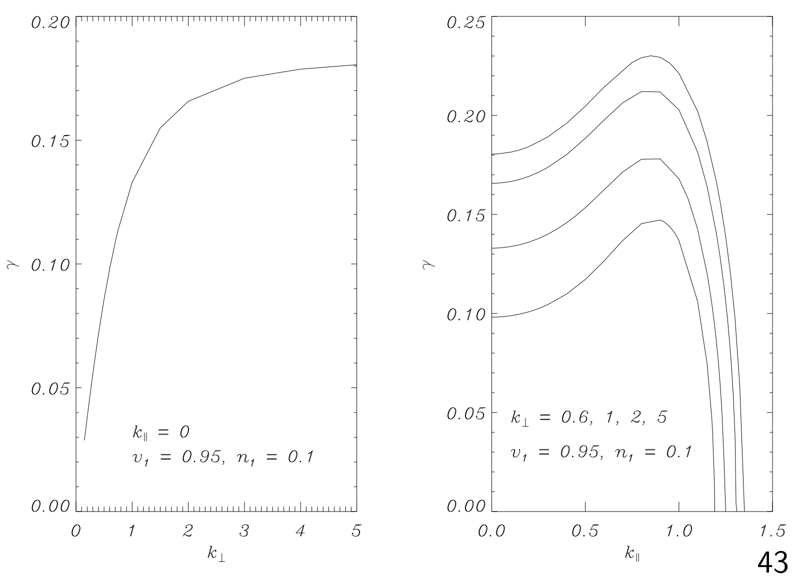

3D fluid simulation of the CF instability

3D fluid simulation of the CF instability

Simulation example:
$n_1/n_2 = 9$, $v_1 = 0.95c$, $v_2 = -0.10556c$.

3D fluid simulation of the CF instability

Simulation example:

$n_1/n_2 = 9$, $v_1 = 0.95c$, $v_2 = -0.10556c$.

Figure shows isosurfaces of A_z (vector potential component along beam direction), which is representative of the magnetic field structure because $B_z \ll (B_x, B_y)$ is found.

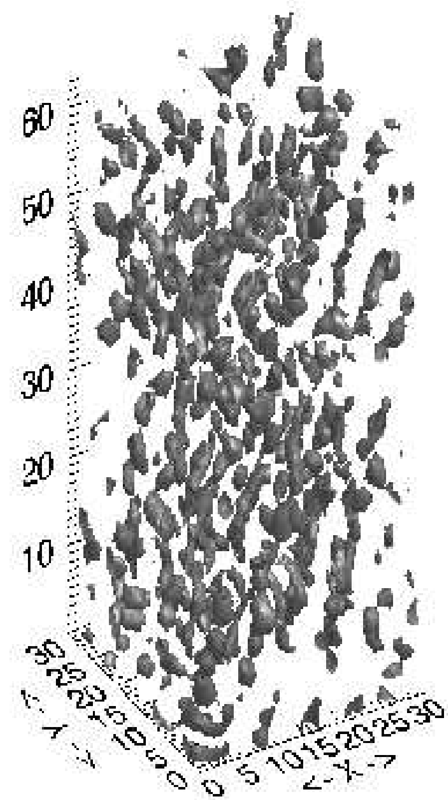

3D fluid simulation of the CF instability

Simulation example:

$n_1/n_2 = 9$, $v_1 = 0.95c$, $v_2 = -0.10556c$.

Figure shows isosurfaces of A_z (vector potential component along beam direction), which is representative of the magnetic field structure because $B_z \ll (B_x, B_y)$ is found.

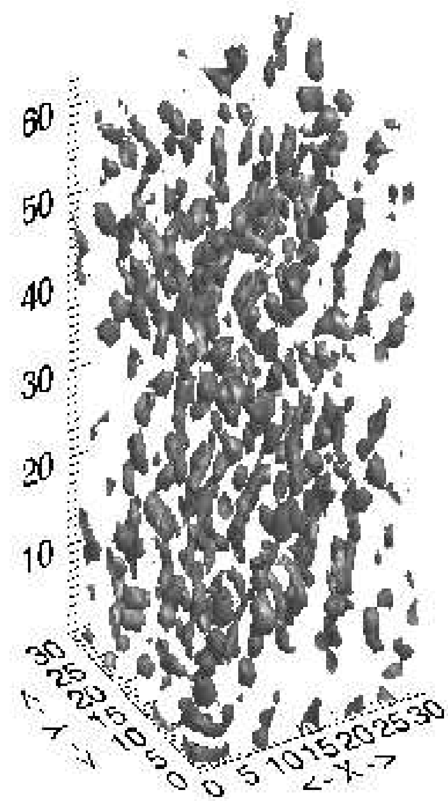

3D "bubble–like" magnetic structures are formed with typical length scales $\sim d_e = c/\omega_p$. No extended filaments in beam direction are observed.

[Simulations by F. Califano;
Macchi et al, Nucl. Fus. **43**, 362 (2003)]

TSWD and fast electron generation

TSWD and fast electron generation

- We have seen that electron heating at a step laser–plasma interface is dominated by the force component normal to the surface.

TSWD and fast electron generation

- We have seen that electron heating at a step laser–plasma interface is dominated by the force component normal to the surface.
- Surface waves excited in “grating” targets have strong normal components and affect electron heating

TSWD and fast electron generation

- We have seen that electron heating at a step laser–plasma interface is dominated by the force component normal to the surface.

- Surface waves excited in "grating" targets have strong normal components and affect electron heating
  [C. Riconda et al, Phys. Plasmas **11**, 1669 (2004)]

TSWD and fast electron generation

- We have seen that electron heating at a step laser–plasma interface is dominated by the force component normal to the surface.

- Surface waves excited in "grating" targets have strong normal components and affect electron heating
  [C. Riconda et al, Phys. Plasmas **11**, 1669 (2004)]

- The standing SW produced by the TSWD parametric instability may lead to localized, spatially periodic heating of electrons.

TSWD and fast electron generation

- We have seen that electron heating at a step laser–plasma interface is dominated by the force component normal to the surface.

- Surface waves excited in "grating" targets have strong normal components and affect electron heating
  [C. Riconda et al, Phys. Plasmas **11**, 1669 (2004)]

- The standing SW produced by the TSWD parametric instability may lead to localized, spatially periodic heating of electrons.

$\longrightarrow$ We performed test particle simulations of electron motion in the pump+SW fields involved in TSWD.

Enhanced acceleration near SW maxima

Enhanced acceleration near SW maxima

Top: (y, p_x) phase space projections from PIC simulations at two subsequent times

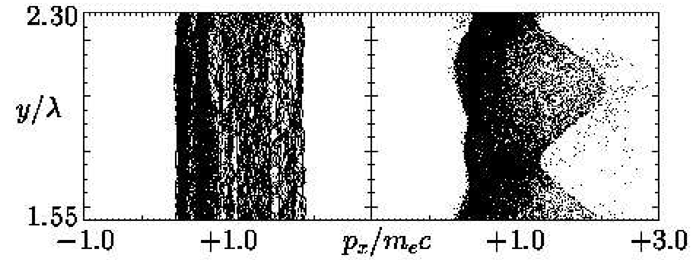

Enhanced acceleration near SW maxima

Top: (y, p_x) phase space projections from PIC simulations at two subsequent times

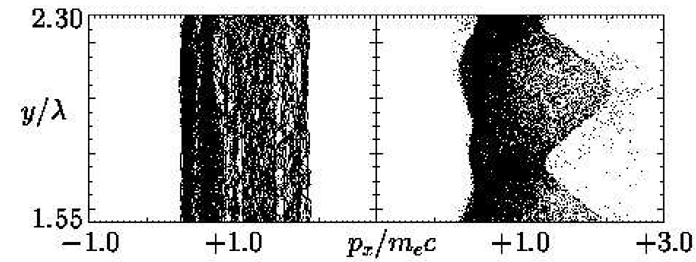

Bottom: same phase space projection from test particle simulations

Enhanced acceleration near SW maxima

Top: (y, p_x) phase space projections from PIC simulations at two subsequent times

Bottom: same phase space projection from test particle simulations

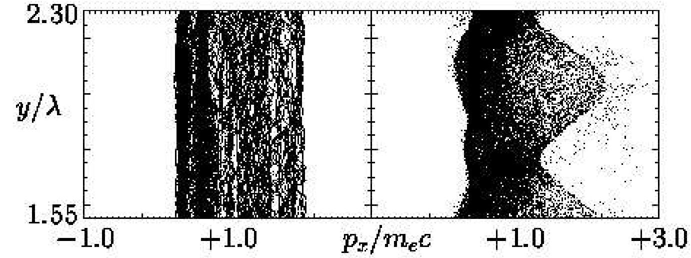

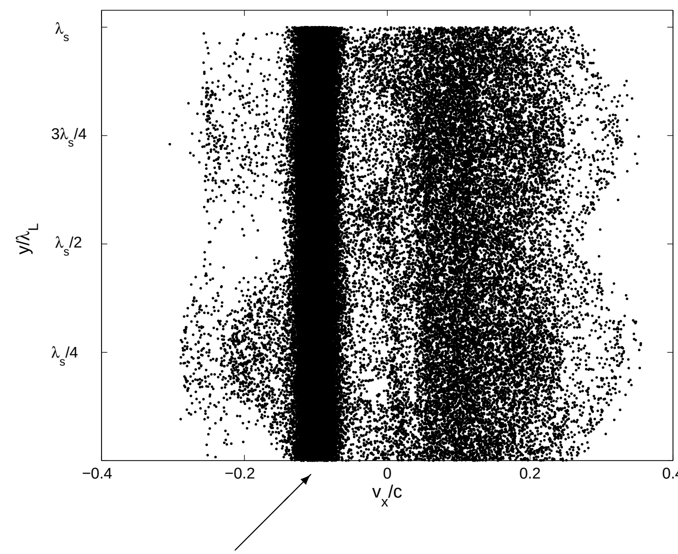

"Black stripe": initial conditions

Enhanced acceleration near SW maxima

Top: (y, p_x) phase space projections from PIC simulations at two subsequent times

Bottom: same phase space projection from test particle simulations

PIC and test-particle simulations both show enhanced electron heating near SW maxima

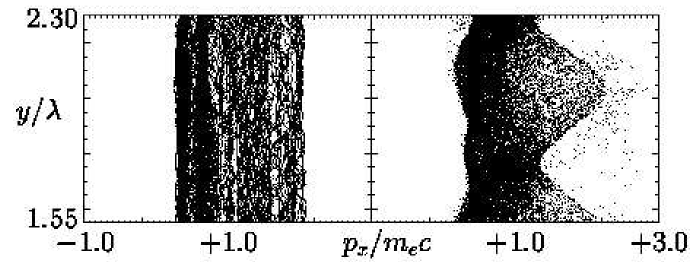

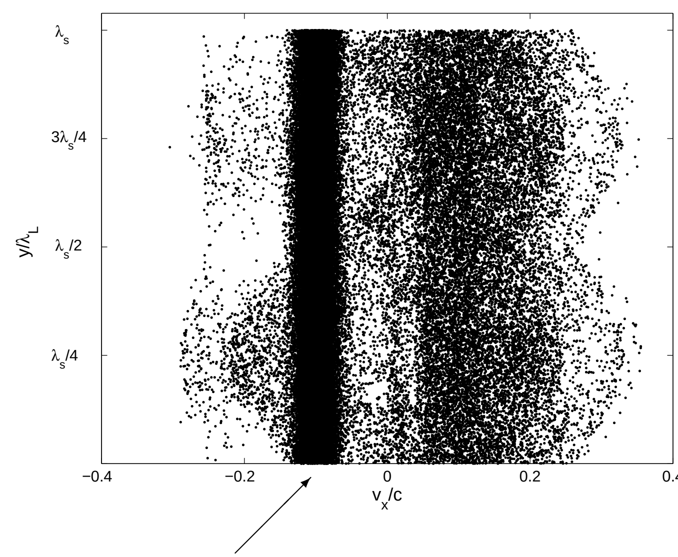

"Black stripe": initial conditions

Enhanced acceleration near SW maxima

Top: (y, p_x) phase space projections from PIC simulations at two subsequent times

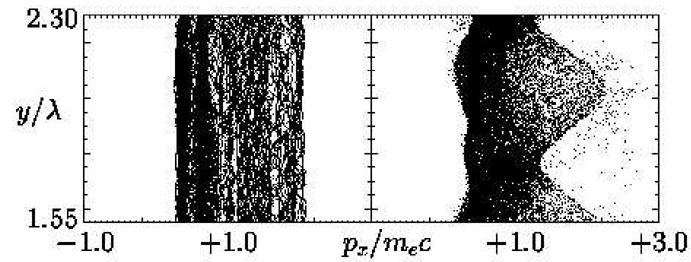

Bottom: same phase space projection from test particle simulations

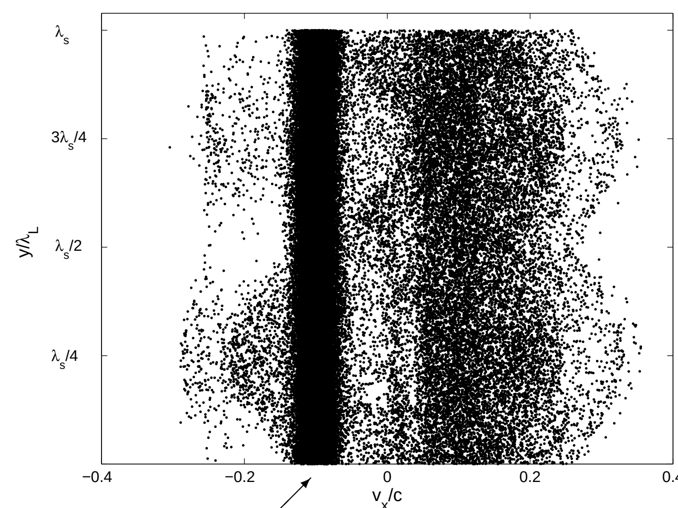

"Black stripe": initial conditions

PIC and test-particle simulations both show enhanced electron heating near SW maxima

A. Macchi et al, Appl. Phys. B **78**, 915 (2004).

Enhanced acceleration near SW maxima

Top: (y, p_x) phase space projections from PIC simulations at two subsequent times

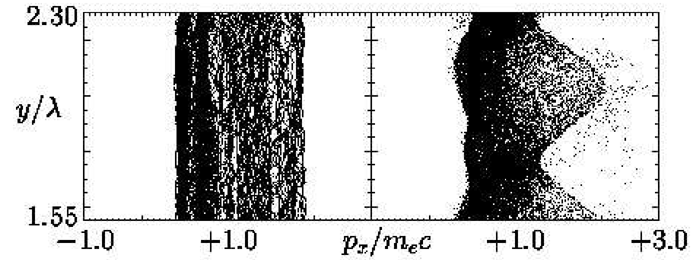

Bottom: same phase space projection from test particle simulations

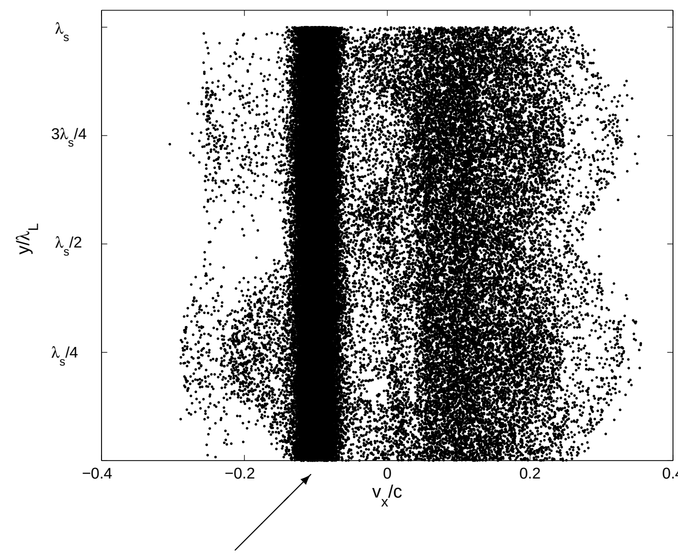

"Black stripe": initial conditions

PIC and test-particle simulations both show enhanced electron heating near SW maxima

A. Macchi et al, Appl. Phys. B **78**, 915 (2004).

Induced modulation of electron current

Induced modulation of electron current

The electron current density $J_{e,x}$ is reconstructed from test particle phase space.

Induced modulation of electron current

The electron current density $J_{e,x}$ is reconstructed from test particle phase space.

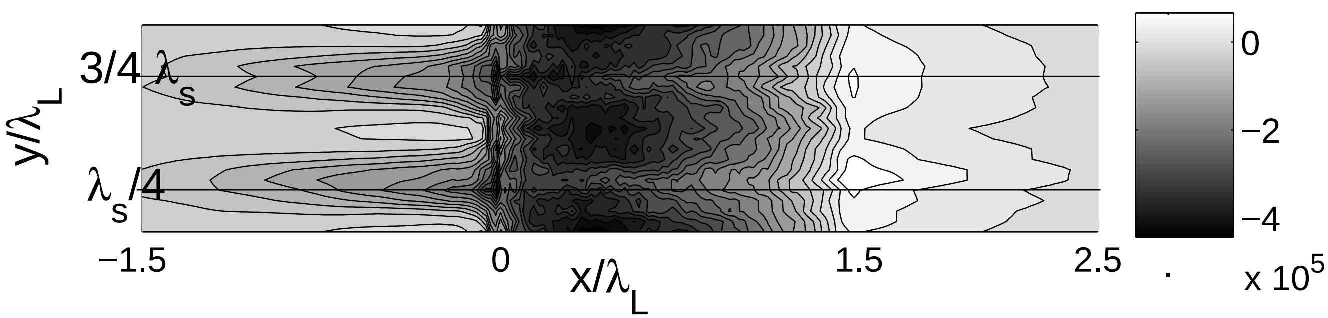

$J_{e,x}$ is spatially modulated in y with the SW periodicity.

Induced modulation of electron current

The electron current density $J_{e,x}$ is reconstructed from test particle phase space.

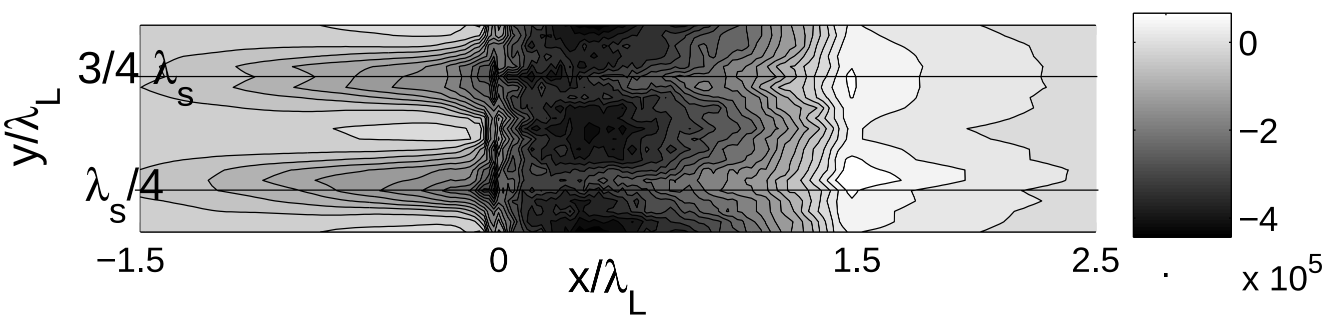

$J_{e,x}$ is spatially modulated in y with the SW periodicity.

Spatial imprint for current filamentation?

Laser–cluster interaction

Laser–cluster interaction

Clusters bridge the gap between bulk material and single atoms:

Laser–cluster interaction

Clusters bridge the gap between bulk material and single atoms:

radius $R \approx 10^{-6} - 10^{-7}$ cm, number of atoms $N \approx 10^2 - 10^6$

Laser–cluster interaction

Clusters bridge the gap between bulk material and single atoms:

radius $R \approx 10^{-6} - 10^{-7}$ cm, number of atoms $N \approx 10^{2} - 10^{6}$

density $n \approx 10^{22} - 10^{23}$ cm^{-3}, average $\bar{n} \approx 10^{18}$ cm^{-3} (gas).

Laser–cluster interaction

Clusters bridge the gap between bulk material and single atoms:

radius $R \approx 10^{-6} - 10^{-7}$ cm, number of atoms $N \approx 10^2 - 10^6$

density $n \approx 10^{22} - 10^{23}$ cm^{-3}, average $\bar{n} \approx 10^{18}$ cm^{-3} (gas).

$(n_e/n_c)(R/\lambda) \ll 1$ for $\lambda \approx 1$ μm

Laser–cluster interaction

Clusters bridge the gap between bulk material and single atoms:

radius $R \approx 10^{-6} - 10^{-7}$ cm, number of atoms $N \approx 10^2 - 10^6$

density $n \approx 10^{22} - 10^{23}$ cm^{-3}, average $\bar{n} \approx 10^{18}$ cm^{-3} (gas).

$(n_e/n_c)(R/\lambda) \ll 1$ for $\lambda \approx 1$ μm

$\longrightarrow$ laser field penetrates into the cluster: *volume* interaction

Laser–cluster interaction

Clusters bridge the gap between bulk material and single atoms:

radius $R \approx 10^{-6} - 10^{-7}$ cm, number of atoms $N \approx 10^2 - 10^6$

density $n \approx 10^{22} - 10^{23}$ cm^{-3}, average $\bar{n} \approx 10^{18}$ cm^{-3} (gas).

$(n_e/n_c)(R/\lambda) \ll 1$ for $\lambda \approx 1$ μm

$\longrightarrow$ laser field penetrates into the cluster: *volume* interaction

Rapid field ionization at high intensities $\longrightarrow$ any cluster becomes a *nanoplasma*.

Laser–cluster interaction

Clusters bridge the gap between bulk material and single atoms:

radius $R \approx 10^{-6} - 10^{-7}$ cm, number of atoms $N \approx 10^2 - 10^6$

density $n \approx 10^{22} - 10^{23}$ cm^{-3}, average $\bar{n} \approx 10^{18}$ cm^{-3} (gas).

$(n_e/n_c)(R/\lambda) \ll 1$ for $\lambda \approx 1$ μm

$\longrightarrow$ laser field penetrates into the cluster: *volume* interaction

Rapid field ionization at high intensities $\longrightarrow$ any cluster becomes a *nanoplasma*.

Energy is confined (no trasport): strong heating

Enhanced absorption in clusters

Enhanced absorption in clusters

The field inside the cluster is *enhanced* with respect to the laser field due to the Mie resonance at $\omega = \omega_p/\sqrt{3}$

$$E = \frac{3E_L}{\epsilon + 2} \simeq \frac{E_L}{1 - \omega_p^2/3\omega^2 + i\omega_p^2\nu/3\omega^3}$$

Collective Mie oscillations

Enhanced absorption in clusters

The field inside the cluster is *enhanced* with respect to the laser field due to the Mie resonance at $\omega = \omega_p/\sqrt{3}$

$$E = \frac{3E_L}{\epsilon + 2} \simeq \frac{E_L}{1 - \omega_p^2/3\omega^2 + i\omega_p^2\nu/3\omega^3}$$

$t = t_1$

n_e

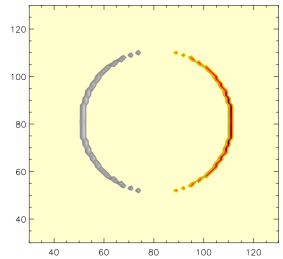

Collective Mie oscillations

Enhanced absorption in clusters

The field inside the cluster is *enhanced* with respect to the laser field due to the Mie resonance at $\omega = \omega_p/\sqrt{3}$

$$E = \frac{3E_L}{\epsilon + 2} \simeq \frac{E_L}{1 - \omega_p^2/3\omega^2 + i\omega_p^2\nu/3\omega^3}$$

$t = t_1$ $\qquad\qquad$ $t = t_1 + \pi\sqrt{3}/\omega_p$

n_e

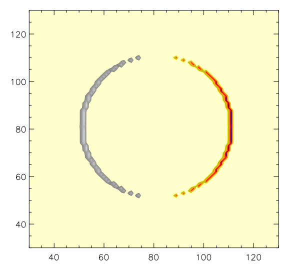

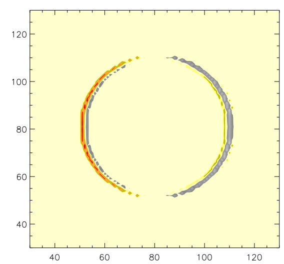

Collective Mie oscillations

Enhanced absorption in clusters

The field inside the cluster is *enhanced* with respect to the laser field due to the Mie resonance at $\omega = \omega_p/\sqrt{3}$

$$E = \frac{3E_L}{\epsilon + 2} \simeq \frac{E_L}{1 - \omega_p^2/3\omega^2 + i\omega_p^2\nu/3\omega^3}$$

$t = t_1$ $\quad\quad$ $t = t_1 + \pi\sqrt{3}/\omega_p$

n_e

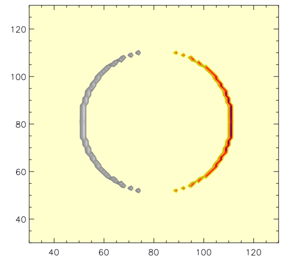

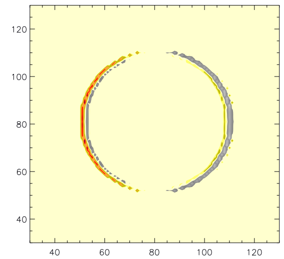

Collective Mie oscillations

In *nanoshells* the resonance frequency depends on the shell thickness and can be tuned (applications in medicine).

Ionization ignition in clusters

Ionization ignition in clusters

The ionization of clusters in short laser pulses is higher than for single atoms, because after first ionization “strong electric fields build up enhancing ionization” [Rose Petruck et al, Phys. Rev. A 55, 1182 (1997)].

Ionization ignition in clusters

The ionization of clusters in short laser pulses is higher than for single atoms, because after first ionization "strong electric fields build up enhancing ionization" [Rose Petruck et al, Phys. Rev. A 55, 1182 (1997)].

This is somewhat different from the model of the cluster as a (quasi-neutral) nanoplasma [Ditmire et al., Phys. Rev. A 53, 3379 (1996)].

Ionization ignition in clusters

The ionization of clusters in short laser pulses is higher than for single atoms, because after first ionization "strong electric fields build up enhancing ionization" [Rose Petruck et al, Phys. Rev. A 55, 1182 (1997)].

This is somewhat different from the model of the cluster as a (quasi-neutral) nanoplasma [Ditmire et al., Phys. Rev. A 53, 3379 (1996)].

What is the dynamics behind this "ionization ignition"?

Ionization ignition in clusters

The ionization of clusters in short laser pulses is higher than for single atoms, because after first ionization "strong electric fields build up enhancing ionization" [Rose Petruck et al, Phys. Rev. A 55, 1182 (1997)].

This is somewhat different from the model of the cluster as a (quasi-neutral) nanoplasma [Ditmire et al., Phys. Rev. A 53, 3379 (1996)].

What is the dynamics behind this "ionization ignition"?

A one-dimensional model of rare gas clusters has been investigated quantum mechanically by means of time-dependent density functional theory.
[D. Bauer and A. Macchi, Phys. Rev. A **68**, 033201 (2003)]

Dynamical Ionization ignition

Dynamical Ionization ignition

A wave packet bouncing between the "cluster" boundaries at the laser frequency is observed.

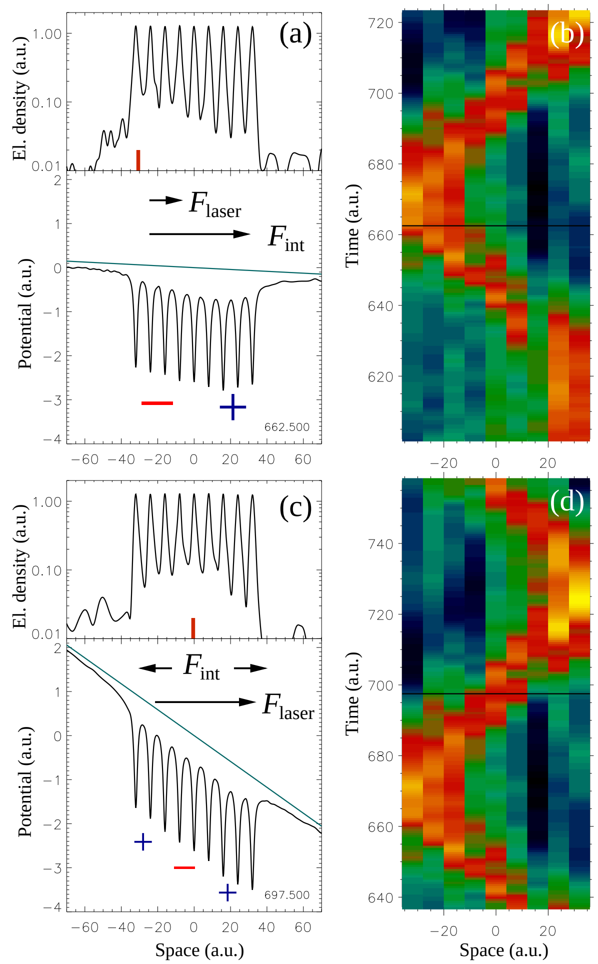

Dynamical Ionization ignition

A wave packet bouncing between the “cluster” boundaries at the laser frequency is observed.
This leads to field enhancement and thus to high absorption and ionization.

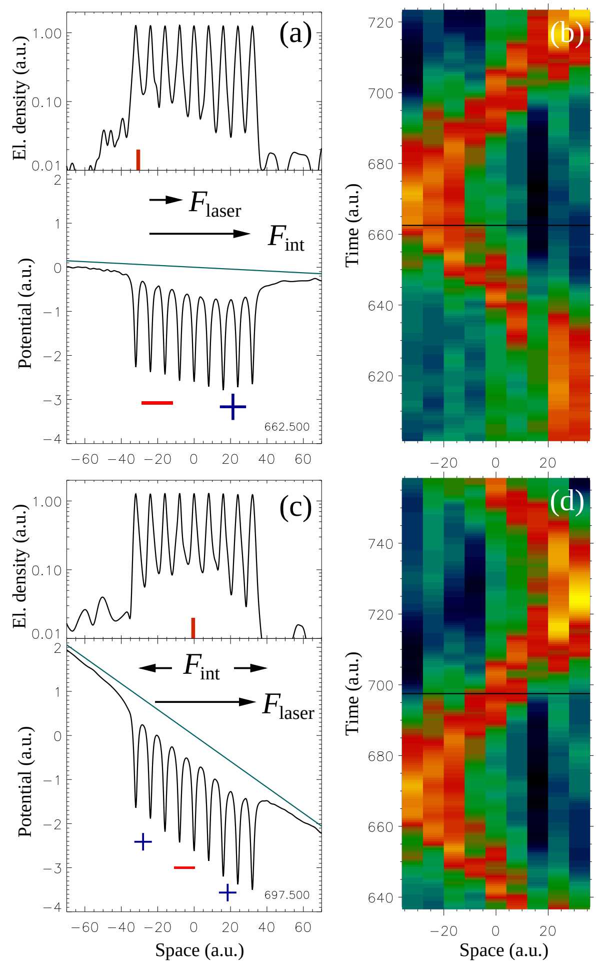

Dynamical Ionization ignition

A wave packet bouncing between the "cluster" boundaries at the laser frequency is observed.
This leads to field enhancement and thus to high absorption and ionization.
Absorption and field enhancement are collective but "not–so–resonant".

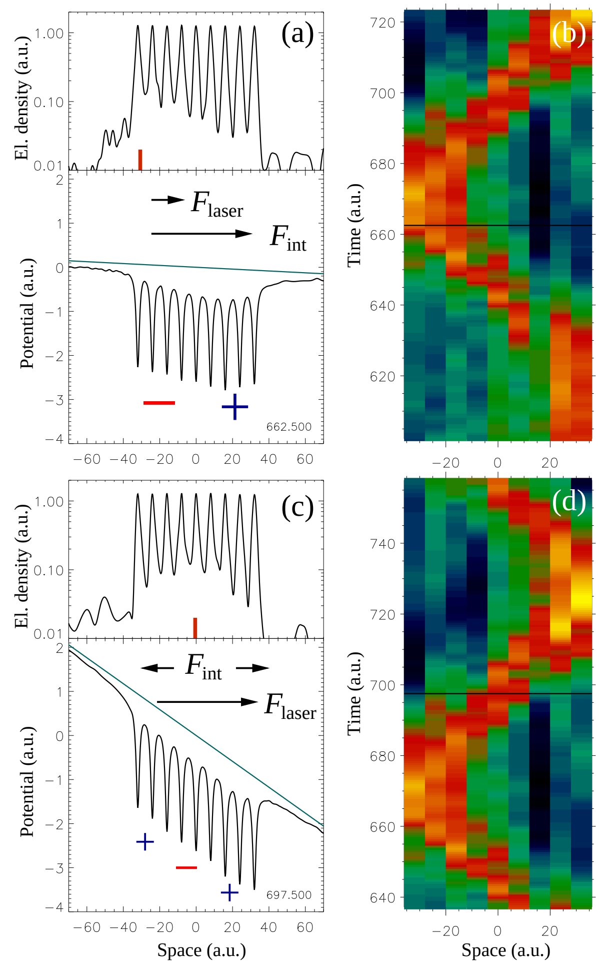

How is the wavepacket excited?

How is the wavepacket excited?

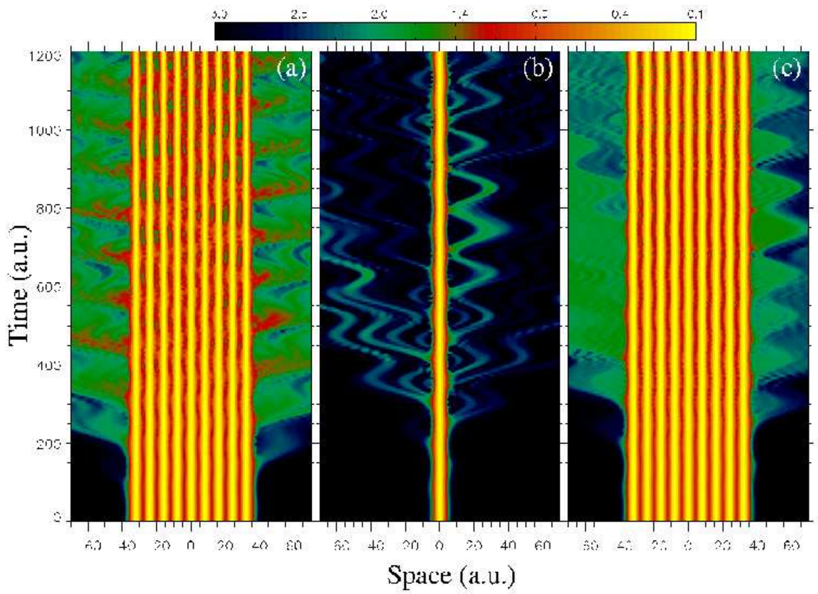

How is the wavepacket excited?

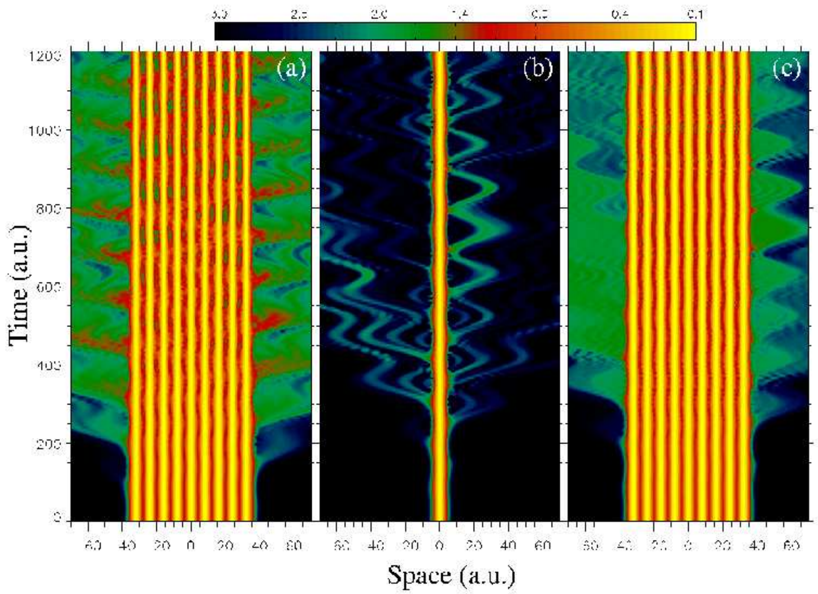

a) cluster, self-consistent field
b) single atom
c) cluster of *non–interacting* atoms

The wavepacket is excited by laser-assisted collisions with the boundaries.

How is the wavepacket excited?

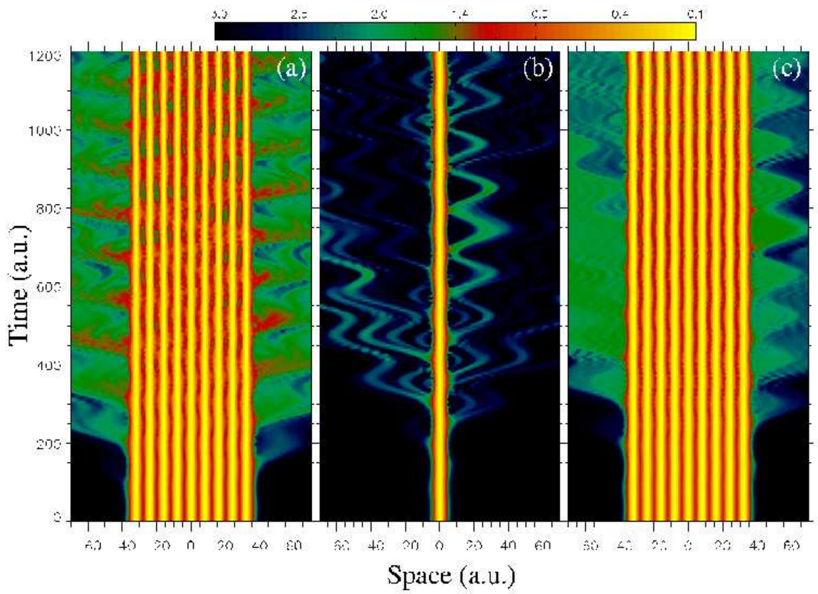

a) cluster, self-consistent field
b) single atom
c) cluster of *non–interacting* atoms

The wavepacket is excited by laser-assisted collisions with the boundaries.

The heating mechanism is reminiscent of “vacuum heating”

D. Bauer and A. Macchi, Phys. Rev. A **68**, 033201 (2003); effect also observed in 3D MD simulations: D. Bauer, preprint physics/0403016 (2004).

Acknowledgments

Acknowledgments

These slides were prepared on a Linux laptop,

Acknowledgments

These slides were prepared on a Linux laptop, using the PPower4 package to post–process a LaTeXsource,

Acknowledgments

These slides were prepared on a Linux laptop, using the PPower4 package to post–process a LaTeXsource, with some figures prepared with OpenOffice.

Acknowledgments

These slides were prepared on a Linux laptop, using the PPower4 package to post–process a LaTeXsource, with some figures prepared with OpenOffice.

This was a 100% Open–Source, Microsoft–free presentation!

Acknowledgments

These slides were prepared on a Linux laptop, using the PPower4 package to post–process a LaTeXsource, with some figures prepared with OpenOffice.

This was a 100% Open–Source, Microsoft–free presentation!

Financial Support for mobility between Italy and UK by British Council is also acknowledged.

EXTRA SLIDES

EXTRA SLIDES

Fresnel formulas for p–polarization

Fresnel formulas for p–polarization

$$\mathsf{n} = 1 - \omega_p^2/\omega^2 < 0 \qquad (\omega_p = \sqrt{4\pi n_i e^2/m_e})$$

$$B_z(x,t) = B_z(0^+)e^{iky\sin\theta - x/l_p - i\omega t} + \text{ c. c.},$$

$$E_y(x,t) = -\frac{i\omega l_p}{c} B_z(0^+)e^{iky\sin\theta - x/l_p - i\omega t} + \text{ c. c.},$$

$$E_x(x,t) = \left(\frac{\omega l_p}{c}\right)^2 \sin\theta B_z(0^+)e^{iky\sin\theta - x/l_p - i\omega t} + \text{ c. c.},$$

$$l_p = \frac{c}{\omega_p}\left(\cos\theta(1-\omega^2\cos^2\theta/\omega_p^2)\right)^{-1/2},$$

$$\frac{B_z(0^+)}{B_{z,i}} = \frac{2\mathsf{n}^2\cos\theta}{\sqrt{\mathsf{n}^2 - \sin^2\theta} + \mathsf{n}^2\cos\theta}$$

Set–up of test particle simulations

Set–up of test particle simulations

- Force: superposition of 1D “pump” field $\sim \cos 2\omega t$

Set–up of test particle simulations

- Force: superposition of 1D “pump” field $\sim \cos 2\omega t$
  plus 2D standing SW field $\sim \sin \omega t \sin(2\pi y/\lambda_s)$

Set–up of test particle simulations

- Force: superposition of 1D “pump” field $\sim \cos 2\omega t$
  plus 2D standing SW field $\sim \sin \omega t \sin(2\pi y/\lambda_s)$

- Amplitudes: $a_0^{(\omega)} = 0.2$, $a_0^{(2\omega)} = 0.019$

Set–up of test particle simulations

- Force: superposition of 1D "pump" field $\sim \cos 2\omega t$
  plus 2D standing SW field $\sim \sin \omega t \sin(2\pi y/\lambda_s)$
- Amplitudes: $a_0^{(\omega)} = 0.2$, $a_0^{(2\omega)} = 0.019$
- Plasma density: $n_e/n_c = \omega_p^2/\omega^2 = 5$
- Initial spatial distribution: uniform in y along one λ_s length

Set–up of test particle simulations

- Force: superposition of 1D "pump" field $\sim \cos 2\omega t$
  plus 2D standing SW field $\sim \sin \omega t \sin(2\pi y/\lambda_s)$
- Amplitudes: $a_0^{(\omega)} = 0.2$, $a_0^{(2\omega)} = 0.019$
- Plasma density: $n_e/n_c = \omega_p^2/\omega^2 = 5$
- Initial spatial distribution: uniform in y along one λ_s length
- Initial velocity distribution: drifting in x with average $v_x = -0.1$
  (particles move from the plasma towards the surface)

Enhanced acceleration in time domain

Enhanced acceleration in time domain

(x, p_x) phase space

Black: all electrons in simulation

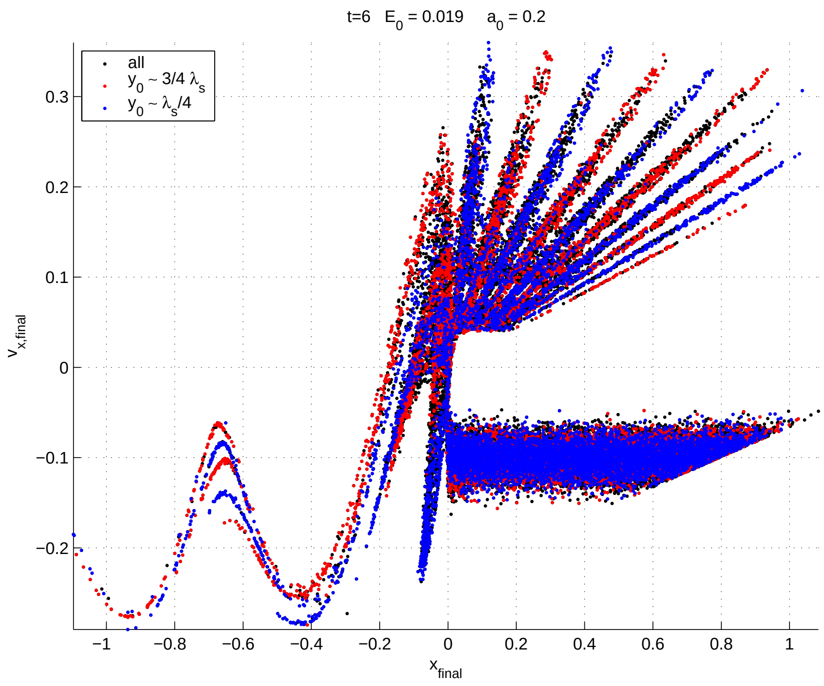

Enhanced acceleration in time domain

(x, p_x) phase space

Black: all electrons in simulation
Blue: electrons starting around $y = \lambda_s/4$

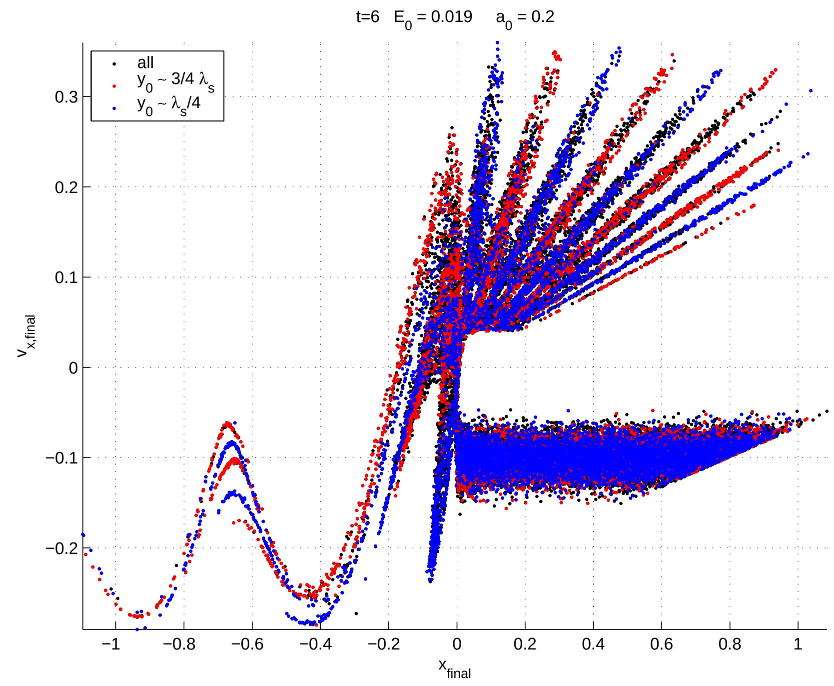

Enhanced acceleration in time domain

(x, p_x) phase space

Black: all electrons in simulation
Blue: electrons starting around $y = \lambda_s/4$
Red: electrons starting around $y = 3\lambda_s/4$

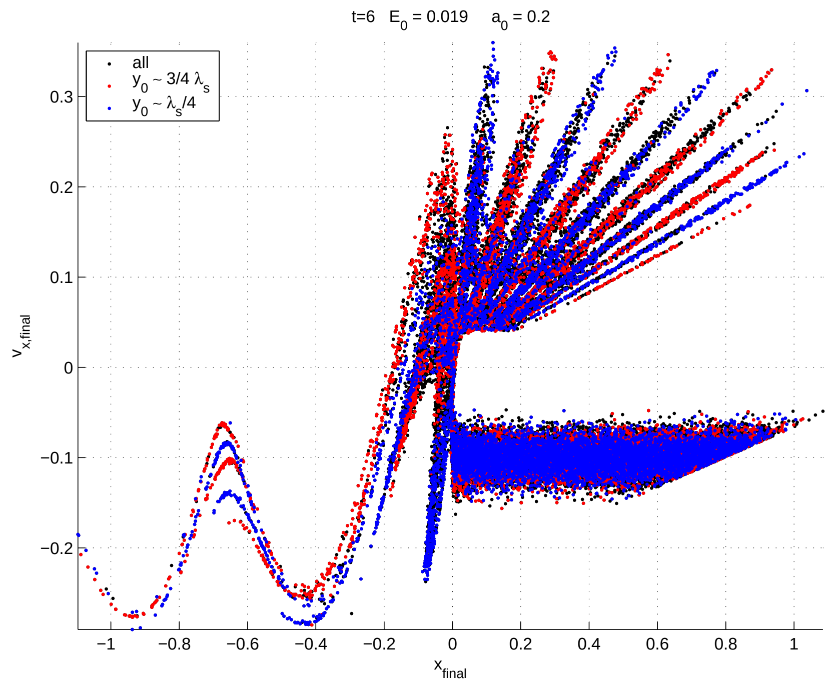

Enhanced acceleration in time domain

(x, p_x) phase space

Black: all electrons in simulation
Blue: electrons starting around $y = \lambda_s/4$
Red: electrons starting around $y = 3\lambda_s/4$

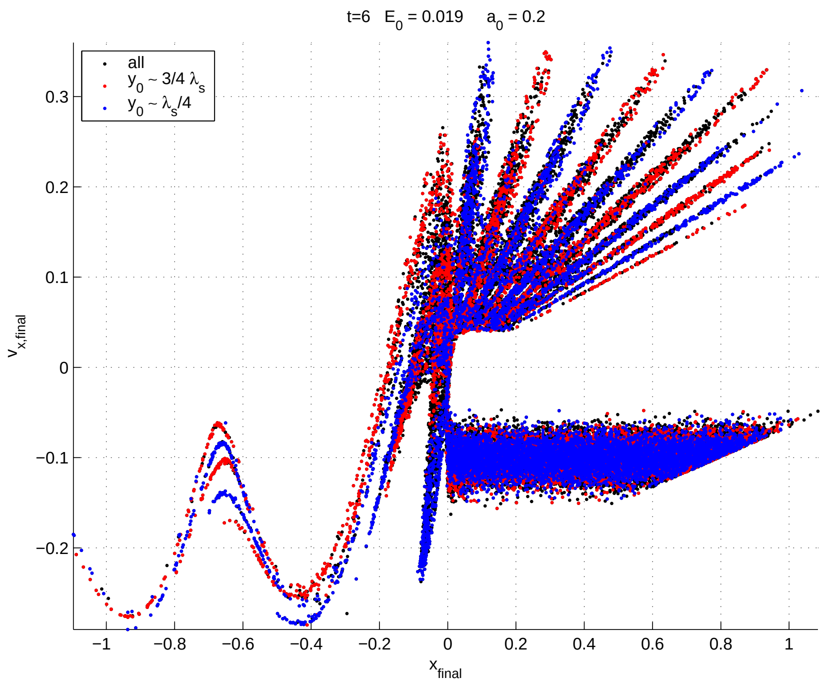

– "Jets" are produced at 2ω rate (by $\mathbf{v} \times \mathbf{B}$ force).

Enhanced acceleration in time domain

(x, p_x) phase space

Black: all electrons in simulation
Blue: electrons starting around $y = \lambda_s/4$
Red: electrons starting around $y = 3\lambda_s/4$

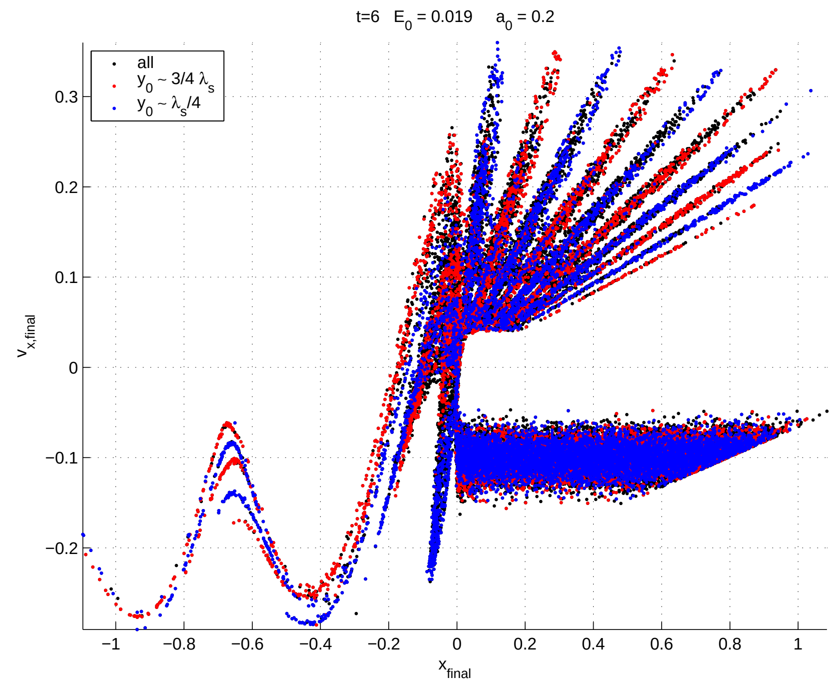

– "Jets" are produced at 2ω rate (by $\mathbf{v} \times \mathbf{B}$ force).
– Enhanced acceleration by SW occurs at ω rate.

Enhanced acceleration in time domain

(x, p_x) phase space

Black: all electrons in simulation
Blue: electrons starting around $y = \lambda_s/4$
Red: electrons starting around $y = 3\lambda_s/4$

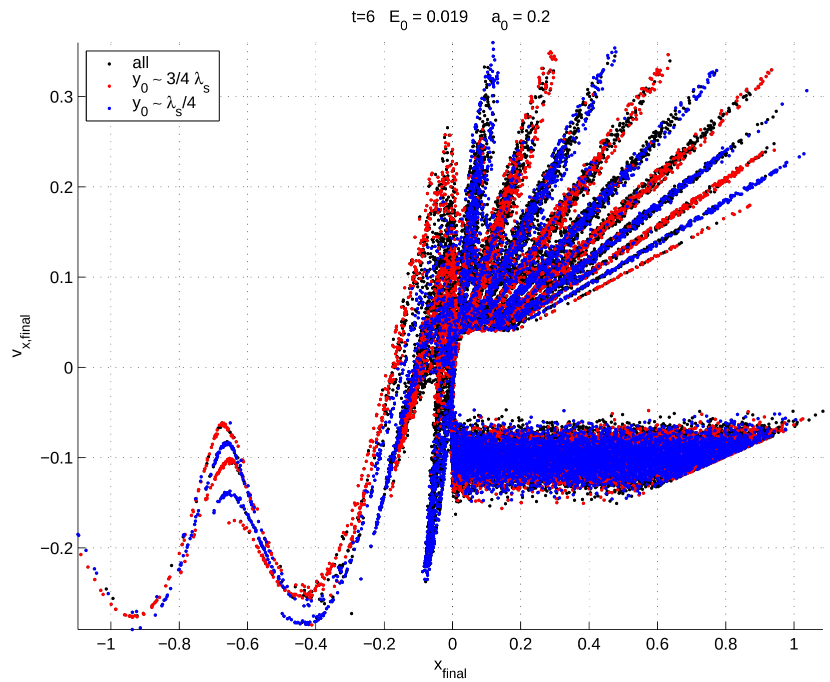

– "Jets" are produced at 2ω rate (by $\mathbf{v} \times \mathbf{B}$ force).

– Enhanced acceleration by SW occurs at ω rate.

– Near SW maxima some electrons are emitted into vacuum ($x < 0$)
(p_x modulated by $\mathbf{v} \times \mathbf{B} \sim \cos 2k_L x$ in vacuum)

Resistivity effects

Resistivity effects

"Fast" electrons (energy > 100 keV) penetrating into a solid material ($n \approx 10^{23}$cm^{-3}) are not significantly stopped by collisions ($\tau_s > 1$ ps, $l_s > 100\ \mu$m).

Resistivity effects

"Fast" electrons (energy > 100 keV) penetrating into a solid material ($n \approx 10^{23}$cm^{-3}) are not significantly stopped by collisions ($\tau_s > 1$ ps, $l_s > 100\ \mu$m).

The "return" current of slow, collisional electrons depends on the material via Ohm's law: $\mathbf{j}_s = \sigma_s \mathbf{E} = \mathbf{E}/\eta_s$.

Resistivity effects

“Fast” electrons (energy > 100 keV) penetrating into a solid material ($n \approx 10^{23}$cm^{-3}) are not significantly stopped by collisions ($\tau_s > 1$ ps, $l_s > 100\ \mu$m).

The “return” current of slow, collisional electrons depends on the material via Ohm’s law: $\mathbf{j}_s = \sigma_s \mathbf{E} = \mathbf{E}/\eta_s$.

The field $\mathbf{E}$ has a slowing effect for fast electrons

Resistivity effects

"Fast" electrons (energy > 100 keV) penetrating into a solid material ($n \approx 10^{23}$cm^{-3}) are not significantly stopped by collisions ($\tau_s > 1$ ps, $l_s > 100$ μm).

The "return" current of slow, collisional electrons depends on the material via Ohm's law: $\mathbf{j}_s = \sigma_s \mathbf{E} = \mathbf{E}/\eta_s$.

The field $\mathbf{E}$ has a slowing effect for fast electrons$\Rightarrow$ collisions affect fast electron transport.

A model for electrostatic inhibition

A model for electrostatic inhibition

[Bell et al.,Plasma Phys. Contr. Fusion **39**, 653 (1997)]

Boltzmann electrostatic equilibrium

$n_f = n_0 \exp(e\Phi/T_f)$

A model for electrostatic inhibition

[Bell et al.,Plasma Phys. Contr. Fusion **39**, 653 (1997)]

Boltzmann electrostatic equilibrium
$n_f = n_0 \exp(e\Phi/T_f)$
$+\ j_f = -j_s = -\sigma E$
$+$ Poisson & continuity eqs.
yield diffusion equation :

$$\partial_t n_f = \partial_x \left[\left(\frac{\sigma_s T_f}{n_f} \right) \partial_x n_f \right]$$

A model for electrostatic inhibition

[Bell et al.,Plasma Phys. Contr. Fusion **39**, 653 (1997)]

Boltzmann electrostatic equilibrium
$n_f = n_0 \exp(e\Phi/T_f)$
$+\ j_f = -j_s = -\sigma E$
$+$ Poisson & continuity eqs.
yield diffusion equation :

$$\partial_t n_f = \partial_x \left[\left(\frac{\sigma_s T_f}{n_f} \right) \partial_x n_f \right]$$

Solutions before and after the laser pulse (duration τ_L):

$$n_f(x,t) = \begin{cases} n_0 \left(\frac{t}{\tau_L}\right) \left(\frac{x_0}{x+x_0}\right)^2 & (t < \tau_L), \\ \frac{2n_0 x_0}{\pi} \frac{L(t)}{x^2+L^2(t)} & (t > \tau_L). \end{cases}$$

$$n_0 = (2I_{abs}^2 \tau_L)/(9eT_f^3\sigma_s)\ ,$$
$$x_0 = 3T_0^3\sigma_s/I_{abs}\ ,$$
$$L(t) = x_0 \ \ (t-\tau_L)(5\pi\sigma_s T_0)/(3en_0x_0^2) + 1 \ \ ^{3/5}.$$

Models for field generation

Models for field generation

To study fast electron transport, once assigned models for $\mathbf{j}_f$ (e.g. kinetic, Fokker–Planck eqs. or Monte Carlo)

Models for field generation

To study fast electron transport, once assigned models for $\mathbf{j}_f$ (e.g. kinetic, Fokker–Planck eqs. or Monte Carlo)and $\mathbf{j}_s$ (e.g. Ohm's law),

Models for field generation

To study fast electron transport, once assigned models for $\mathbf{j}_f$ (e.g. kinetic, Fokker–Planck eqs. or Monte Carlo)and $\mathbf{j}_s$ (e.g. Ohm's law),a model for quasi–steady fields generation must be taken.

Models for field generation

To study fast electron transport, once assigned models for $\mathbf{j}_f$ (e.g. kinetic, Fokker–Planck eqs. or Monte Carlo)and $\mathbf{j}_s$ (e.g. Ohm's law),a model for quasi–steady fields generation must be taken.

Many transport codes assume $\boldsymbol{\nabla} \cdot \mathbf{E} = 0$, $\partial_t \mathbf{E} \simeq 0$ (i.e. no space–charge effects), $\mathbf{j}_s = \mathbf{E}/\eta$ and compute fields by

$$\partial_t \mathbf{B} = \boldsymbol{\nabla} \times (\eta \mathbf{j}_f) \quad , \qquad \mathbf{E} = -\eta[\mathbf{j}_f - (c/4\pi)\boldsymbol{\nabla} \times \mathbf{B}].$$

[Sometimes: $\mathbf{j}_f = -\mathbf{j}_s$, $\mathbf{E} = -\eta \mathbf{j}_f$.]

Models for field generation

To study fast electron transport, once assigned models for $\mathbf{j}_f$ (e.g. kinetic, Fokker–Planck eqs. or Monte Carlo)and $\mathbf{j}_s$ (e.g. Ohm's law),a model for quasi–steady fields generation must be taken.

Many transport codes assume $\boldsymbol{\nabla} \cdot \mathbf{E} = 0$, $\partial_t \mathbf{E} \simeq 0$ (i.e. no space–charge effects), $\mathbf{j}_s = \mathbf{E}/\eta$ and compute fields by

$$\partial_t \mathbf{B} = \boldsymbol{\nabla} \times (\eta \mathbf{j}_f) \quad , \qquad \mathbf{E} = -\eta[\mathbf{j}_f - (c/4\pi)\boldsymbol{\nabla} \times \mathbf{B}].$$

[Sometimes: $\mathbf{j}_f = -\mathbf{j}_s$, $\mathbf{E} = -\eta \mathbf{j}_f$.]

Much additional physics is (or *should* be) inserted: target heating, slow electron diffusion, ionization, . . .

Electrothermal instability

Electrothermal instability

[Haines, PRL **47**, 917 (1981).]

If the background electrons have a Spitzer–Harm conductivity $\sigma \sim T_s^{3/2}$, a transverse modulation of T_s leads to a modulation of σ and thus of $\mathbf{j}_s$.

Electrothermal instability

[Haines, PRL **47**, 917 (1981).]

If the background electrons have a Spitzer–Harm conductivity $\sigma \sim T_s^{3/2}$, a transverse modulation of T_s leads to a modulation of σ and thus of $\mathbf{j}_s$.

Joule heating by $\mathbf{j}_s \cdot \mathbf{E} = \sigma E^2$ increases/decreases where T_s is high/low

Electrothermal instability

[Haines, PRL **47**, 917 (1981).]

If the background electrons have a Spitzer–Harm conductivity $\sigma \sim T_s^{3/2}$, a transverse modulation of T_s leads to a modulation of σ and thus of $\mathbf{j}_s$.

Joule heating by $\mathbf{j}_s \cdot \mathbf{E} = \sigma E^2$ increases/decreases where T_s is high/low $\Rightarrow$ modulation of T_s is increased.

Resulting modulation of $\mathbf{j}$ leads to filamentation and generation of $\mathbf{B}$ that enforces instability;

Electrothermal instability

[Haines, PRL **47**, 917 (1981).]

If the background electrons have a Spitzer–Harm conductivity $\sigma \sim T_s^{3/2}$, a transverse modulation of T_s leads to a modulation of σ and thus of $\mathbf{j}_s$.

Joule heating by $\mathbf{j}_s \cdot \mathbf{E} = \sigma E^2$ increases/decreases where T_s is high/low $\Rightarrow$ modulation of T_s is increased.

Resulting modulation of $\mathbf{j}$ leads to filamentation and generation of $\mathbf{B}$ that enforces instability;magnetic induction generates $\mathbf{E}$ that stabilizes long wavelength modes.

Electrothermal instability

[Haines, PRL **47**, 917 (1981).]

If the background electrons have a Spitzer–Harm conductivity $\sigma \sim T_s^{3/2}$, a transverse modulation of T_s leads to a modulation of σ and thus of $\mathbf{j}_s$.

Joule heating by $\mathbf{j}_s \cdot \mathbf{E} = \sigma E^2$ increases/decreases where T_s is high/low $\Rightarrow$ modulation of T_s is increased.

Resulting modulation of $\mathbf{j}$ leads to filamentation and generation of $\mathbf{B}$ that enforces instability;magnetic induction generates $\mathbf{E}$ that stabilizes long wavelength modes.

Growth rate $\gamma \approx (2m_e/M_I)\nu_{eI}$,

Electrothermal instability

[Haines, PRL **47**, 917 (1981).]

If the background electrons have a Spitzer–Harm conductivity $\sigma \sim T_s^{3/2}$, a transverse modulation of T_s leads to a modulation of σ and thus of $\mathbf{j}_s$.

Joule heating by $\mathbf{j}_s \cdot \mathbf{E} = \sigma E^2$ increases/decreases where T_s is high/low $\Rightarrow$ modulation of T_s is increased.

Resulting modulation of $\mathbf{j}$ leads to filamentation and generation of $\mathbf{B}$ that enforces instability;magnetic induction generates $\mathbf{E}$ that stabilizes long wavelength modes.

Growth rate $\gamma \approx (2m_e/M_I)\nu_{eI}$,wavelength $\lambda \approx (M_I/m_e)^{1/2}\ell_{mfp}$.

(Ion mass appears because Ohmic dissipation is balanced by equipartition to ions.)

The “Weibel” counterstreaming instability

The "Weibel" counterstreaming instability

The fast electron current may penetrate into the target only if almost exactly balanced by a "slow" return current: $n_f v_f = -n_s v_s$, $v_f \gg v_s$, $n_f \ll v_s$.

The "Weibel" counterstreaming instability

The fast electron current may penetrate into the target only if almost exactly balanced by a "slow" return current: $n_f v_f = -n_s v_s$, $v_f \gg v_s$, $n_f \ll v_s$.

An equilibrium configuration with two electron populations carrying opposite and neutralizing currents $(n_1 v_1 = -n_2 v_2)$ is unstable due to the magnetic repulsion of currents; this is a particular case of the Weibel transverse instability.

The "Weibel" counterstreaming instability

The fast electron current may penetrate into the target only if almost exactly balanced by a "slow" return current: $n_f v_f = -n_s v_s$, $v_f \gg v_s$, $n_f \ll v_s$.

An equilibrium configuration with two electron populations carrying opposite and neutralizing currents ($n_1 v_1 = -n_2 v_2$) is unstable due to the magnetic repulsion of currents; this is a particular case of the Weibel transverse instability.

The "Weibel" instability has been invoked to explain filamentation of currents observed in PIC simulations (moderate densities, relativistic electrons, collisions not important).

Simple model of transverse “Weibel” instability – I

Simple model of transverse "Weibel" instability – I

Equilibrium $$f_0 = \frac{e^{-v_y^2/v_{te}^2}}{\pi(v_1+v_2)v_{te}}\left[v_2\delta(v_x - v_1) + v_1\delta(v_x + v_2)\right]$$

Simple model of transverse "Weibel" instability – I

Equilibrium $f_0 = \frac{e^{-v_y^2/v_{te}^2}}{\pi(v_1+v_2)v_{te}}\left[v_2\delta(v_x - v_1) + v_1\delta(v_x + v_2)\right]$ (1)

Perturbation $f(y, v_x, v_y, t) = f_0(v_x, v_y^2) + f_1(v_x, v_y)e^{(iky - i\omega t)}$

Simple model of transverse "Weibel" instability – I

Equilibrium $f_0 = \dfrac{e^{-v_y^2/v_{te}^2}}{\pi(v_1+v_2)v_{te}}\left[v_2\delta(v_x - v_1) + v_1\delta(v_x + v_2)\right]$ (1)

Perturbation $f(y, v_x, v_y, t) = f_0(v_x, v_y^2) + f_1(v_x, v_y)e^{(iky - i\omega t)}$

Linearized Vlasov+Maxwell equations

$$(-i\omega + ikv_y)f_1 = \tfrac{e}{m}\left[\left(E_x + \tfrac{v_y}{c}B_z\right)\partial_{v_x} - \tfrac{v_x}{c}B_z\partial_{v_y}\right]f_0,$$

$$ikB_z = \tfrac{4\pi}{c}J_x - i\tfrac{\omega}{c}E_x\,, \qquad -ikE_x = i\tfrac{\omega}{c}B_z\,.$$

Simple model of transverse "Weibel" instability – I

Equilibrium $f_0 = \dfrac{e^{-v_y^2/v_{te}^2}}{\pi(v_1+v_2)v_{te}}\left[v_2\delta(v_x - v_1) + v_1\delta(v_x+v_2)\right]$ (1)

Perturbation $f(y, v_x, v_y, t) = f_0(v_x, v_y^2) + f_1(v_x, v_y)e^{(iky - i\omega t)}$

Linearized Vlasov+Maxwell equations

$$(-i\omega + ikv_y)f_1 = \tfrac{e}{m}\left[\left(E_x + \tfrac{v_y}{c}B_z\right)\partial_{v_x} - \tfrac{v_x}{c}B_z\partial_{v_y}\right]f_0,$$

$$ikB_z = \tfrac{4\pi}{c}J_x - i\tfrac{\omega}{c}E_x\,, \qquad -ikE_x = i\tfrac{\omega}{c}B_z\,.$$

Dispersion relation $\omega = \omega(k)$ $\qquad (v_0^2 = v_1 v_2)$

$$\omega^2 - k^2c^2 = \omega_p^2\left(1 + \frac{v_0^2}{v_{te}^2}\int dv_y \frac{1}{\sqrt{\pi}v_{te}}e^{-v_y^2/v_{te}^2}\frac{kv_y}{\omega - kv_y}\right)$$

Simple model of transverse "Weibel" instability – II

Simple model of transverse "Weibel" instability – II

Long– and short–wavelength limits of $\omega = \omega(k)$:

Simple model of transverse “Weibel” instability – II

Long– and short–wavelength limits of $\omega = \omega(k)$:

$$\omega^2 - k^2c^2 = \begin{cases} \omega_p^2 \left(1 + \frac{k^2 v_0^2}{\omega^2}\right) & (kv_y \ll \omega), \\ \omega_p^2 \left(1 - \frac{v_0^2}{v_{te}^2}\right) & (kv_y \gg \omega). \end{cases}$$

Simple model of transverse “Weibel” instability – II

Long– and short–wavelength limits of $\omega = \omega(k)$:

$$\omega^2 - k^2c^2 = \begin{cases} \omega_p^2 \left(1 + \frac{k^2 v_0^2}{\omega^2}\right) & (kv_y \ll \omega), \\ \omega_p^2 \left(1 - \frac{v_0^2}{v_{te}^2}\right) & (kv_y \gg \omega). \end{cases}$$

Imaginary root $\omega = i\gamma, \gamma > 0$

Simple model of transverse "Weibel" instability – II

Long– and short–wavelength limits of $\omega = \omega(k)$:

$$\omega^2 - k^2c^2 = \begin{cases} \omega_p^2\left(1 + \frac{k^2 v_0^2}{\omega^2}\right) & (kv_y \ll \omega), \\ \omega_p^2\left(1 - \frac{v_0^2}{v_{te}^2}\right) & (kv_y \gg \omega). \end{cases}$$

Imaginary root $\omega = i\gamma, \gamma > 0 \rightarrow$ unstable branch $\gamma = \gamma(k)$

Simple model of transverse "Weibel" instability – II

Long– and short–wavelength limits of $\omega = \omega(k)$:

$$\omega^2 - k^2c^2 = \begin{cases} \omega_p^2 \left(1 + \frac{k^2 v_0^2}{\omega^2}\right) & (kv_y \ll \omega), \\ \omega_p^2 \left(1 - \frac{v_0^2}{v_{te}^2}\right) & (kv_y \gg \omega). \end{cases}$$

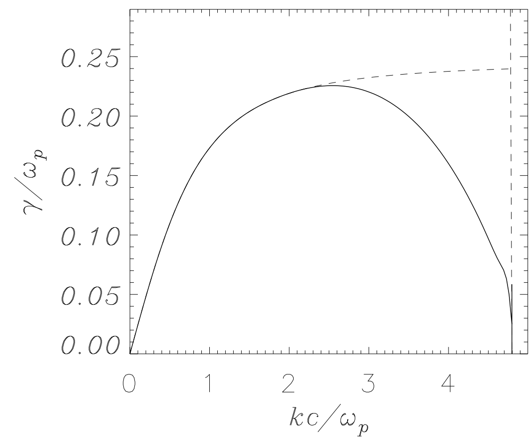

Imaginary root $\omega = i\gamma, \gamma > 0 \rightarrow$ unstable branch $\gamma = \gamma(k)$

Simple model of transverse "Weibel" instability – II

Long– and short–wavelength limits of $\omega = \omega(k)$:

$$\omega^2 - k^2c^2 = \begin{cases} \omega_p^2 \left(1 + \frac{k^2 v_0^2}{\omega^2}\right) & (kv_y \ll \omega), \\ \omega_p^2 \left(1 - \frac{v_0^2}{v_{te}^2}\right) & (kv_y \gg \omega). \end{cases}$$

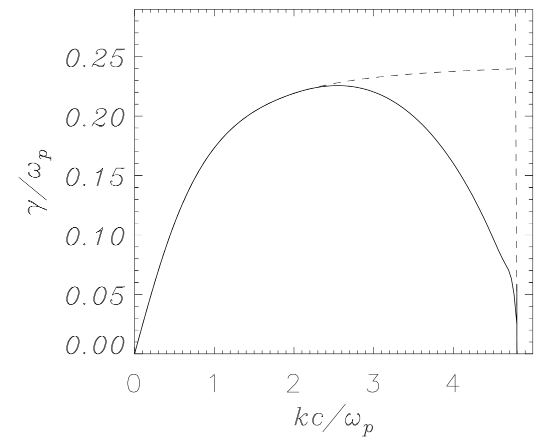

Imaginary root $\omega = i\gamma, \gamma > 0 \rightarrow$ unstable branch $\gamma = \gamma(k)$

Range of the unstable wavevectors $k^2c^2 < \omega_p^2 \left(v_0^2/v_{te}^2 - 1\right)$

Simple model of transverse “Weibel” instability – II

Long– and short–wavelength limits of $\omega = \omega(k)$:

$$\omega^2 - k^2c^2 = \begin{cases} \omega_p^2 \left(1 + \frac{k^2 v_0^2}{\omega^2}\right) & (kv_y \ll \omega), \\ \omega_p^2 \left(1 - \frac{v_0^2}{v_{te}^2}\right) & (kv_y \gg \omega). \end{cases}$$

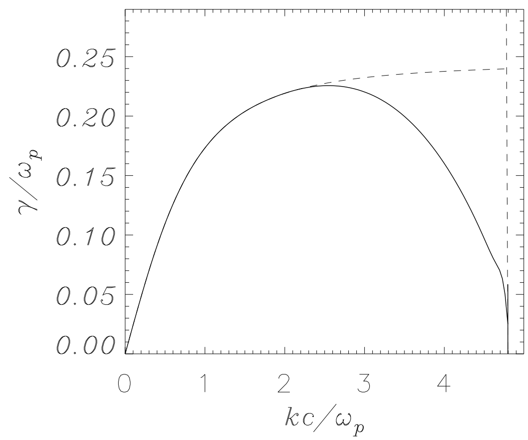

Imaginary root $\omega = i\gamma, \gamma > 0 \rightarrow$ unstable branch $\gamma = \gamma(k)$

Range of the unstable wavevectors $k^2c^2 < \omega_p^2 \left(v_0^2/v_{te}^2 - 1\right)$

Similar to the Bennett condition for pinch stability (thermal and magnetic pressures balance each other).

Simple model of transverse “Weibel” instability – II

Long– and short–wavelength limits of $\omega = \omega(k)$:

$$\omega^2 - k^2c^2 = \begin{cases} \omega_p^2 \left(1 + \frac{k^2 v_0^2}{\omega^2}\right) & (kv_y \ll \omega), \\ \omega_p^2 \left(1 - \frac{v_0^2}{v_{te}^2}\right) & (kv_y \gg \omega). \end{cases}$$

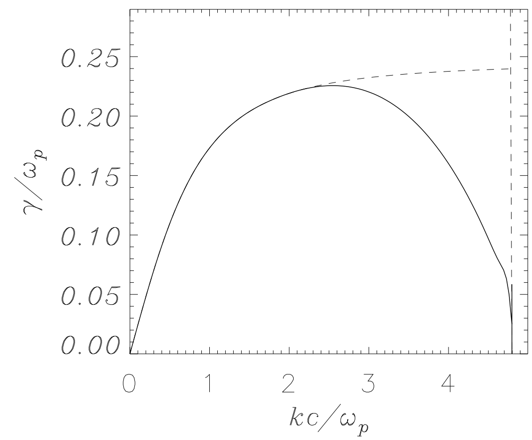

Imaginary root $\omega = i\gamma, \gamma > 0 \rightarrow$ unstable branch $\gamma = \gamma(k)$

Range of the unstable wavevectors $k^2c^2 < \omega_p^2 \left(v_0^2/v_{te}^2 - 1\right)$

Similar to the Bennett condition for pinch stability (thermal and magnetic pressures balance each other).

Saturation when $B^2/8\pi \approx n_e m v_0^2/2$ ($\approx$ energy equipartition)

[Califano et al. PRE 1998]

Generalized 3D current filamentation instability

Generalized 3D current filamentation instability

The distribution function (1) is also unstable with respect to electrostatic, longitudinal perturbations (two–stream instability).

Generalized 3D current filamentation instability

The distribution function (1) is also unstable with respect to electrostatic, longitudinal perturbations (two–stream instability). In the relativistic regime $(v_1 \rightarrow c)$ the longitudinal modes are coupled to the transverse "Weibel" modes for asymmetrical initial equilibria $(v_1 \neq v_2)$ [Califano et al. PRE 1998].

Generalized 3D current filamentation instability

The distribution function (1) is also unstable with respect to electrostatic, longitudinal perturbations (two–stream instability). In the relativistic regime $(v_1 \to c)$ the longitudinal modes are coupled to the transverse "Weibel" modes for asymmetrical initial equilibria $(v_1 \neq v_2)$ [Califano et al. PRE 1998].

$$f(x, y, v_x, \mathbf{v}_\perp, t) = f_0(v_x, v_\perp^2) + f_1(v_x, \mathbf{v}_\perp) e^{i(k_\parallel x + ik_\perp \mathbf{r}_\perp - \omega t)}$$

The most unstable wavevector $\mathbf{k} = (k_\parallel, \mathbf{k}_\perp)$ has $k_\perp \neq 0$
$\rightarrow$ fields structures have finite length along the beams direction.

Generalized 3D current filamentation instability

The distribution function (1) is also unstable with respect to electrostatic, longitudinal perturbations (two–stream instability). In the relativistic regime ($v_1 \rightarrow c$) the longitudinal modes are coupled to the transverse "Weibel" modes for asymmetrical initial equilibria ($v_1 \neq v_2$) [Califano et al. PRE 1998].

$$f(x, y, v_x, \mathbf{v}_\perp, t) = f_0(v_x, v_\perp^2) + f_1(v_x, \mathbf{v}_\perp) e^{i(k_\parallel x + ik_\perp \mathbf{r}_\perp - \omega t)}$$

The most unstable wavevector $\mathbf{k} = (k_\parallel, \mathbf{k}_\perp)$ has $k_\perp \neq 0$ $\rightarrow$ fields structures have finite length along the beams direction.

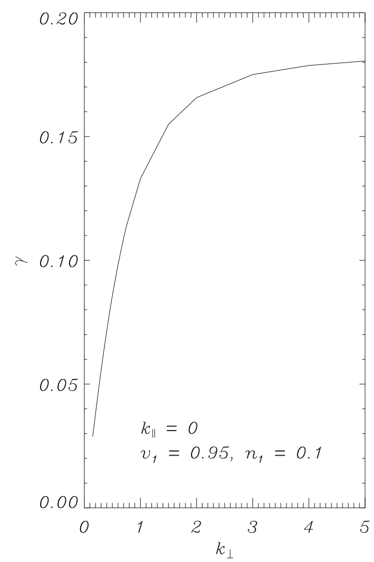

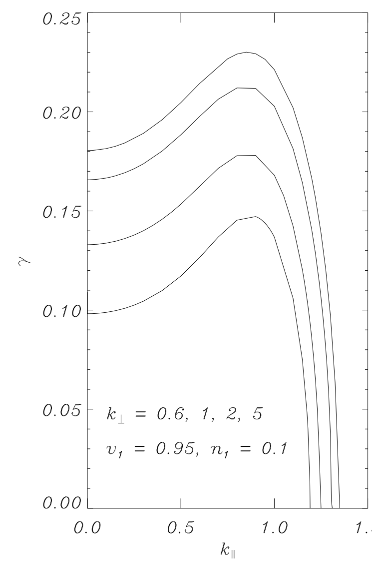

3D fluid simulation of the CF instability

3D fluid simulation of the CF instability

Simulation example:
$n_1/n_2 = 9$, $v_1 = 0.95c$, $v_2 = -0.10556c$.

3D fluid simulation of the CF instability

Simulation example:
$n_1/n_2 = 9$, $v_1 = 0.95c$, $v_2 = -0.10556c$.
Figure shows isosurfaces of A_z (vector potential component along beam direction), which is representative of the magnetic field structure because $B_z \ll (B_x, B_y)$ is found.

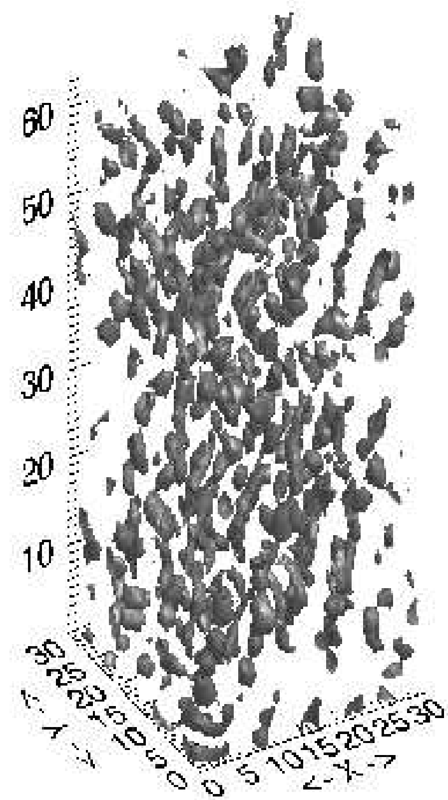

3D fluid simulation of the CF instability

Simulation example:

$n_1/n_2 = 9$, $v_1 = 0.95c$, $v_2 = -0.10556c$.

Figure shows isosurfaces of A_z (vector potential component along beam direction), which is representative of the magnetic field structure because $B_z \ll (B_x, B_y)$ is found.

3D "bubble–like" magnetic structures are formed with typical length scales $\sim d_e = c/\omega_p$. No extended filaments in beam direction are observed.

[Simulations by F. Califano;
Macchi et al, Nucl. Fus. **43**, 362 (2003)]